

5-2019

Reconstructing Barrier Island Behavior from Overstepped Deposits and Relict Onshore Morphology : Modeling and Field Approaches

Daniel James Ciarletta
Montclair State University

Follow this and additional works at: <https://digitalcommons.montclair.edu/etd>



Part of the [Geomorphology Commons](#)

Recommended Citation

Ciarletta, Daniel James, "Reconstructing Barrier Island Behavior from Overstepped Deposits and Relict Onshore Morphology : Modeling and Field Approaches" (2019). *Theses, Dissertations and Culminating Projects*. 298.
<https://digitalcommons.montclair.edu/etd/298>

This Dissertation is brought to you for free and open access by Montclair State University Digital Commons. It has been accepted for inclusion in Theses, Dissertations and Culminating Projects by an authorized administrator of Montclair State University Digital Commons. For more information, please contact digitalcommons@montclair.edu.

RECONSTRUCTING BARRIER ISLAND BEHAVIOR FROM OVERSTEPPED DEPOSITS
AND RELICT ONSHORE MORPHOLOGY: MODELING AND FIELD APPROACHES

A DISSERTATION

Submitted to the Faculty of
Montclair State University in partial fulfillment
of the requirements
for the degree of Doctor of Philosophy

by

DANIEL J. CIARLETTA

Montclair State University

Upper Montclair, NJ

May 2019

Dissertation Chair: Dr. Jorge Lorenzo-Trueba

MONTCLAIR STATE UNIVERSITY

THE GRADUATE SCHOOL

DISSERTATION APPROVAL

We hereby approve the Dissertation

RECONSTRUCTING BARRIER ISLAND BEHAVIOR FROM OVERSTEPPED DEPOSITS

AND RELICT ONSHORE MORPHOLOGY: MODELING AND FIELD APPROACHES

of

Daniel J. Ciarletta

Candidate for the Degree:

Doctor of Philosophy

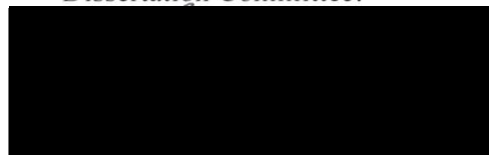
Graduate Program: Environmental
Science and Management

Dissertation Committee:

Certified by:



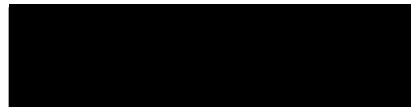
Dr. M. Scott Henness
Vice Provost for Research and
Dean of the Graduate School



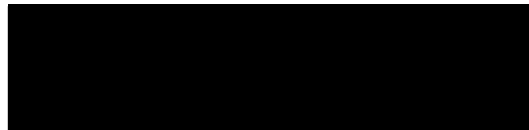
Dr. Jorge Lorenzo-Trueba
Dissertation Chair



Dr. Sandra Passchier



Dr. Mark Chopping



Mr. Charles Dill (AOSS, Inc.)

Date

4-22-19

Copyright © 2019 by Daniel James Ciarletta. All rights reserved.

ABSTRACT

RECONSTRUCTING BARRIER ISLAND BEHAVIOR FROM OVERSTEPPED DEPOSITS AND RELICT ONSHORE MORPHOLOGY: MODELING AND FIELD APPROACHES

by Daniel J. Ciarletta

Barrier Islands comprise 10% of the Earth's shorelines, fringing every continent except Antarctica. Despite their ubiquity, much about the medium to long-term evolution of these coastal systems remain poorly understood, mostly due to the destruction of the geologic record as barriers migrate landward under the influence of rising sea level. Even where modern barriers and related strandplain systems have prograded and regressed, leaving evidence of their former geometries in the form of relict shorelines, field investigations often require intensive labor and time commitments to interpret past evolution. In this work, several investigations are undertaken to use novel numerical modeling techniques coupled with field interpretation and comparison to gain insights into the evolution of barrier islands from relict geomorphic features preserved on the continental shelf seabed and the surfaces of modern barriers. Much of these efforts focus on 'drowned' barrier features, or the remnants of barrier islands left stranded on the shelf during landward migration that occurred in the late Pleistocene and early Holocene, as well as patterns of abandoned foredune ridges generated during late Holocene shoreline progradation. Among the most intriguing results herein is the possibility that the internal dynamics of barrier islands can lead to periodic backstepping and partial deposition of the barrier structure without the need to invoke changing environmental forcing. Moreover, it can be shown that combinations of internal dynamic state and environmental forcing from relatively sudden changes in rate of sea-level rise could lead to a rich suite of barrier retreat behaviors. This might explain the morphologies of drowned barrier features produced during glacial meltwater and outburst flood 'pulses' prior to 8

kya. More importantly, these insights may prove practical in modern systems, where anthropogenic climate change threatens barrier islands with historically unprecedented rates of sea-level rise.

Keywords: coastal geomorphology, barrier islands, sea level, beach ridges, modeling

ACKNOWLEDGEMENTS

Foremost, I would like to thank Dr. Jorge Lorenzo-Trueba for giving me the opportunity work on these investigations, as well as my dissertation committee members, Dr. Sandra Passchier, Dr. Mark Chopping, and Mr. Charles Dill, for offering their time and expertise. I would like to thank the National Science Foundation and New Jersey Sea Grant Consortium for financially supporting these investigations, as well as acknowledge my collaborators at the Virginia Institute of Marine Science and Woods Hole Oceanographic Institution, especially Andrew Ashton, Christopher Hein, and Justin Shawler. I would also like to thank all the students of the Coastal Research Group, including Christopher Tenebruso, Isamar Cortes, Arye Janoff, Jesse Kolodon, and Will Anderson, for their support, as well as the both graduate offices in CELS for their exceptional camaraderie over the course of these investigations and during my studies at Montclair State University. And I would especially like to thank my family and friends for all their support, as well as my girlfriend, Kim, who has stood with me for the duration of my doctoral studies.

TABLE OF CONTENTS

INTRODUCTION	1
CHAPTER 1 - AN AUTOGENIC ORIGIN OF RELICT BARRIERS	6
1.0 Summary	7
1.1 Introduction: An Unexplored Mechanism	7
1.2 Background: Relict Deposits on Modern Margins	10
1.3 Methods.....	11
1.4 Results.....	14
1.5 Discussion: Model Implications for Real-World Comparison	15
1.6 Conclusions.....	17
CHAPTER 2 - QUASI-PERIODIC BARRIER OVERSTEPPING	18
2.0 Summary	19
2.1 Introduction: Incomplete Periodicity	19
2.2 Background & Methods.....	20
2.3 Results.....	24
2.5 Conclusions.....	28
CHAPTER 3 - SEA-LEVEL DRIVEN AUTOGENIC-ALLOGENIC INTERACTION DURING PERIODIC BARRIER RETREAT	29
3.0 Summary	30
3.1 Introduction: Autogenic-Allogenic Interaction.....	30
3.2 Background: Periodicity and Sea-Level Pulses	33
3.2.1 Morphodynamic Model	33
3.2.2 Sea Level Interaction	35
3.3 Model Setup.....	37
3.4 Results.....	40
3.5 Discussion: A Complicated Response	45
3.6 Conclusions.....	47
CHAPTER 4 - QUANTIFYING SEDIMENT BUDGET FROM SUBAERIAL BARRIER RIDGE AND SWALE MORPHOLOGY.....	48
4.0 Summary	49
4.1 Introduction: Ridge and Swale Systems as Records of Past Change.....	50
4.2 Background: Concept to Quantification	52
4.2.1 Development of Ridge Morphology	54
4.3 Model Setup and Methods	57
4.3.1 Exploration of Model Behaviors.....	60
4.3.2 Field Comparison.....	64
4.4 Model Validation: Analysis of the Growth of Fishing Point, Virginia.....	65
4.4.1 Fishing Point Overview	66
4.4.2 Deriving Input Fluxes from the Historical Record	67
4.4.3 Modeled Fluxes and Morphology	69
4.5 Model Application: Reconstructing the Growth of Parramore Island, Virginia.....	72
4.5.1 Parramore Island Overview	72
4.5.2 Modeled Fluxes and Morphology	73
4.6 Discussion.....	77
4.6.1 Parramore Island	77

4.6.2 Broader Application.....	78
4.6.3 Considerations and Future Work	80
4.7 Conclusions.....	81
CONCLUDING SYNTHESIS AND FUTURE WORK	83
REFERENCES	87
APPENDICES	97
Chapter 1 Appendix	98
Model Sensitivity to Input Parameters.....	98
Chapter 4 Appendix	104
Tables.....	104
Figures.....	107

Tables

Table 1.1 – Field Sites	10
Table 1.2 – Model Input Parameters.....	14
Table 2.1 – Model Barrier Parameters.....	24
Table 3.1 – Model Input Parameters.....	39
Table 4.1 – State Variables	60
Table 4.2 – Model Input Parameters.....	60
Table 4.3 – Modeled vs. Field Measurements	69

Figures

Figure 1.1 – Upper Panel: Idealized transgressive barrier sequence with alternating remnant sand bodies and ravinement surfaces. Lower Panels: Profiles through Sand Key, West Florida, after Locker et al. (2003); New Jersey outer continental shelf, seaward of the Mid-Shelf Wedge, after Nordfjord et al. (2009); Long Island off Cedar Beach, after Rampino and Sanders (1980); Hastings Bank (English Channel), after Mellet et al. (2012); KwaZulu-Natal shelf off Durban, South Africa, after Pretorius et al. (2016); Gulf of Orsitano, Sardinia, after De Falco et al. (2015). Numbers in meters are depth relative to mean sea level.....	9
Figure 1.2 – Model output depicting cycle of periodic retreat. A remnant deposit (tan) is left on the seabed as the barrier (yellow) migrates (A, B) following a previous aggradational episode, culminating in erosion of the shelf and a return to aggradation (C, D). The size of the black arrow indicates the magnitude of fluxes at the shoreface. The red arrow indicates active migration through overwash, while the red circle indicates aggradation (no overwash). Green lines in subplots indicate time during production of corresponding cross-section. Seabed elevation is anomaly in seabed topography relative to initial (linearly sloping) seabed.....	13
Figure 1.3 – Modeled remnant seabed deposit wavelength (spacing) and volume produced by a barrier undergoing periodic retreat overlain with field site interpretations. Results are shown for constant sea-level rise rates (SLRR) from 0.01 to 18 mm/yr and a run time of 20 kyrs (see Table 1.2 for input parameters; see Appendix Figures A1.1-A1.11 for additional input sensitivity analysis).....	14
Figure 2.1 – Cross section of barrier undergoing periodic retreat at 6 kyrs. Subplot tracks seabed anomaly with time, depicting deposition (aggradation) and ravinement (migration). Star corresponds to Figure 2.3	21

Figure 2.2 – Cross section of barrier undergoing deflation drowning at 3 kyrs post-initialization. Subplots track seabed anomaly with time, depicting deposition (aggradation) and ravinement (migration). Star corresponds to Figure 2.3..... 22

Figure 2.3 – Behavioral response of a modestly sized barrier (see Table 2.1) to combinations of maximum rate of overwash and rate of sea-level rise. Starred points correspond with Figures 2.1 and 2.2. 23

Figure 2.4 – Temporary increase in the volume of the barrier with each migration-aggradation cycle during transition to consistent periodicity. Here, change in volume per cycle stops after 7 kyrs..... 23

Figure 2.5 – Time to drowning for modestly sized barrier (solid black line) vs. large barrier (dashed black line) at 4 mm/yr sea-level rise and 2 m/km shelf slope. See Table 2.1 for additional inputs. $Q_{OW,max}$ = Maximum overwash rate..... 25

Figure 2.6 – Annotated time to drowning plot for a large barrier. Note that deflation drowning occurs between 4 and 16.5 kyrs, demonstrating an extended time in periodic transition. 25

Figure 2.7 – Large barrier undergoing deflation drowning, producing two quasi-periodic deposits on the seabed during an incomplete transition to consistent periodicity. Max overwash rate = 525 m³/m/yr..... 26

Figure 2.8 – Three quasi-periodic deposits produced on the seabed prior to deflation drowning. Max overwash rate = 505 m³/m/yr. 27

Figure 2.9 – Detail of deflation region for a large barrier. The number of quasi-periodic deposits increases as the rate of overwash moves closer to values that can sustain consistent periodicity..... 27

Figure 3.1 – Periodic barrier retreat, defined by an autogenic cycle of alternating episodes of migration (red) and aggradation (green), modeled under constant forcing from rate of sea-level rise and shelf slope. Recurring phases of aggradation lead to the deposition of remnant barrier sands, as eventual migration causes a portion of the lower shoreface below the depth of closure to become stranded on the shelf seabed..... 34

Figure 3.2 – Barrier undergoing dynamic rollover at shoreface response $K = 9000$ m³/m/yr. (A) Example with constant forcing and balance between shoreface fluxes and overwash fluxes. (B) The barrier is subjected to a 200-yr pulse (duration and distance affected highlighted in magenta), beginning 800 years into the model run, with a magnitude of 20 mm/yr..... 38

Figure 3.3 – Setup of sea-level interaction experiment. A periodically retreating barrier encounters a pulse in rate of sea-level rise (in this example, 18 mm/yr) comparable to the duration of the 8.2 kyr rise event. The timing of the pulse is shifted through periodic cycles (migration and aggradation) for pulse rates of rise up to 30 mm/yr. The barrier also migrates along a shelf with a 1 m/km slope, comparable to many passive margins..... 39

Figure 3.4 – Range of behavioral/depositional responses of a periodically retreating barrier subjected to a pulse in rate of sea-level rise. Pink highlights correspond to duration and distance affected by pulse. (A) Periodic deposition (autogenic), with no pulse; dashed lines in subsequent subplots (B, C, D) refer to plots shown here. (B) 20 mm/yr pulse coinciding with the aggradational phase of periodic retreat; amplified deposit produced. (C) 10 mm/yr pulse coinciding with migrational phase of periodic retreat; no deposition/ravinement. (D) 20 mm/yr pulse coinciding with migrational phase of periodic retreat; deposition occurs where periodic retreat suggests none should occur..... 40

Figure 3.5 – Regime plots depicting the barrier response to a 200-yr sea level pulse, with pulse initiation (relative to start of model run) on the y-axis, and pulse rate of rise on the x-axis. Response shown for barriers with a shoreface response of (A) 2000 m³/m/yr, (B) 3000 m³/m/yr, and (C) 6000 m³/m/yr. Red and green regions occur where remnant barrier deposits are detected and the barrier does not completely drown; red regions correspond with the migrational phase of the periodic cycle, while green regions correspond with the aggradational phase. Dark blue regions highlight dynamic rollover, orange regions

highlight width drowning, and light blue regions highlight height drowning. Drowning is least pronounced when the pulse is initiated near the transition from migration (red) to aggradation (green), which corresponds with the timing of maximum landward-directed shoreface fluxes during the periodic cycle. At the highest shoreface response rate ($6000 \text{ m}^3/\text{m}/\text{yr}$), the phase of the periodic cycle exerts relatively little influence on whether the barrier drowns, as autogenic influence is minimized. 42

Figure 3.6 – Classification of a full periodic cycle (migration-aggradation) based on the amplitudes of resulting deposits. Allogenic influence from the pulse occurs readily in the transition from autogenic deposition/ravinement to the width drowning regime. During the aggradational phase, pulses can amplify deposits that would already be created during purely periodic retreat. Conversely, in the migrational phase, where ravinement would occur autogenically, emergent allogenic deposits (with amplitudes smaller than autogenic deposits), as well as large allogenic deposits (with amplitudes greater than autogenic deposits) can form. 43

Figure 3.7 – TOP: Classification of a full periodic cycle with decreasing autogenic influence. As shoreface response rate K increases, the periodic cycle shortens, drowning becomes less variable with respect to pulse rate of rise, and amplification and production of allogenic deposits gradually dominate the regime space. At $K=6000 \text{ m}^3/\text{m}/\text{yr}$, no autogenic deposits are produced, and dynamic rollover begins to dominate the barrier response at low pulse rates or rise. BOTTOM: Corresponding plots of deposit amplitude. White regions indicate to no detection of a deposit or complete drowning of the barrier. 44

Figure 4.1 – (a) Processes responsible for shoreline progradation. Sand is first transported to the beach (largely through onshore bar migration and contributions from longshore transport) and later transported to the active beach/foredune ridge by aeolian and wave transport. The shoreline advances seaward with time, and new dunes form with a characteristic crest spacing, producing an alternating pattern of ridges and swales. In this example, swales are progressively flooded by rising sea level and experience upland marsh migration from the back-barrier margin. In cases of falling sea level and decreasing shoreface accommodation (also included in model development), this would not occur. (b) Model idealized geometry and processes. (c) Depiction of new dune line emplacement. An incipient foredune forms when the width of the beach and dune flank $L + H/\Gamma_l$ is greater than or equal to the critical ridge spacing plus the setback distance $L_C + L_S$. The crest of the new dune forms at $x_s - L_S$ so that the incipient dune is inland of the shoreline. 53

Figure 4.2 – (a) Map overview of the Virginia Eastern Shore (VES), at the southern end of the Delmarva Peninsula on the United States Atlantic coast. (b) Hillshaded LiDAR-derived digital elevation models of Fishing Point and (c) North Parramore Island, showing orientation of ridge and swale systems. Highest elevations on Fishing Point are $> 3 \text{ m}$, while some points on North Parramore reach $> 7 \text{ m}$ above mean higher high water (MHHW). (d) Ridge-perpendicular transects of Fishing Point and (e) Parramore Island showing elevation profiles referenced to MHHW. Individual ridges are numbered from landward to seaward, unless otherwise named. 61

Figure 4.3 – Regime plot showing the types of subaerial ridge and swale patterns modeled over the timescale of Fishing Point (100 years) for combinations of shoreface fluxes Q_S and foredune fluxes Q_D . The characterization of ridge heights is based on the tallest ridges observed in the Virginia system (8 m). The rate of rise was set to $2 \text{ mm}/\text{yr}$, and the critical ridge spacing was 109 m . To distinguish patterns, n =number of ridges and H =height of ridge. 62

Figure 4.4 – Modeled pattern of cross-shore changes in ridge geometry resulting from adjustments in the rate of progradation by modulating Q_S . (a) Washboard pattern of regularly spaced ridges, with steady Q_S . (b) Episode of fast progradation that suppresses ridge height and results in a wide flat on the barrier platform (c) Sustained episode of slow progradation, allowing time to build a large, complex ridge. For all cases, $L_C = 200 \text{ m}$, $L_S = 5 \text{ m}$, with rate of rise of $1 \text{ mm}/\text{yr}$ 63

Figure 4.5 – (a) Calculated shoreline fluxes for the Fishing Point transect for 1919–2013. The average flux for this period is 134 m³/m/yr. (b) Calculated foredune fluxes for the Fishing Point transect for 1958–2016. The average flux for this period is 13 m³/m/yr. 68

Figure 4.6 – (a) Elevation cross section of Fishing Point along its widest dimension measured from LiDAR data. (b) Modeled profile of Fishing Point using a time series of shoreface and foredune fluxes derived from the historical record. While the average height of the modeled profile is 50% taller than the field average, remaining parameters are within 20% of field measurements (Table 3). (c) Modeled geomorphological profile of Fishing Point using a time-invariant shoreface flux Q_S of 134 m³/m/yr and a foredune flux Q_D of 13 m³/m/yr, the long-term average flux values derived from the historical record.... 70

Figure 4.7 – Sensitivity plots of (a) number of ridges produced, (b) average ridge height, (c) cross-sectional dune volume, and (d) final shoreline location, as a function of input-flux combinations. Bolded contours represent measurements of the four morphologic parameters obtained from the field at Fishing Point. (e) A morphological calibration in which the area bound by the intersection of the four parameter lines—the *region of similarity*—indicates the range of flux combinations that produce results similar to field measurements. 71

Figure 4.8 – Evaluation of the “Back Four” ridges of North Parramore Island using morphological calibration plots to constrain the balance of Q_S and Q_D fluxes consistent with field sites parameters over timescales of (a) 200 years and (b) 600 years. The area bound by the intersection of the four parameter lines—the *region of similarity*—indicates the range of flux combinations that produce results similar to the field. 74

Figure 4.9 – (a) Modeled geomorphological profile of North Parramore Island using a shoreline flux Q_S of 13 m³/m/yr for 200 years, 1.6 m³/m/yr for 600 years, and 15 m³/m/yr for the last 200 years—with a constant foredune flux Q_D of 0.7 m³/m/yr. Changes in (b) rate of shoreline progradation and (c) ridge height are shown for the 1000 yr run time of the model. 75

LIST OF ABBREVIATIONS

CoNED – Coastal National Elevation Database
GPR – Ground Penetrating Radar
LiDAR – Light Detecting and Ranging
LIS – Laurentide Ice Sheet
LTA – Lorenzo-Trueba & Ashton (cross-shore barrier model)
MHHW – Mean Higher High Water
NAVD88 – North American Vertical Datum of 1988
OSL – Optically Stimulated Luminescence
SLRR – Sea-Level Rise Rate
VES – Virginia Eastern Shore

INTRODUCTION

Barrier islands are a widely distributed landform on the Earth's surface, fronting the equivalent of 10% of all continental shorelines (Stutz and Pilkey, 2011), not considering the estimated 15,000+ fetch-limited barrier islands that exist in bays, behind reefs, and within other semi-enclosed or restricted water bodies (Pilkey et al., 2009). Coastal systems containing barrier islands contribute at least 9.2% of worldwide ecosystem services, valued at slightly more than \$3 trillion per year (Feagin et al., 2010; Martínez et al., 2007; Pilkey and Fraser, 2003)—coastal ecosystems more broadly account for an estimated 77% of the world's ecosystem services, valued at \$33 trillion (Martínez et al., 2007). Within the United States alone, tourism related to barrier islands and beaches fuels an industry worth an estimated \$322 billion (Feagin et al., 2010; Houston, 2008), and an estimated 1.4 million people were living directly on east coast barrier islands in 2000, marking an increase in population by 14% during the 1990s (Zhang and Leatherman, 2011). More broadly, 39 percent of the United States' population in 2010 lived in coastal counties, the vast majority on the east coast fronted by barrier islands (Zhang and Leatherman, 2011; NOAA, 2010) that not only protect island communities, but also marshes and infrastructure on the mainland shoreline (Gedan et al., 2011).

Despite the ubiquity and value of coastal barrier islands, knowledge of how barriers behave over decadal to centennial scales remains poorly constrained, and many of the underlying concepts describing their long-term evolution have changed little since they were originally proposed by Gilbert (1885) and Johnson (1919). This poses a substantial risk for future coastal management, as current policies largely lack guidance pertaining to long-term barrier evolution—despite that anthropogenic sea-level rise will undoubtedly lead to historically unprecedented changes in barrier coastlines in the next century (McNamara and Lazarus, 2018). One of the major reasons for the relative dearth of knowledge arises because barrier islands

generally destroy evidence of their former geometries, with much of their superstructures recycled through landward overwash of sediments (Swift, 1975). Even where barriers have prograded, growing seaward and leaving behind ample geologic evidence of their former configurations, it was not until relatively recently that surface geomorphology was understood well enough to conceptualize how relict and active features could, for example, serve as a proxy for beach sediment budget (Psuty, 2004; Psuty, 1988).

However, while landward-retreating barriers have generally obliterated most of the geologic record of their former dispositions, in some cases remnant barrier features have been preserved on modern continental shelf seabeds. Rampino and Sanders (1980; 1981; 1982; 1983) studying the shelf off Long Island, New York, wrote a succession of studies and responses to studies, detailing the finding of a well-preserved ‘drowned’ or ‘overstepped’ barrier complex that existed prior to 7 kya—believed to have been overcome by a rapid increase in sea-level rise. While they were not the first to identify overstepped barriers, they were the first to suggest that overstepping could involve a range of behaviors from complete barrier drowning to partial overstepping of the lower shoreface and back-barrier marsh/lagoon with simultaneous landward retreat. Specifically, Rampino and Sanders (1982) proposed that this could occur due to an out-of-equilibrium shoreface geometry and the failure of the barrier to immediately respond to a change in rate of sea level. At the time, this was a contentious argument, especially as Swift (1975) proposed that barriers generally retreated with steady-state geometry.

Many more overstepped barrier islands have been found since the 1980s, including several systems which have recently been correlated to late Pleistocene and early Holocene glacial meltwater pulses, following the advent of optically stimulated luminescence (OSL) dating (Mellet & Plater, 2018). Generally, most modern literature assumes drowned barriers are related

to rapid changes in sea level, or forcing from antecedent topography and changes in sediment supply (Cooper et al., 2016). However, results from a cross-shore morphodynamic model of barrier island evolution (Lorenzo-Trueba and Ashton, 2014) suggest an alternative: Even under constant forcing from sea-level rise and shelf topography, the internal dynamics of barrier islands can lead to novel autogenic retreat behaviors, including the production of relict barrier deposits. Uniquely, this model allows out-of-equilibrium shoreface geometries as a function of differentials between shoreface response and rate of overwash, potentially validating some of the concepts put forth by Rampino and Sanders (1982). More importantly, the model's ability to capture the production of relict deposits could allow a quantitative means to explore and extract the signatures of pre-historic barrier behavior from modern shelf seabeds.

In the first two chapters of this compendium, the model of Lorenzo-Trueba and Ashton (2014) is initially applied to identify the signatures of barrier autogenic deposition and compare with real-world field sites, determining if transgressive barriers could plausibly produce such deposits in nature. In the third chapter, this model is used to explore the interaction of autogenic deposition with changes in external 'allogenic' forcing, particularly rapid changes in rate of sea-level rise. Finally, in the fourth chapter, the focus of investigation shifts to the subaerial domain, using a novel cross-shore model of prograding barrier island dune ridge and swale morphology to derive time-varying beach sediment budgets. This last component expands on the conceptual work of Psuty (2004), who proposed that the size of dune ridges, as well as the frequency of new ridge creation, scales in proportion to beach sediment flux—concepts which have been backed by recent field observations (Bristow & Pucillo, 2006; Nooren et al., 2017; Oliver et al., 2018). Here, this work quantifies the magnitude of past changes in sediment budget based on the pattern

of relict dune ridge morphology preserved on modern prograded barriers, complementing the investigation of transgressive systems.

CHAPTER 1 - AN AUTOGENIC ORIGIN OF RELICT BARRIERS

The contents of this chapter appear in:

Ciarletta, D. J., Lorenzo-Trueba, J., & Ashton, A. D. (2019). Mechanism for retreating barriers to autogenically form periodic deposits on continental shelves. *Geology* 47(3), 239-242.

1.0 Summary

Drowned barrier deposits are common to passive margins around the world. In many cases, such deposits form horizontally discontinuous sequences, with several deposits spaced multiple kilometers apart. Previous research has shown these complexes can result from allogenic overstepping processes, in which barriers are wholly or partly drowned as a function of episodes of increased sea-level rise, or spatially discrete changes in the shelf slope/topography. However, using a simple morphodynamic model of a retreating barrier, it can be shown that regularly spaced deposits could arise during transgression from autogenic feedbacks between shoreface dynamics and landward overwash of barrier sediment. This mode of barrier retreat is described as periodic, internal dynamics driving cyclic alternations between episodes of barrier aggradation and rapid migration. The response creates regular patterns of low-relief cross-shore deposits with kilometer-scale spacing that increases for more gradual shelf slopes. Similar observations are made of deposits at real-world field sites, suggesting that autogenic abandonment of the lower shoreface offers an alternative to allogenic overstepping.

1.1 Introduction: An Unexplored Mechanism

Continental shelves around the world preserve deposits produced during barrier island transgression, including barrier sand/gravel and back-barrier mud. These deposits comprise either the partially or wholly drowned remnants of barrier islands that existed from the time of the last glacial maximum up to the present day (Mellet et al., 2018; Pretorius et al, 2016; Forbes et al., 1991). Typically, the emplacement of barrier remnants, a process described as ‘overstepping’ (Cooper et al., 2016), is ascribed to changes in allogenic forcing, including increases in rate of sea-level rise, fluctuations in sediment supply, or variations in antecedent topography (Rampino and Sanders, 1980; Mellet et al., 2012; De Falco et al., 2015). Because

remnant barrier deposits provide insight into the past response of transgressive shorelines to changes in environmental forcing, recent studies have examined these features to understand how modern barriers might adjust to historically undocumented conditions, including predicted increases in rate of sea-level rise (Donoghue, 2011; Cooper et al., 2016). Such studies are imperative to understand future socioeconomic risks, especially since centennial-scale processes driving transgressive barrier evolution are not well understood or commonly considered in modern coastal management (McNamara and Lazarus, 2018).

Until recently, it had been assumed that landward-migrating barrier islands retreat only under the influence of external forcing (Swift, 1975). In the last decade, however, it has become clear that sedimentary systems such as barriers may evolve, at least partly, under the influence of internal dynamics. Such internally-driven ‘autogenic’ processes can drive changes in the rate and mechanisms of sediment deposition (Hajek and Straub, 2017), and have been known to occur in the alongshore domain of barrier islands during the creation of sand spits (Ashton et al., 2016). Autogenic deposition is also a widely studied phenomenon in alluvial-deltaic systems (Li et al., 2016; Kim et al., 2014). In the context of this investigation, Lorenzo-Trueba and Ashton (2014) have shown in a cross-shore model that barrier islands can exhibit periodic behavior, in which the barrier alternates between landward migration and aggradation, occurring strictly as a function on internal dynamics (with no change in external forcing).

Using the model of Lorenzo-Trueba and Ashton (2014), this investigation seeks to demonstrate that the periodic cycle of aggradation and migration can cause a portion of the lower shoreface to become stranded on the seabed, leaving relict barrier sediments on the continental shelf (Figure 1.1; Table 1.1). This work subsequently explores the spacing and volume of such deposits using the model, investigating shelf slopes and rates of sea-level rise consistent with periodic retreat and comparing to observations of relict barrier deposits at real-world field locations. As a result of

this effort, it is hypothesized that internally driven periodic retreat could arise readily in nature, offering a plausible mechanism to emplace relict sediments at globally distributed sites.

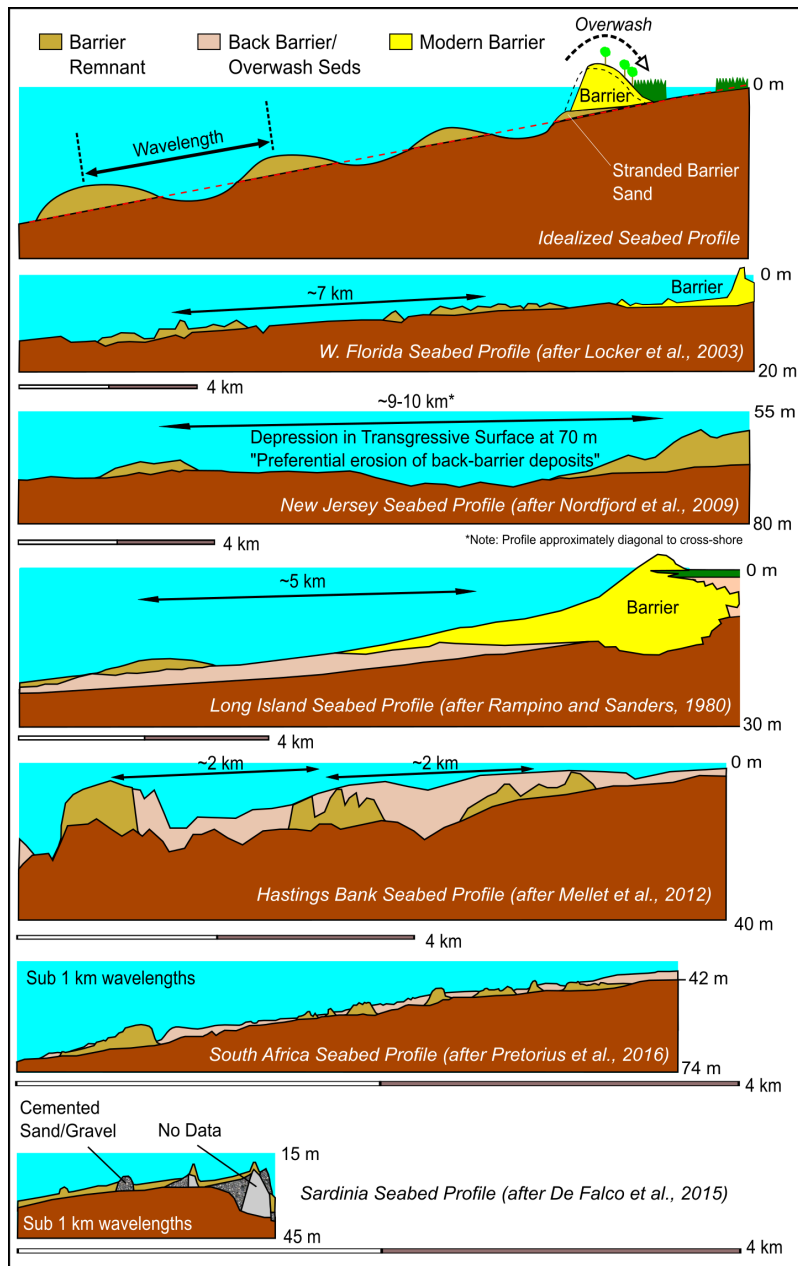


Figure 1.1 – Upper Panel: Idealized transgressive barrier sequence with alternating remnant sand bodies and ravinement surfaces. Lower Panels: Profiles through Sand Key, West Florida, after Locker et al. (2003); New Jersey outer continental shelf, seaward of the Mid-Shelf Wedge, after Nordfjord et al. (2009); Long Island off Cedar Beach, after Rampino and Sanders (1980); Hastings Bank (English Channel), after Mellet et al. (2012); KwaZulu-Natal shelf off Durban, South Africa, after Pretorius et al. (2016); Gulf of Orsitano, Sardinia, after De Falco et al. (2015). Numbers in meters are depth relative to mean sea level.

Table 1.1 – Field Sites

Location	Number of Oscillations	λ (km)	Estimated Volume (m ³ /m)	Shelf Slope (m/km)	Sea Level Rise Rate (mm/yr)	Timeframe
Long Island ¹	1	5	<1800–3000	2	≤5	7–8 kya
Sardinia ²	3	0.3	200–10000	5–7	10–15	7.5–9.5 kya
Florida ³	1–2	6–11	<3000–12000	1	~3	3–8 kya
Hastings ⁴	2	2	2700–18000	3	~0.3–3.6	8.3–9.5 kya
New Jersey ⁵	2	8–17	12000–72000	1	~14	11.4–12.8 kya
S. Africa ⁶	≥4	0.01–1	850–2975	≥5	~2.9	5.5–11.7 kya

[1] Rampino and Sanders (1980). [2] De Falco et al. (2015). [3] Locker et al. (2003). [4] Mellett et al. (2012). [5] Nordfjord et al. (2009). [6] Pretorius et al. (2016).

1.2 Background: Relict Deposits on Modern Margins

Continental margins around the world preserve evidence of cross-shore depositional features that are associated with barrier transgression (Figure 1.1; Table 1.1). In all existing literature, the production of these deposits is attributed to a form of overstepping, where a barrier is completely or partially drowned due to a change in the rate of sea-level rise, an increase in back-barrier accommodation (topographic forcing), a change in sediment supply, or a combination of allogenic agents (Cooper et al., 2016, DeFalco et al, 2015, Mellet et al., 2012). In terms of morphology, remnant barrier deposits are generally observed to have kilometer-scale spacing, with an amplitude or thickness of only a few meters (Mellet et al., 2018). The upper portions of these deposits are likely to be reworked into subaqueous sand waves/dunes (Locker et al., 2003), and are observed to sometimes occur in a series, as they are seen on the South Florida shelf (Locker et al., 1996). At the South Florida site, Locker et al. (1996) epitomizes the paradigm of allogenic overstepping, hypothesizing that closely spaced remnant shoreline features originated from variations in sea-level rise during glacial meltwater pulse events in the late Pleistocene and early Holocene.

In terms of geologic framework factors controlling the morphology of deposits, Cattaneo and Steel (2003) posit that shelf slope plays a key role, with deposits potentially becoming more

widely spaced along more subdued shelf gradients—for every vertical unit of sea-level rise, the corresponding distance covered by shoreline migration grows greater for decreasing slopes. Locker et al. (2003) additionally observed that the maximum thicknesses of deposits spaced along the West Florida shelf corresponded with increasing shelf gradient.

1.3 Methods

This exploration utilizes the morphodynamic model of barrier evolution described by Lorenzo-Trueba and Ashton (2014)—‘LTA model’. It is constructed as a reduced complexity framework, focusing on the interplay of sea-level rise, shoreface dynamics, and overwash. The barrier is represented two-dimensionally in the cross-shore and is defined by three moving boundaries, which include a shoreface toe, an ocean shoreline, and back-barrier shoreline. During sea-level rise, the barrier shorelines are translated landward by overwash, while shoreface dynamics adjust the position of the ocean shoreline and shoreface toe towards a steady-state configuration. The position of the shoreface toe is further constrained in the vertical direction by a ‘depth of closure’—this represents the depth at which sediment exchange between the barrier shoreface and the shelf becomes insignificant (Ortiz and Ashton, 2016).

The LTA model expresses periodic retreat as a cyclical alternation between episodes of aggradation and landward migration, producing regularly spaced deposits on the seabed (a form of partial overstepping). It also produces several other behaviors, including complete barrier drowning and rollover. In rollover, shoreface dynamics and overwash are balanced, and the barrier maintains a fixed geometry, migrating at the rate of sea-level rise over the slope of the shelf. Drowning occurs when the barrier’s height or width is reduced to zero. While drowning would produce remnant deposits through complete overstepping, this project focuses on deposits that appear to be only partly overstepped, being low relief and evenly spaced (periodic).

The periodic response occurs in the model from a temporal lag between overwash and shoreface dynamics, which causes the barrier to oscillate around a state of dynamic equilibrium, where the barrier would retreat in a manner consistent with rollover. Figure 1.2 describes the periodic cycle, starting with a phase of migration. Initially, fluxes of sediment to the shoreface cannot keep up with overwash, and the barrier thins as the shorelines retreat at a faster rate than the shoreface toe (Figure 1.2A). Eventually, fluxes of sediment from the lower shoreface to the barrier increase as the toe begins to excavate the shelf and the shoreface flattens. At the same time, as the barrier starts to move into shallower water, it begins to slow and widen as a function of decreasing back-barrier accommodation to overwash (Figure 1.2B). The barrier finally grows wide enough that overwash no longer reaches the back-barrier, and as a result, starts to aggrade (Figure 1.2C). The shoreface does not immediately respond during the cessation of overwash, and further widening occurs. Afterwards, the barrier shoreline slowly erodes and steepens the shoreface—this process, which occurs in the aggradational phase, accounts for the majority of time in the periodic cycle (Figure 1.2D). Ultimately, increasing sea level and continued shoreline erosion narrows the barrier so that overwash can reach the back-barrier, restarting the periodic cycle. Immediately following aggradation, a portion of the barrier below the elevation of the shoreface toe becomes stranded on the shelf as an isolated body, similar to the remnant deposits observed in natural systems (Figure 1.1). Worth noting is that the mass of the barrier in the LTA model is conserved during periodic retreat, such that the cross sectional volume of deposition is compensated by corresponding erosion of the seabed during migration, reflecting the oscillation around dynamic equilibrium.

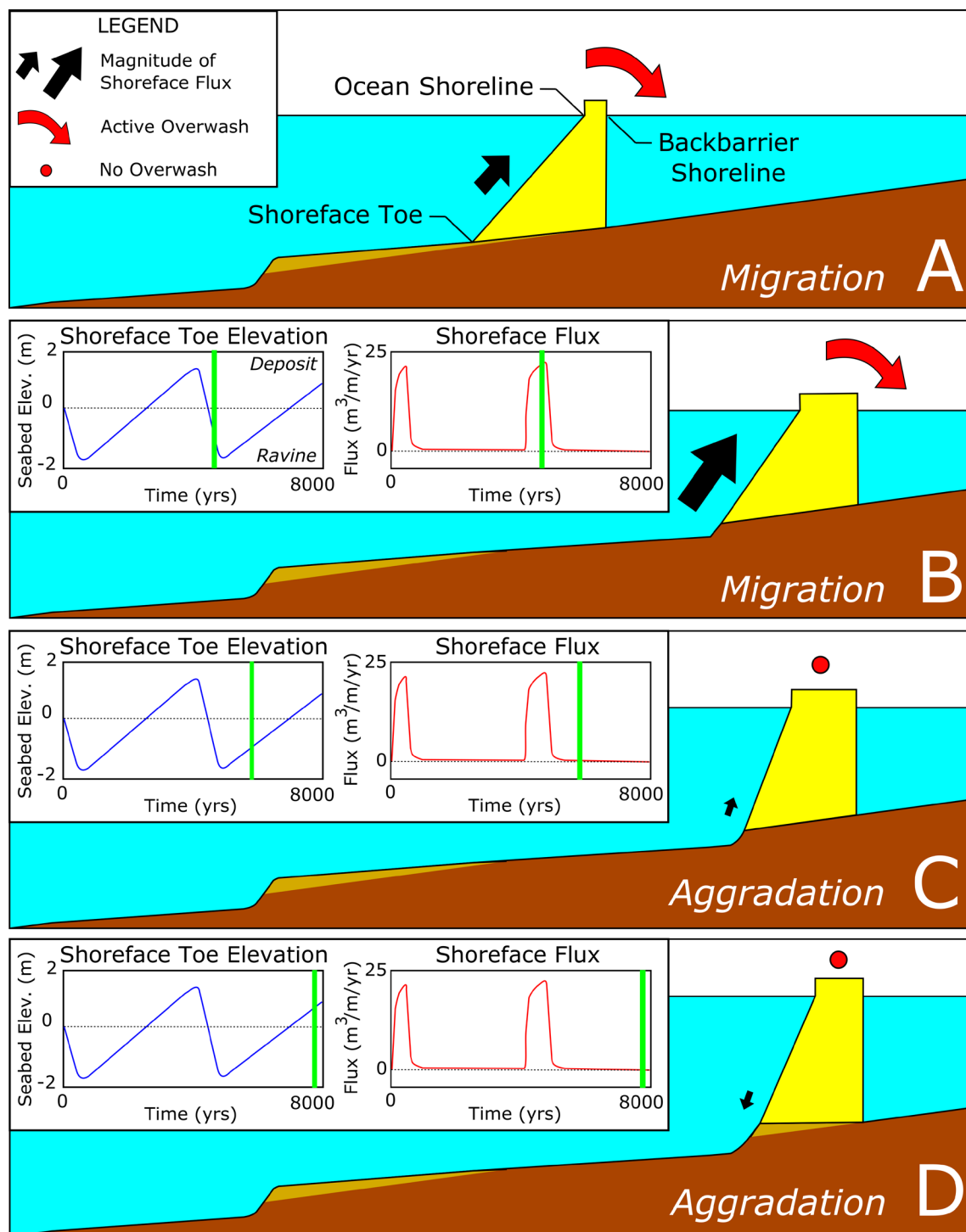


Figure 1.2 – Model output depicting cycle of periodic retreat. A remnant deposit (tan) is left on the seabed as the barrier (yellow) migrates (A, B) following a previous aggradational episode, culminating in erosion of the shelf and a return to aggradation (C, D). The size of the black arrow indicates the magnitude of fluxes at the shoreface. The red arrow indicates active migration through overwash, while the red circle indicates aggradation (no overwash). Green lines in subplots indicate time during production of corresponding cross-section. Seabed elevation is anomaly in seafloor topography relative to initial (linearly sloping) seabed.

1.4 Results

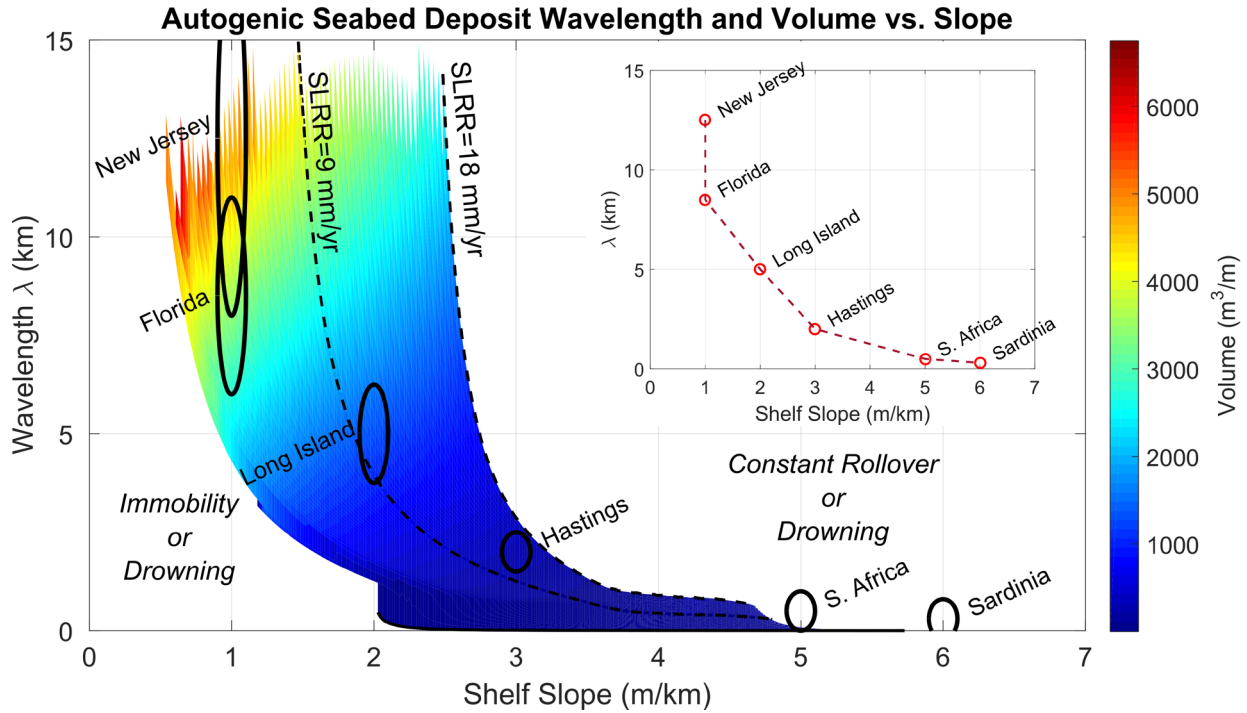


Figure 1.3 – Modeled remnant seabed deposit wavelength (spacing) and volume produced by a barrier undergoing periodic retreat overlain with field site interpretations. Results are shown for constant sea-level rise rates (SLRR) from 0.01 to 18 mm/yr and a run time of 20 kyrs (see Table 1.2 for input parameters; see Appendix Figures A1.1-A1.11 for additional input sensitivity analysis).

Table 1.2 – Model Input Parameters

Parameter	Symbol	Inputs (Fig 2)	Inputs (Fig 3)
Slope (m/km)	β	1,2,3	*0-6
Shoreface Toe Depth (m)	D_t	15	15
Equilibrium Width (m)	W_e	800	800
Equilibrium Height (m)	H_e	2	2
Eq. Shoreface Slope	a_e	0.02	0.02
Max Overwash ($m^3/m/yr$)	$Q_{OW,max}$	100	100
Max Deficit Volume ($m^3/m/yr$)	$V_{d,max}$	$0.5 \cdot H_e \cdot W_e$	$0.5 \cdot H_e \cdot W_e$
Shoreface Response ($m^3/m/yr$)	K	2000	2000
Sea-Level Rise Rate (mm/yr)	\dot{z}	2	*0.01-18

*Denotes a range of tested values.

The modeled wavelengths of remnant deposits produced by periodic retreat are inversely related to shelf slope, decreasing from a maximum of ~ 15 km at 1–3 m/km shelf slopes to approaching the sub-kilometer scale at shelf slopes greater than 6 m/km (Figure 3). This inverse trend is also apparent for field sites, with measured wavelengths decaying rapidly with increasing

slope. Although the number of field sites is small, and in some cases only a few oscillations can be measured, the general agreement with the model trend strongly suggests periodic deposition follows the paradigm of deposit spacing described by Cattaneo and Steel (2003) and observed by Locker et al. (2003).

Similar to the inverse relationship between wavelength and slope, the greatest cross sectional volumes of remnant deposits occur on shelf slopes of 1–3 m/km and quickly decrease at slopes of 5+ m/km, suggesting that shallow to moderately sloping shelves provide the ideal conditions for producing periodic deposits (Figure 3). Significant volumes are modeled at rates of sea-level rise up to 18 mm/yr for slopes approaching 3 m/km. Beyond this rate, and at higher slopes, constant rollover and drowning dominates the barrier behavioral response, resulting in negligible deposition, or conversely, complete overstepping.

1.5 Discussion: Model Implications for Real-World Comparison

Although a simple morphological model is employed, it captures patterns of deposition found on shelf seabeds around the world. In particular, modeled deposit wavelengths and volumes compare similarly with the dimensions of seabed features apparent at gently sloping shelf sites, including Long Island, Florida, and New Jersey (Table 1). This apparent match between model results and field observations suggests internally driven periodicity plausibly explains the behavior of a variety of transgressional barriers throughout the Holocene.

However, while the wavelengths observed in nature for steeper shelves compare favorably with the model, deposit volume is inconsistent, particularly for South Africa and Sardinia. Observations for deposits on slopes in excess of 4 m/km are up to two orders of magnitude larger than predicted by the model, which constrains volumes to $\sim 500 \text{ m}^3/\text{m}$ or less.

The most likely explanation is that volume accumulation is subject to additional processes that are not accounted for in the current framework, including variable sedimentology.

This investigation does not explore all the conditions where periodicity is possible, but as autogenic influence is demonstrable with up to 18 mm/yr of sea-level rise, it is plausible that internal dynamics are a key driver of barrier evolution in nature. Consequently, periodic retreat behavior likely poses a previously unknown risk for modern barriers. As the aggradational phase accounts for the longest portion of the periodic retreat cycle, barriers thought to be stable could undergo abrupt changes in behavioral state, reverting to rapid migration. In systems with minimal human intervention, this could lead to rapid destruction of back-barrier marshes, which provide protection to coastal infrastructure and coincident natural systems (Gedan et al., 2011). Back-barrier marshes also store significant quantities of sequestered carbon, which retreating barriers may release back into the environment, further contributing to the disruption of the global carbon cycle (Pendleton et al., 2012; Theuerkauf and Rodriguez, 2017).

Fundamentally, the results demonstrate a novel retreat behavior that offers a non-exclusive alternative to current interpretation of relict barrier deposits. While some repetitive deposits can probably be accounted for by modulation of allogenic forcing (e.g., Locker et al., 1996), this study demonstrates that periodicity can arise readily from internal barrier dynamics alone. Future work with this model framework could also incorporate variable stratigraphy and back-barrier processes to explore the structure and variety of deposits that can be generated by internal dynamics. For example, Forbes et al. (1991) describe a gravel barrier in Atlantic Canada in which the lower and upper portions of the barrier superstructure became separated, partly due to rapid sea-level rise and a reduction in sediment supply. The upper portion of the barrier, owing to its reduced volume, migrated rapidly landward across a sand/mud back-barrier platform, while

the lower portion remained stranded offshore. In the context of periodic deposition, a comparable outcome could hypothetically occur during the transition from aggradation to migration, conceivably producing a deposit similar to Long Island, where back-barrier sediments are extensively preserved in the landward direction (Rampino and Sanders, 1980).

1.6 Conclusions

Modeling remnant deposits produced by internally driven periodic retreat, this investigation demonstrates an inverse relationship between shelf gradient and deposit spacing, which is also observed at field sites. Additionally, the volumes of individual deposits at field sites with shelf slopes of 1–3 m/km compare reasonably with those produced by the model, implying that autogenic periodicity occurring under constant external forcing plausibly explains the behavior of some Holocene barriers. Projecting into the future, this suggests the long-term retreat of modern barriers may deviate significantly from current conceptual models, posing unknown risks.

CHAPTER 2 - QUASI-PERIODIC BARRIER OVERSTEPPING

The contents of this chapter appear in:

Ciarletta, D. J., Lorenzo-Trueba, J., & Ashton, A. D. (2019). Quasi-Periodic Barrier Overstepping. In *The Proceedings of the Coastal Sediments 2019*, World Scientific Pub Co Inc., San Diego, USA.

2.0 Summary

Drowned barrier deposits exist on passive margins around the world, their origins usually ascribed to allogenic forcing from antecedent topography and changes in the rate of sea-level rise. Here, a cross-shore morphodynamic model is used to explore a novel transgressive barrier behavior, ‘deflation drowning’, which occurs during a transition to autogenic periodic retreat. The investigation demonstrates that autogenic sequences of increasingly amplified quasi-periodic relict barrier deposits can occur in conjunction with deflation drowning during an incomplete changeover to periodicity. Results suggest this behavior may arise most readily for large, voluminous barriers.

2.1 Introduction: Incomplete Periodicity

Drowned barrier remnants are found on continental shelves around the world, interpreted to reflect changes in paleocoastal environments throughout the Holocene (Mellet et al., 2018). These remnant deposits are thought to form through an ‘overstepping’ process, whereby a barrier is partly or wholly drowned by a rapid sea-level increase (Cooper et al., 2016), possibly in conjunction with changes in sediment supply or antecedent topography (De Falco et al., 2015; Mellet et al., 2018). Until recently, it was believed that drowned barriers only resulted from changes in allogenic forcing (e.g. episodic rapid sea-level rise). However, morphodynamic modeling of long-term barrier evolution under constant allogenic forcing produces a mode of internally driven, autogenic retreat, characterized by cycles of alternating migration and aggradation (Lorenzo-Trueba and Ashton, 2014). This intermittent, self-organized process can create periodic remnant deposits on the shelf seabed, which appear similar to many deposits observed in nature (Locker et al., 2003; Nordfjord et al., 2009; Pretorius et al., 2016).

Here, it is shown that autogenic periodicity can sometimes be incomplete at relatively high rates of overwash, resulting in a mode of ‘deflation drowning’ and complete overstepping. This process represents another form of width drowning—where the barrier thins until collapse (Lorenzo-Trueba and Ashton, 2014)—which occurs specifically due to an excessive loss of overwash-driven sediments to back-barrier accommodation following an aggradational episode.

It is later shown that for large barriers there is a behaviorally significant transition to consistent periodicity that can span multiple aggradation-migration cycles, sometimes producing quasi-periodic deposits for input parameters where sustained periodicity should not occur. In these cases, deflation drowning can arise on the third or fourth cycle (following initialization), creating a limited pattern of increasingly amplified quasi-periodic relict deposits. These results suggest that internal dynamics could plausibly support a mechanism to produce sequences of outsized periodic-like remnant barriers on transgressive margins that are not representative of the long-term barrier trajectory.

2.2 Background & Methods

This exploration uses the morphodynamic model presented by Lorenzo-Trueba and Ashton (2014), which considers the interplay between sea-level rise, shoreface dynamics, and overwash for transgressive barriers. Functionally, driven by sea-level rise, overwash in this framework moves the beach and back-barrier shorelines landward with time while the shoreface geometry dynamically corrects towards a steady-state shape. During periodic retreat, the barrier oscillates around a dynamic equilibrium profile as landward directed fluxes from the shoreface lag behind overwash-driven fluxes. Episodically, as the barrier migrates landward into shallower water, the decrease in back-barrier accommodation causes the barrier to widen until overwash-driven retreat ceases. This produces aggradation under continued sea-level rise, and the barrier

shoreface steepens as a consequence. Eventually, sea-level rise causes the direction of shoreface fluxes to reverse (moving offshore), narrowing the barrier until overwash becomes active again—creating a self-sustaining cycle of migration and aggradation (Figure 2.1).

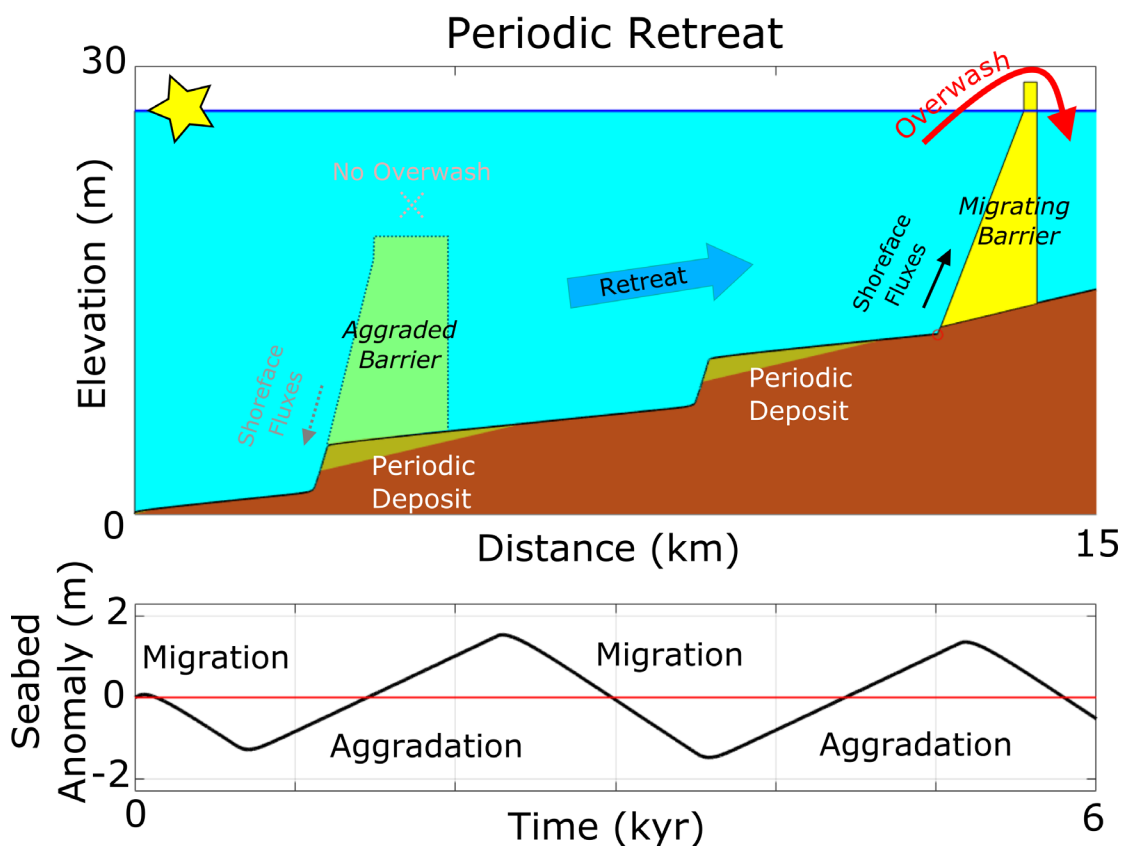


Figure 2.1 – Cross section of barrier undergoing periodic retreat at 6 kyr. Subplot tracks seabed anomaly with time, depicting deposition (aggradation) and ravinement (migration). Star corresponds to Figure 2.3

Deflation drowning follows a similar behavioral pattern, with a lag between shoreface dynamics and overwash, but the cycle never goes to completion (Figure 2.2). In other the words, during deflation drowning the barrier begins to oscillate around a dynamic equilibrium (as would occur in true periodic retreat), but undergoes width drowning before this is achieved due to an unsustainable lag in shoreface response to overwash. This similarity to the periodic response begins to explain why deflation drowning and periodicity occupy a similar region of regime space defined by rate of overwash and sea-level rise (Figure 2.3). Indeed, closer analysis of periodic barrier behavior shows that a form of non-drowning deflation occurs during a transition

to dynamic equilibrium, where a barrier undergoes several periodic-like cycles before settling in to a mode of consistent periodicity (Figure 2.4).

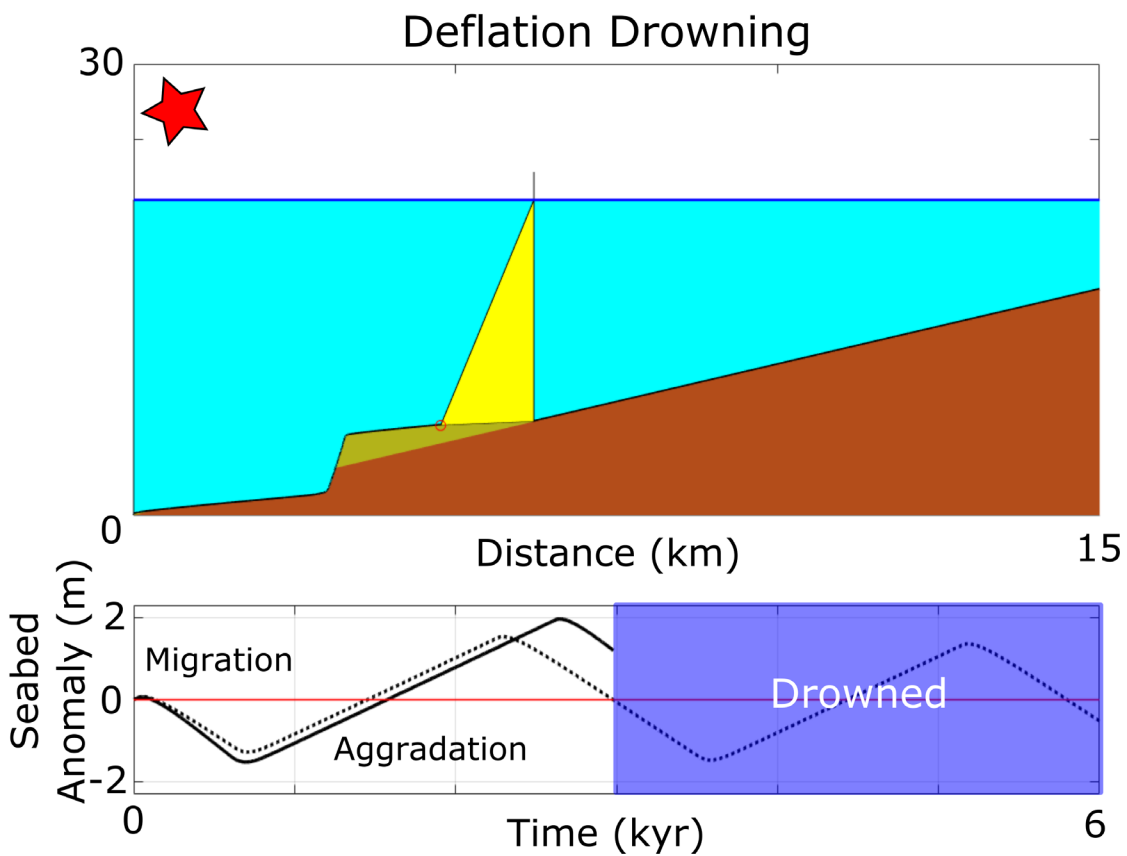


Figure 2.2 – Cross section of barrier undergoing deflation drowning at 3 kyrs post-initialization. Subplots track seabed anomaly with time, depicting deposition (aggradation) and ravinement (migration). Star corresponds to Figure 2.3.

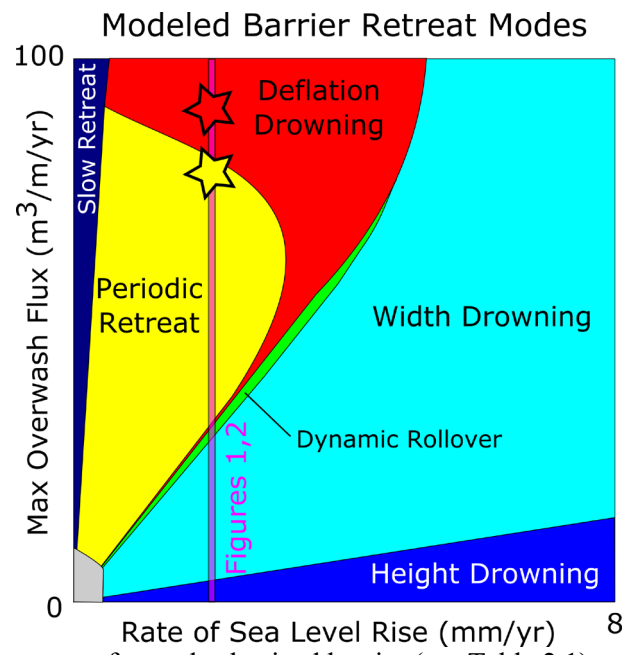


Figure 2.3 – Behavioral response of a modestly sized barrier (see Table 2.1) to combinations of maximum rate of overwash and rate of sea-level rise. Starred points correspond with Figures 2.1 and 2.2.

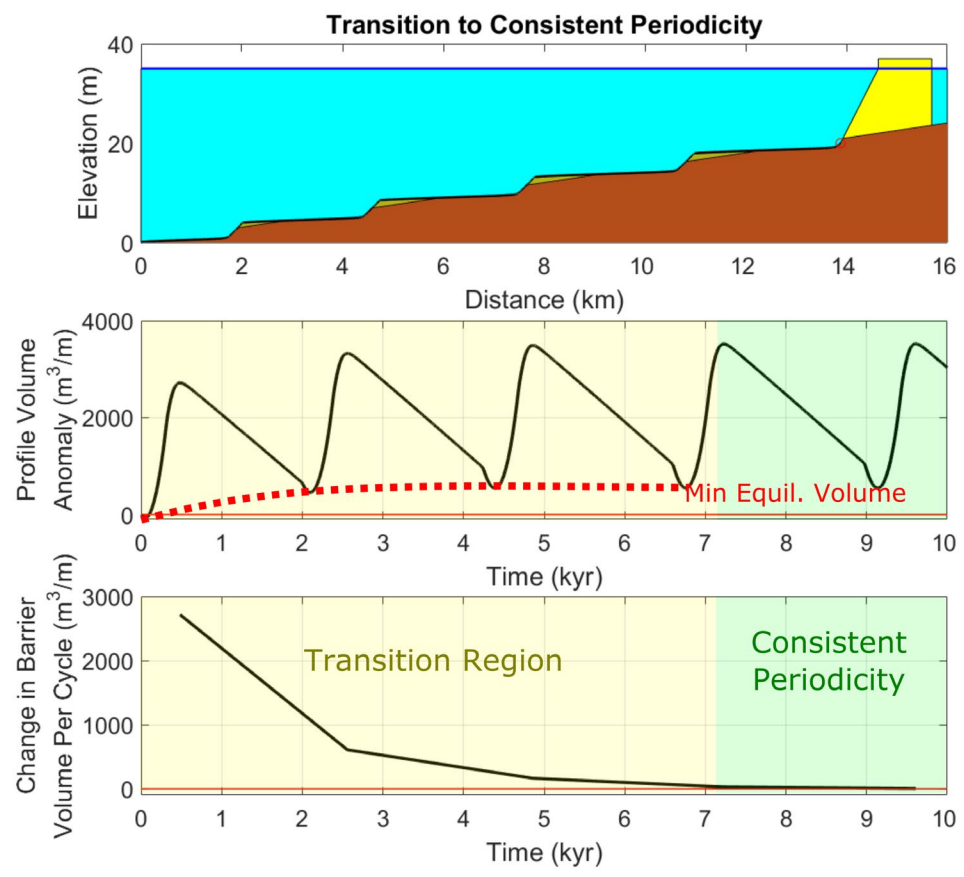


Figure 2.4 – Temporary increase in the volume of the barrier with each migration-aggradation cycle during transition to consistent periodicity. Here, change in volume per cycle stops after 7 kyrs.

Next, the production of sequences of quasi-periodic deposits created in the lead-up to deflation drowning is explored. Inspired by real-world field sites (Green et al., 2018), a large barrier with correspondingly large overwash flux is modeled against a modestly sized barrier (Table 2.1), showing that the transition period asserts a more dominant role in the behavior of voluminous barriers. It is subsequently quantified how adjusting the rate of overwash affects the time to deflation drowning for a large barrier, identifying the timescales under which limited sequences of quasi-periodic retreat can occur without fully transitioning to periodic retreat.

Table 2.1 – Model Barrier Parameters

Parameter	Symbol	Modest-sized Barrier (Figs. 2.1-2.5)	Large Barrier (Figs. 2.5-2.9)
Back-barrier Slope (m/km)	β	1-2	2
Shoreface Toe Depth (m)	D_t	15	22.5
Equilibrium Width (m)	W_e	800	1200
Equilibrium Height (m)	H_e	2	6
Eq. Shoreface Slope	α_e	0.02	0.05
Max Overwash (m ³ /m/yr)	$Q_{OW,max}$	1-900	1-900
Max Deficit Volume (m ³ /m/yr)	$V_{d,max}$	$0.5 \cdot H_e \cdot W_e$	$0.5 \cdot H_e \cdot W_e$
Shoreface Response (m ³ /m/yr)	K	2000	2000
Sea-Level Rise Rate (mm/yr)	\dot{z}	1-4	4

2.3 Results

An initial comparison is made of the time to drowning for a modestly sized barrier to a large barrier (Figure 2.5; see Table 2.1 in Background & Methods for inputs). Results show the deflation drowning region is much larger, and the response can last approximately twice as long, for a large barrier than for a modestly-sized barrier (Figure 2.6).

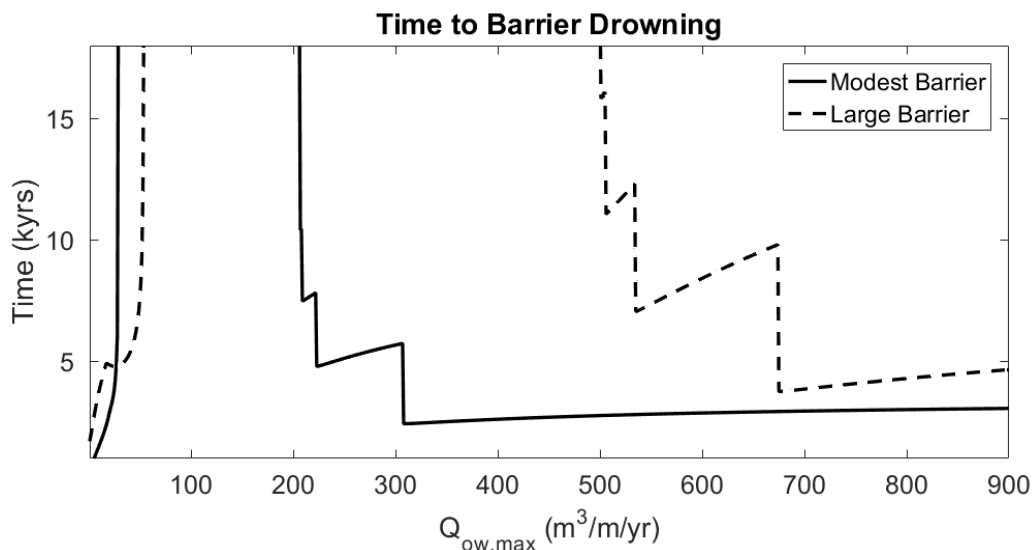


Figure 2.5 – Time to drowning for modestly sized barrier (solid black line) vs. large barrier (dashed black line) at 4 mm/yr sea-level rise and 2 m/km shelf slope. See Table 2.1 for additional inputs. $Q_{OW,max}$ = Maximum overwash rate.

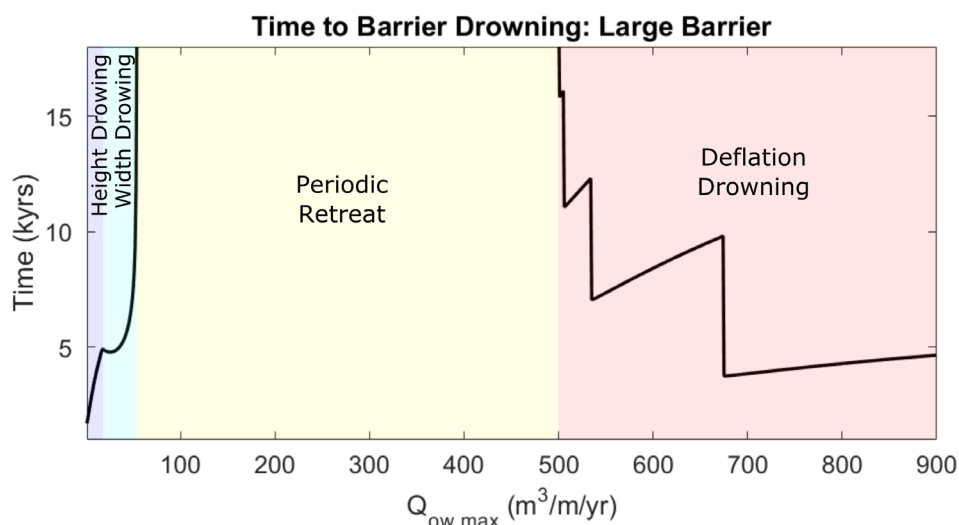


Figure 2.6 – Annotated time to drowning plot for a large barrier. Note that deflation drowning occurs between 4 and 16.5 kyrs, demonstrating an extended time in periodic transition.

The larger barrier remains in the transition to periodicity for timescales comparable to the length of the Late Holocene, allowing it to undergo multiple periodic-like cycles before drowning. These cycles produce a sequence of increasingly amplified quasi-periodic deposits on the shelf seabed (Figure 2.7).

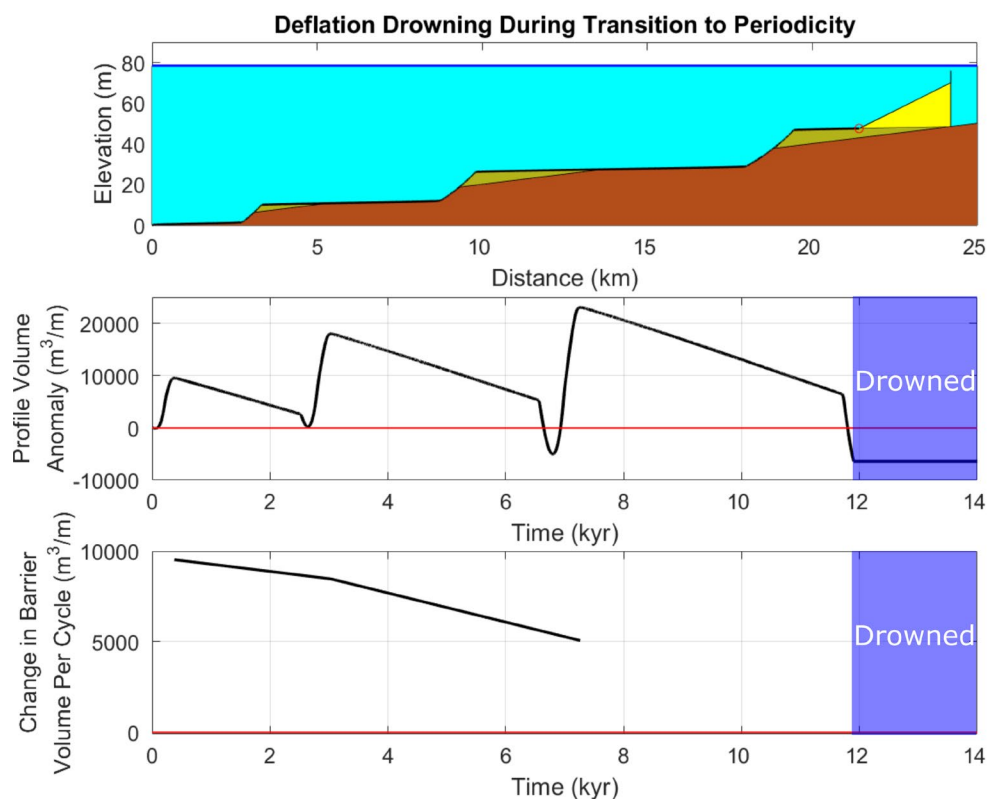


Figure 2.7 – Large barrier undergoing deflation drowning, producing two quasi-periodic deposits on the seabed during an incomplete transition to consistent periodicity. Max overwash rate = $525 \text{ m}^3/\text{m}/\text{yr}$.

Examining the range of overwash values consistent with deflation drowning, it is also shown that the number of quasi-periodic deposits increases for values closer to those giving rise to periodic retreat (Figure 2.8). Moreover, the time to drowning is strongly modulated by the number of periodic-like cycles—time to drowning steps up at a slightly decreasing interval for every additional migration-aggradation cycle completed at a decreasing rate of overwash (Figure 2.9).

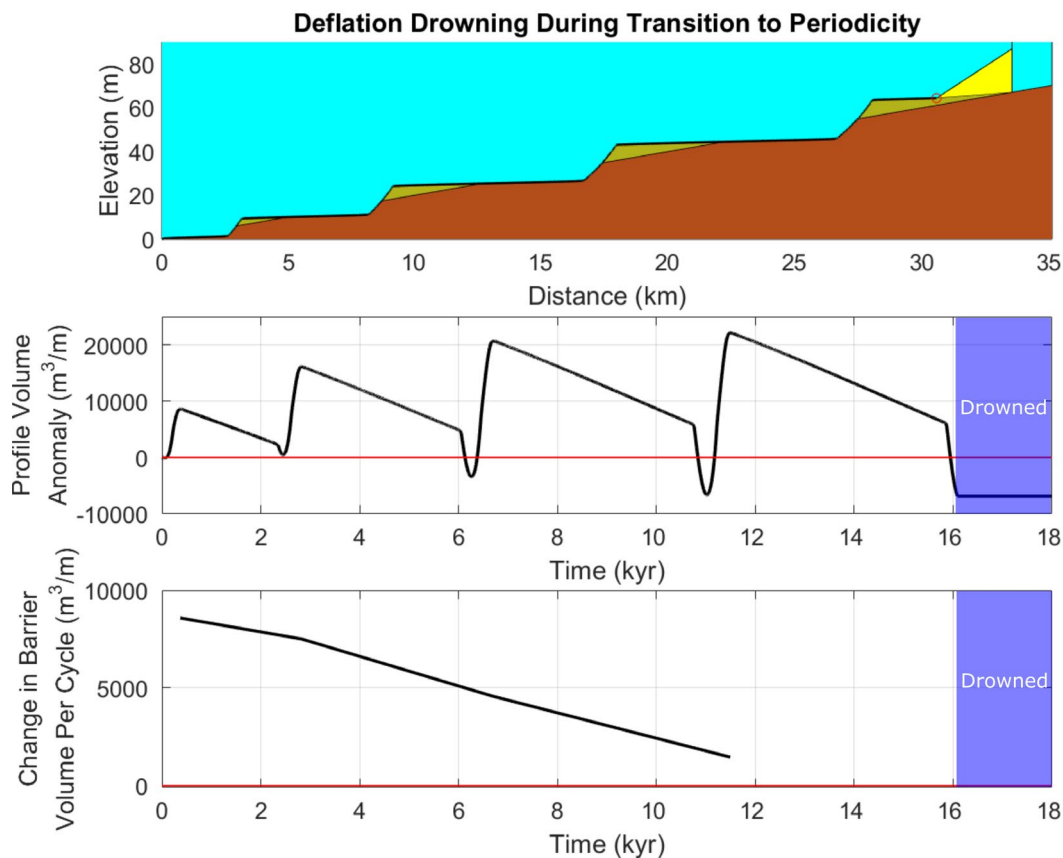


Figure 2.8 – Three quasi-periodic deposits produced on the seabed prior to deflation drowning. Max overwash rate = $505 \text{ m}^3/\text{m}/\text{yr}$.

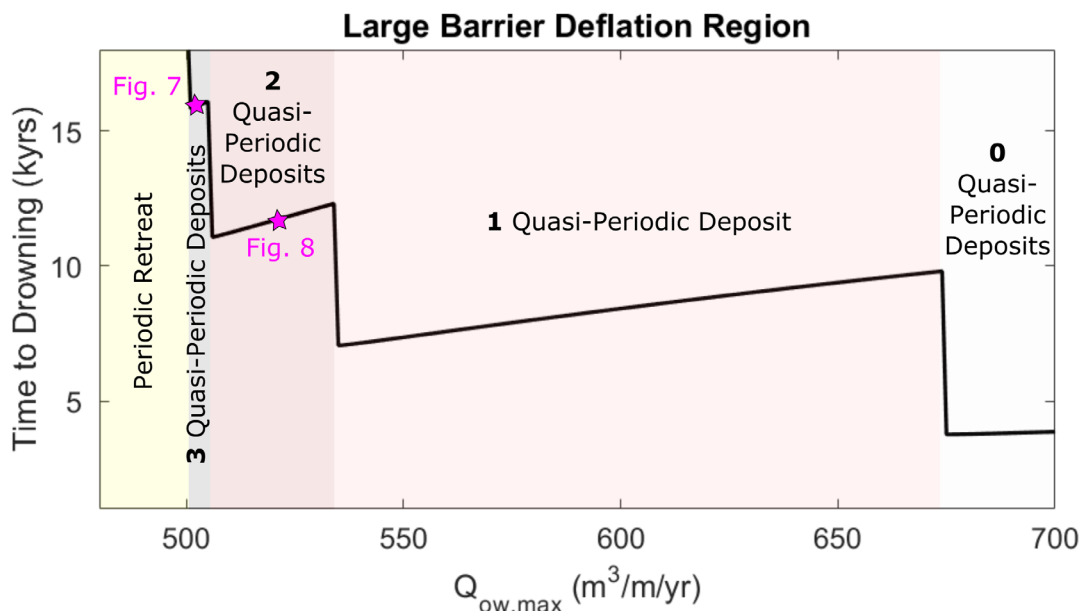


Figure 2.9 – Detail of deflation region for a large barrier. The number of quasi-periodic deposits increases as the rate of overwash moves closer to values that can sustain consistent periodicity.

2.5 Conclusions

The results of this modeling investigation demonstrate a novel mode of transgressive barrier behavior, ‘deflation drowning’, which occurs during a failed transition to periodic retreat. Also shown are sequences of quasi-periodic deposits that can be produced autogenically as a barrier undergoes deflation, demonstrating a heretofore unexplored mechanism of relict barrier emplacement that is especially relevant for large barriers. It is suggested that quasi-periodic deposition could plausibly explain some relict barrier deposits that occur in nature.

**CHAPTER 3 - SEA-LEVEL DRIVEN AUTOGENIC-ALLOGENIC INTERACTION
DURING PERIODIC BARRIER RETREAT**

The contents of this chapter are pending submission to *Frontiers in Earth Science: Sedimentology, Stratigraphy, and Diagenesis*

3.0 Summary

Barrier deposits preserved on continental shelf seabeds provide a record of the paleocoastal environment from the last glacial maximum through the Holocene. The formation of such deposits is often attributed to rapid increases in rate of sea-level rise, especially glacial meltwater pulses, which can lead to partial or complete drowning—overstepping—of migrating barrier islands. However, recent cross-shore modeling and field evidence suggests the internal dynamics of migrating barriers could plausibly drive periodic retreat accompanied by autogenic partial overstepping and deposition of barrier sediment under constant sea-level rise and shelf slope. Here, it is hypothesized that the interaction of periodic retreat with changes in external (allogenic) forcing from sea-level rise may create novel retreat responses, with the potential to be recorded by relict barrier deposits. Barriers are modeled through a range of autogenic-allogenic interactions, exploring the effect of changes in autogenic period with changes in the magnitude of a discrete, centennial-scale pulse in rate of sea-level rise. Results show that, as the autogenic period decreases from millennial- to centennial-scale, deposition of relict barrier sands is increasingly dominated by allogenic forcing imparted by sea-level rise. Paradoxically, decreasing autogenic influence allows barriers to withstand greater magnitudes of sea-level pulses, creating more partial overstepping rather than complete barrier drowning. Additionally, results show that the transition from dominantly autogenic deposition to dominantly allogenic deposition results in complex signal mixing, where deposition of barrier sands is amplified or suppressed.

3.1 Introduction: Autogenic-Allogenic Interaction

Numerous studies indicate transgressive barrier islands are a significant driver of shelf bathymetry and stratigraphy, with remnant barrier deposits common on sandy margins throughout the world (Rampino and Sanders, 1980; Mellet et al., 2012; De Falco et al., 2015).

Deposits are typically considered to be attributable to changes in allogenic forcing, such as changes in the rate of sea-level rise, alteration of sediment supply, or variation in antecedent topography (Cattaneo and Steel, 2003; Storms et al., 2008; Mellet et al., 2012). Because these drowned or ‘overstepped’ barrier features are associated with variations in environmental forcing, recent studies have investigated them to gain insights into how modern barriers might respond to future changes, for example, an increase in rate of sea-level rise (Donoghue, 2011; Cooper et al., 2016). Such studies are imperative to understand future socioeconomic risks, especially since centennial scale processes driving transgressive barrier evolution are not well understood or commonly considered in modern management (McNamara and Lazarus, 2018).

Recently, morphodynamic modeling of barriers by Lorenzo-Trueba and Ashton (2014) and modeling with field comparison (Chapter 1) have implicated internally driven periodic retreat as a plausible driver of remnant barrier deposition. The identification of autogenic processes within cross-shore transgressive continental shelf environments adds to a growing number of sedimentary systems in which internal, autogenic processes are thought to influence deposition and erosion. In the coastal domain, such systems include deltas (Li et al., 2016; Kim et al., 2014), sand spits (Ashton et al., 2016), and storm-influenced beaches (Lazarus et al., 2019).

Among the most intriguing investigations related to internal dynamics in sedimentary systems involve the interaction of autogenic processes with allogenic forcing. Specifically, interpreting environmental signals from the sedimentary record—assigning the driver, timescale, and magnitude of past allogenic forcing—is complicated by internal, nonlinear processes affecting deposition and erosion (Foreman and Straub, 2017). In alluvial systems, for example, channel avulsion and splaying result in spatiotemporally variable deposition that can be

controlled both by internal dynamics and forcing from the environment (Foreman and Straub, 2017). For example, Stouthamer and Berendsen (2007) showed that avulsion frequency in the Rhine-Meuse delta was subject to a 500-600 yr cycle that appeared to be autogenic in origin—at the same time, a longer-term trend in interavulsion period likely fluctuated in response to climate change and human disturbance.

Examining the timescales of autogenic-allogenic interaction using a numerical model, Jerolmack and Paola (2010) demonstrated that environmental (allogenic) signals tend to be preserved in the sedimentary record when they have temporal periods that are longer than the period of autogenic fluctuations—allogenically driven variations in deposition are likely to be destroyed if they fall within the timescales of autogenic processes. However, Jerolmack and Paola (2010) also suggest that allogenic signals with periods shorter than the timescales of autogenic processes can be preserved if their magnitudes are large enough to override any autogenic influence. Li et al. (2016), partly exploring this latter case, showed that for deltas this magnitude directly relates to a storage threshold, based on the spatial extent of the system. Climate signals are attenuated or masked by autogenic processes as the size of the delta system increases in proportion to the depositional potential of allogenic forcing (Li et al., 2016).

The objective of this investigation is to determine if autogenic-allogenic interactions in transgressive barrier island systems follow the paradigms of Jerolmack and Paola (2010), and whether deposits produced by such interaction could be quantified to gain insight into state of the barrier and the magnitude of allogenic forcing. Specifically, a periodically retreating barrier is subjected to a centennial-scale rapid increase in rate of sea-level rise, simulating a glacial meltwater/outburst flood ‘pulse’ of variable magnitude. This investigation subsequently

discusses the implications of interpreting deposits produced by the model as they might appear in nature, as well as the impact of enhanced sea-level rise on modern barriers.

3.2 Background: Periodicity and Sea-Level Pulses

3.2.1 Morphodynamic Model

The exploration herein is primarily constructed as an extension of the work in Chapter 1, which uses the cross-shore morphodynamic model of barrier retreat after Lorenzo-Trueba and Ashton (2014)—the ‘LTA’ model. Within the LTA model, barrier retreat is governed by the interplay of sea-level rise, shoreface dynamics, and overwash, with cross-shore barrier geometry defined by the three moving boundaries: a shoreface toe, ocean shoreline, and backbarrier shoreline (Figure 3.1). As sea level rises, the barrier shorelines are moved landward by storm-driven overwash, while shoreface dynamics—encapsulated by a shoreface response rate K —adjust the configuration of the shoreface toe and ocean shoreline towards a steady-state geometry. The shoreface toe is additionally constrained by a ‘depth of closure’, or a depth at which sediment exchange between the seabed and the shoreface is negligible (Ortiz and Ashton, 2016).

Periodic retreat is expressed within the LTA model as a cyclical alternation between phases of landward migration and aggradation, which creates a regular pattern of ravinement and deposition on the shelf seabed. Deposits produced through this process have volume that increases with more gradual shelf slope, and can be several meters in thickness. The LTA model also produces dynamic rollover (the barrier migrating at the rate of sea-level rise over the slope of the shelf) and drowning, the latter occurring through complete loss of barrier width or barrier height.

During periodic retreat, landward-directed shoreface fluxes lag behind overwash fluxes, causing the barrier to oscillate around a dynamic equilibrium profile. As the barrier migrates landward into shallower water, decreasing back-barrier accommodation space results in widening of the barrier until overwash fluxes fail to reach back-barrier shoreline. Under rising sea level this results in aggradation and steepening of the shoreface, with the direction of shoreface fluxes beginning to reverse ('Aggraded Barrier', Figure 3.1). This causes the barrier to narrow until overwash can again reach the back-barrier shoreline, reinitiating migration ('Migrating Barrier', Figure 3.1) and gradually increasing the rate of landward-directed shoreface fluxes, creating a self-reinforced cycle of migration and aggradation.

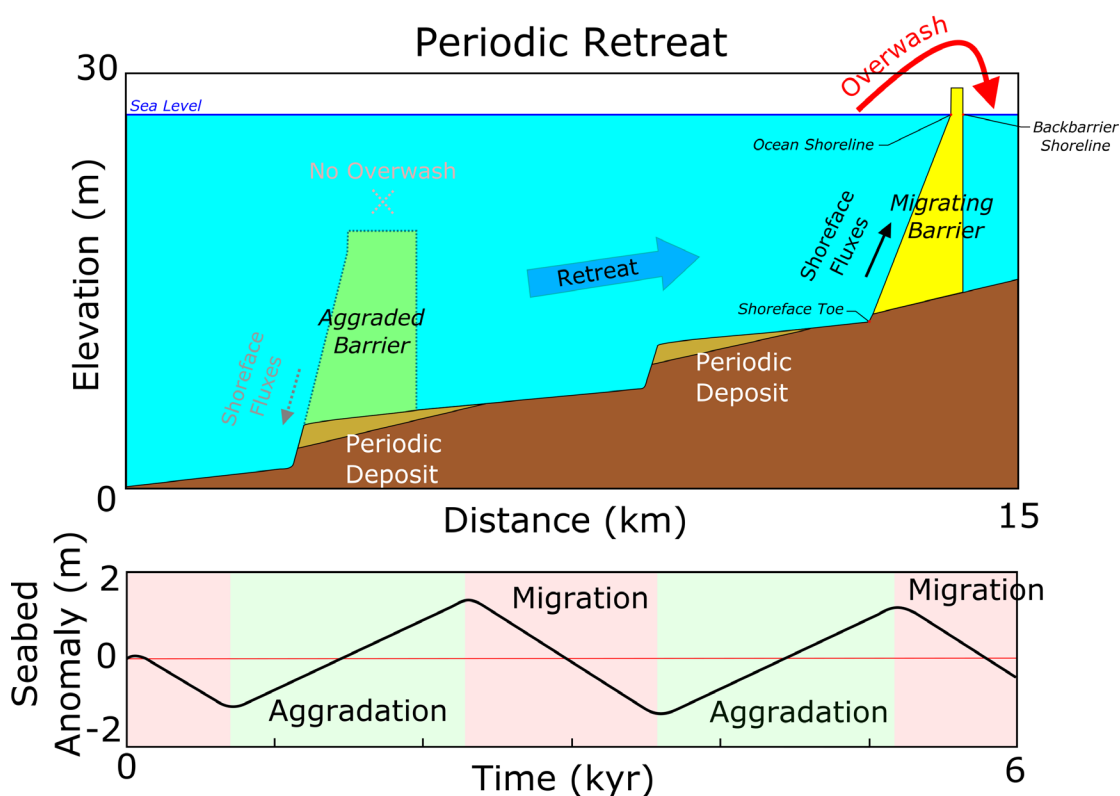


Figure 3.1 – Periodic barrier retreat, defined by an autogenic cycle of alternating episodes of migration (red) and aggradation (green), modeled under constant forcing from rate of sea-level rise and shelf slope. Recurring phases of aggradation lead to the deposition of remnant barrier sands, as eventual migration causes a portion of the lower shoreface below the depth of closure to become stranded on the shelf seabed.

3.2.2 Sea Level Interaction

In this study, barrier islands are modeled through a range of periodic retreats, with very large to very small lags in shoreface response to overwash. Specifically, the periodicity of the barrier is tuned by modulating the shoreface response rate K , which is known to increase deposit wavelength and amplitude as response is reduced (Lorenzo-Trueba and Ashton, 2014). Shoreface response rate in the LTA model is supplied as a constant for the entire shoreface, although it fundamentally describes the rate at which the lower shoreface will respond to changes in the upper shoreface. The model assumes an equilibrium shoreface geometry, where offshore directed flux (driven by gravity) is balanced by onshore directed flux (driven by wave-driven transport). As the upper shoreface (ocean shoreline) is driven landward by storm-driven overwash it distorts the shoreface out of equilibrium, and onshore directed transport responds to this out-of-equilibrium geometry as a function of the response rate—estimable based on wave height/period and grain size/settling velocity (Lorenzo-Trueba and Ashton, 2014 *supplement*). Per the description in the previous section, a low response rate effectively causes changes in the upper shoreface to be dominated by overwash until the shoreface flattens enough that onshore-directed fluxes can counterbalance (and, in the case of periodicity, overcompensate) landward shoreline advance.

Simultaneously with adjustments to shoreface response rate, the barrier is subjected to a discrete interval of sea-level rise—a pulse—and pulse interaction with barrier autogenics is investigated. The inspiration to model this scenario is based on a recently compiled set of chronologically controlled drowned barriers that correlate in time with a sea-level pulse (or pulses) associated with the 8.2 kyr event—an abrupt cooling of global climate linked to glacial

lake outburst floods and enhanced meltwater runoff during the collapse of the Laurentide Ice Sheet (LIS) approximately 8.2 kya (Mellet and Plater, 2018, Hijma & Cohen, 2010).

The timing, duration, and magnitude of the pulse(s) associated with the 8.2 kyr event remains an active area of research, but Hijma and Cohen (2010), using sea level data data from Rotterdam (NL), suggest a pulse beginning 8450 ± 44 yrs BP with a magnitude of 2.11 ± 0.89 m over 200 years—an average rate of rise of 10.6 mm/yr. However, the authors note the pulse could also be divided into two or more discrete jumps in sea level. This suggestion is backed by Lawrence et al. (2016), who used microfossils at the Cree Estuary in Scotland to identify at least three jumps in relative sea level between 8760 and 8218 yrs BP. This series includes a jump beginning at 8595 yrs BP with a mean magnitude of 0.7 m over 130 years—a corresponding rate of rise of 5 mm/yr.

How the pulse(s) associated with the 8.2 kyr event potentially interacted with barrier islands during the early-mid Holocene to produce drowned deposits remains an open question. Rampino and Sanders (1982), in their study of a drowned barrier system off the coast of Long Island (believed to be have experienced a rapid increase in rate of sea-level rise just prior to 7000 yrs BP [Rampino and Sanders, 1981]), suggested that a pulse could induce either complete drowning and overstepping of a barrier, or trigger a mode of combined partial overstepping and retreat. The latter point is intriguing, with Rampino and Sanders (1982) detailing a scenario in which a barrier aggrades during rapid (centennial-scale) sea-level rise before later undergoing migration (as aggradation increasingly fails to maintain pace with rise). In the context of the Long Island system, the authors referred to this concept as a means to describe how both lower shoreface and back-barrier lagoon sediments could be preserved on the modern shelf seabed (Rampino and Sanders, 1983).

Rampino and Sanders (1982) invoked externally driven sediment supply as a mechanism to provide for aggradation even under fast rates of rise. Here, it is proposed that aggradation concurrent with the autogenic cycle provides another means to allow barriers to aggrade during a pulse event. How the resulting seabed deposit records this interaction may be subject to the framework of autogenic-allogenic as described by Jerolmack and Paola (2010). Periodic cycles within the LTA model that produce deposits with amplitudes (seabed anomaly) greater than half a meter tend to occur over centennial to millennial scales, which implies that centennial-scale pulses may have to be relatively high magnitude to be recorded on the seabed.

3.3 Model Setup

A pulse inspired by sea-level rise associated with the 8.2 kyr event is modeled over a 200-yr interval, its magnitude modulated from 0 to 30 mm/yr over a background rate of sea-level rise of 2 mm/yr. 30 mm/yr is chosen in light of insights from Liu and Milliman (2004) who suggest that earlier glacial meltwater pulses had global mean rates of rise from 40 mm/yr to 65 mm/yr—although, tests with the LTA model suggest rates of relative rise in excess of 30 mm/yr generally result in complete drowning of the barrier system over a 200-year interval. Functionally, the pulse injected into the model has a highly simplified square wave or ‘top-hat pulse’ profile, in which the pulse rate of rise is constant for the pulse duration (Figure 3.2).

The modeled barrier subjected to the pulse has an equilibrium geometry described in Table 3.1, transgressing a shelf with a slope of 1 m/km. As a reference case, the barrier is initially modeled with a shoreface response rate K of 9000 m³/m/yr. At this rate, the barrier is in dynamic rollover, as there is no lag between the shoreface response and overwash, the barrier assuming a constant equilibrium geometry as it retreats (Figure 3.2A). Subjecting this barrier to a 20 mm/yr magnitude pulse (Figure 3.2B) temporarily disturbs the barrier from its equilibrium

state, creating purely allogenic deposition with a seabed anomaly ‘amplitude’ over 2 m, followed by corresponding ravinement.

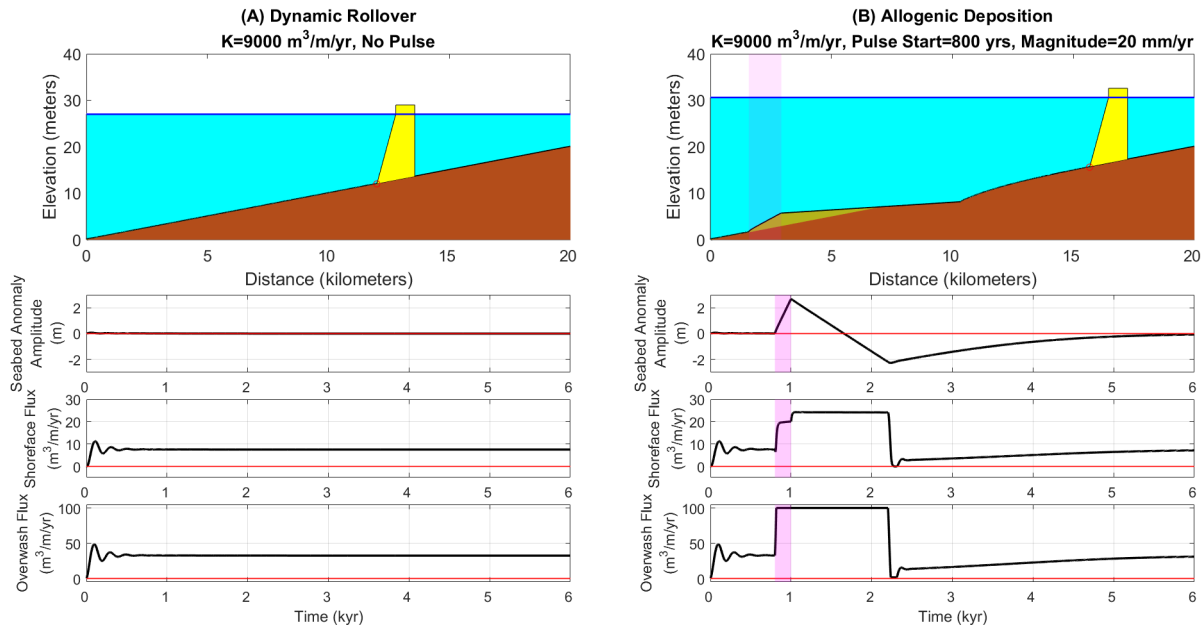


Figure 3.2 – Barrier undergoing dynamic rollover at shoreface response $K = 9000 \text{ m}^3/\text{m}/\text{yr}$. (A) Example with constant forcing and balance between shoreface fluxes and overwash fluxes. (B) The barrier is subjected to a 200-yr pulse (duration and distance affected highlighted in magenta), beginning 800 years into the model run, with a magnitude of 20 mm/yr.

Next, the barrier is modeled with a shoreface response rate K of $2000 \text{ m}^3/\text{m}/\text{yr}$, which for a maximum overwash rate of $100 \text{ m}^3/\text{m}/\text{yr}$ induces a periodic cycle lasting 2900 years. The timing of pulse initiation with respect to the start of the model run is cycled through a 6,000-yr period, ensuring the pulse interacts with the barrier’s periodic cycle at different times (Figure 3.3). In subsequent runs the shoreface response rate is gradually increased, which collapses the duration of the periodic cycle and reduces the amplitudes of autogenic deposits as the barrier transitions towards dynamic rollover (Figure 3.2A). The aim is to model how the pulse interacts with the barrier as autogenic influence is adjusted (through tuning the shoreface response), determining the duration and magnitude thresholds of pulses that result in dominantly allogenic deposition.

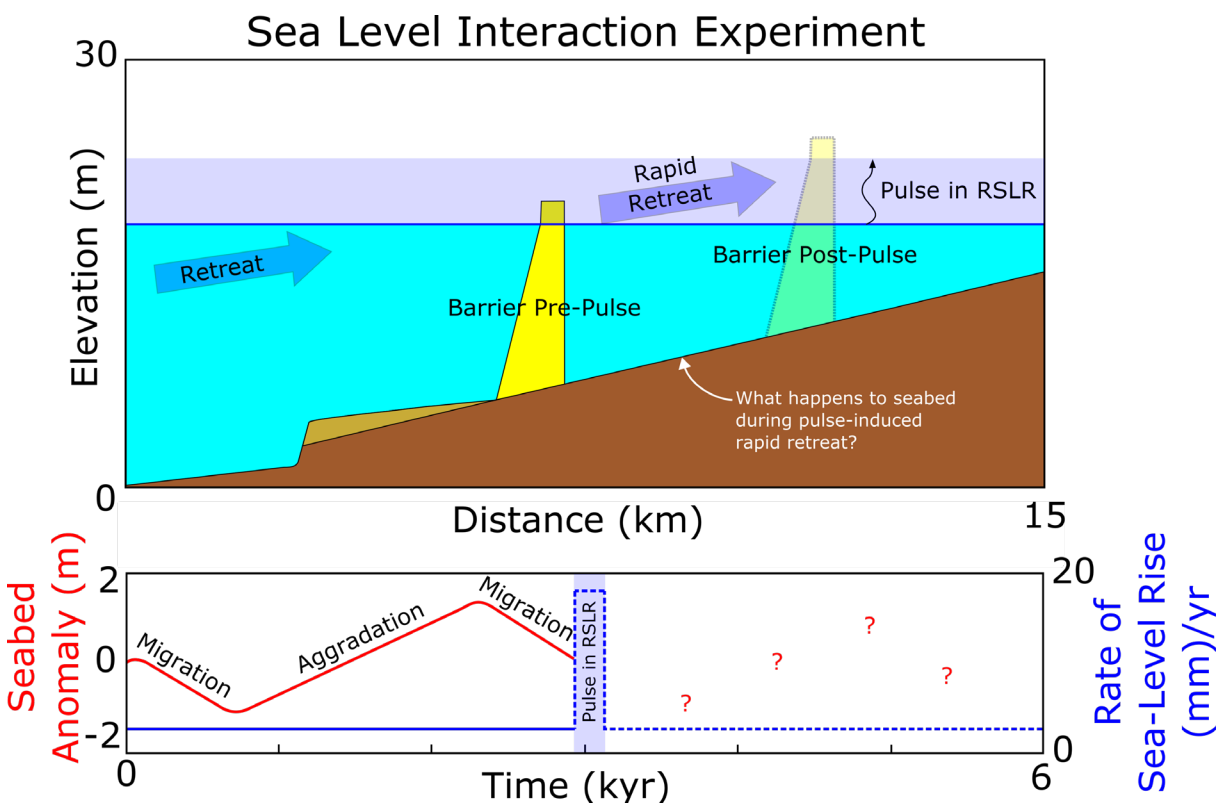


Figure 3.3 – Setup of sea-level interaction experiment. A periodically retreating barrier encounters a pulse in rate of sea level-rise (in this example, 18 mm/yr) comparable to the duration of the 8.2 kyr rise event. The timing of the pulse is shifted through periodic cycles (migration and aggradation) for pulse rates of rise up to 30 mm/yr. The barrier also migrates along a shelf with a 1 m/km slope, comparable to many passive margins.

Table 3.1 – Model Input Parameters

Parameter	Symbol	Inputs (Figs 1-7)
Slope (m/km)	β	1
Shoreface Toe Depth (m)	D_t	15
Equilibrium Width (m)	W_e	800
Equilibrium Height (m)	H_e	2
Eq. Shoreface Slope	α_e	0.02
Max Overwash ($\text{m}^3/\text{m}/\text{yr}$)	$Q_{\text{OW,max}}$	100
Max Deficit Volume ($\text{m}^3/\text{m}/\text{yr}$)	$V_{\text{d,max}}$	$0.5 \cdot H_e \cdot W_e$
Shoreface Response ($\text{m}^3/\text{m}/\text{yr}$)	K	2000-6000
Bkgrnd Sea-Level Rise Rate	\dot{z}	2
Pulse Rate of Rise (mm/yr)	\dot{z}_p	0-30
Pulse Duration (yrs)	t_p	200

*Denotes a range of tested values.

3.4 Results

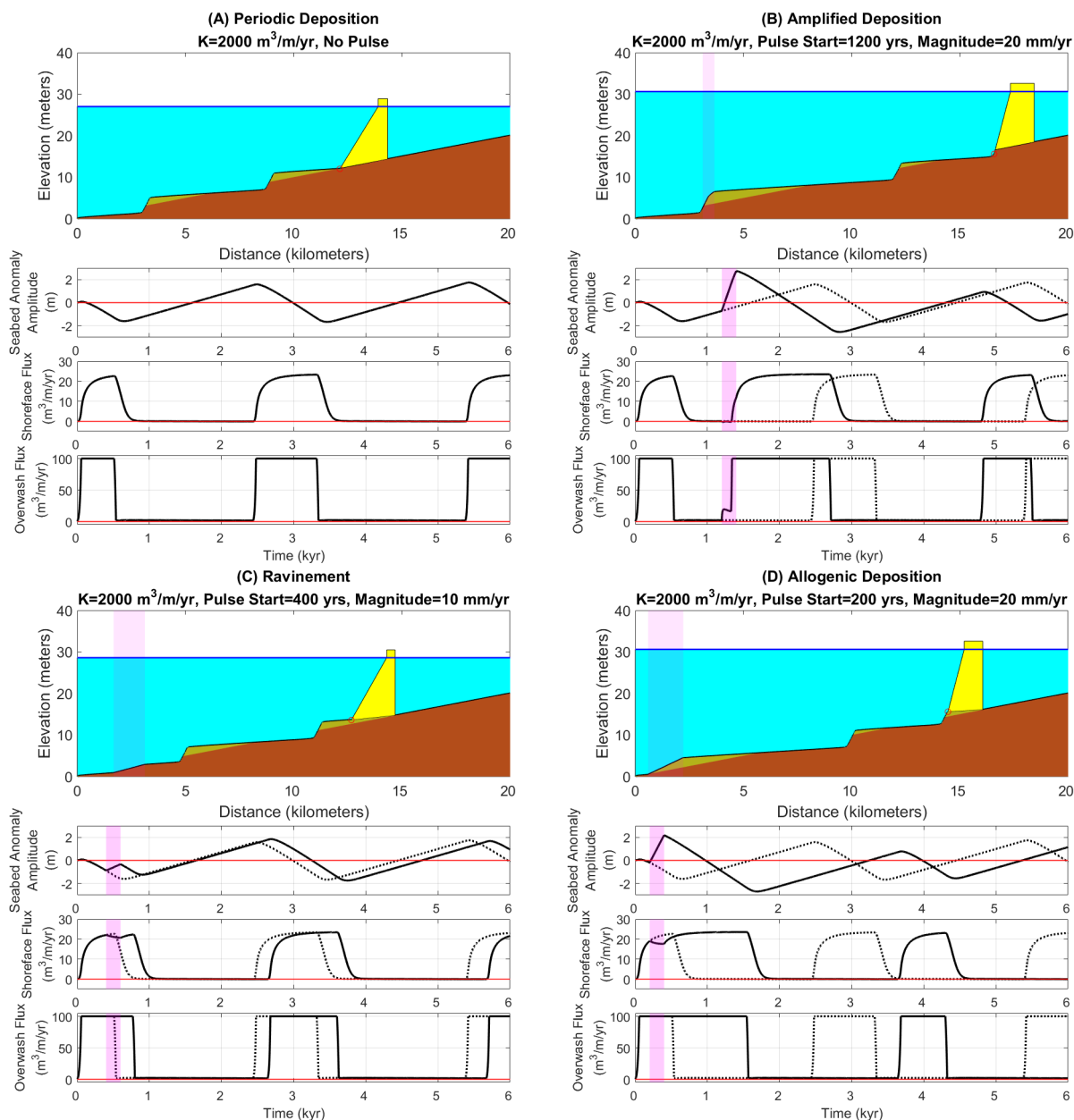


Figure 3.4 – Range of behavioral/depositional responses of a periodically retreating barrier subjected to a pulse in rate of sea-level rise. Pink highlights correspond to duration and distance affected by pulse. (A) Periodic deposition (autogenic), with no pulse; dashed lines in subsequent subplots (B, C, D) refer to plots shown here. (B) 20 mm/yr pulse coinciding with the aggradational phase of periodic retreat; amplified deposit produced. (C) 10 mm/yr pulse coinciding with migrational phase of periodic retreat; no deposition/ravinement. (D) 20 mm/yr pulse coinciding with migrational phase of periodic retreat; deposition occurs where periodic retreat suggests none should occur.

Modeling a periodically retreating barrier with $K = 2000 \text{ m}^3/\text{m}/\text{yr}$ through a range of pulses with variable magnitude and timing yields diverse results in terms of behavior and amplitude of deposits, and suggests strong autogenic influence from the periodic cycle (Figure 3.4). Where the barrier is aggrading during the periodic cycle (Figure 3.4A), interaction with a pulse (Figure 3.4B) initially causes the barrier to grow vertically due to the sudden increase in height accommodation. At the same time, the barrier begins eroding at the shoreward edge, until its width becomes narrow enough that it eventually migrates landward. This sequence of events is evidenced in the double-step that occurs in overwash flux, with shoreface fluxes beginning to increase in tandem with the second step (when pulse-induced migration begins). Conversely, if the barrier is migrating during the periodic cycle, interaction with the pulse leads to two outcomes (Figure 3.4C; 3.4D). If the pulse occurs late enough in the migrational phase, when shoreface fluxes are caught up to overwash fluxes, and/or pulse the magnitude is relatively low, then the pulse will not be able to induce deposition (Figure 3.4C)—the shoreface is already responding, and continued overwash means the barrier can still compensate its geometry for a jump in sea level. If the pulse occurs earlier in the migrational phase, when shoreface fluxes strongly lag behind overwash, and/or the pulse magnitude is relatively high, then the pulse can induce allogenic deposition (Figure 3.4D), overcoming the ability of fluxes to adjust the geometry of the barrier for the sea-level jump.

The influence of autogenic periodicity on barrier response to a sea-level pulse is further emphasized by Figure 3.5A, which shows that regimes of deposition and drowning closely follow the evolution of the periodic cycle. Complete drowning of the barrier occurs most readily in the transition between aggradation to migration, where landward directed shoreface fluxes are initially slow to catch up to overwash fluxes and backbarrier accommodation is maximized.

Conversely, complete drowning is minimized in the transition between migration to aggradation, where landward directed shoreface fluxes are peaking and backbarrier accommodation is reduced. As shoreface response rate K is increased, decreasing internal system lag (Figure 3.5B; 3.5C), variability in complete drowning with respect to pulse rate of rise is diminished; this illustrates the concept of the barrier's depositional response becoming largely dominated by allogenic forcing from sea-level rise, as demonstrated to the extreme in Figure 3.2.

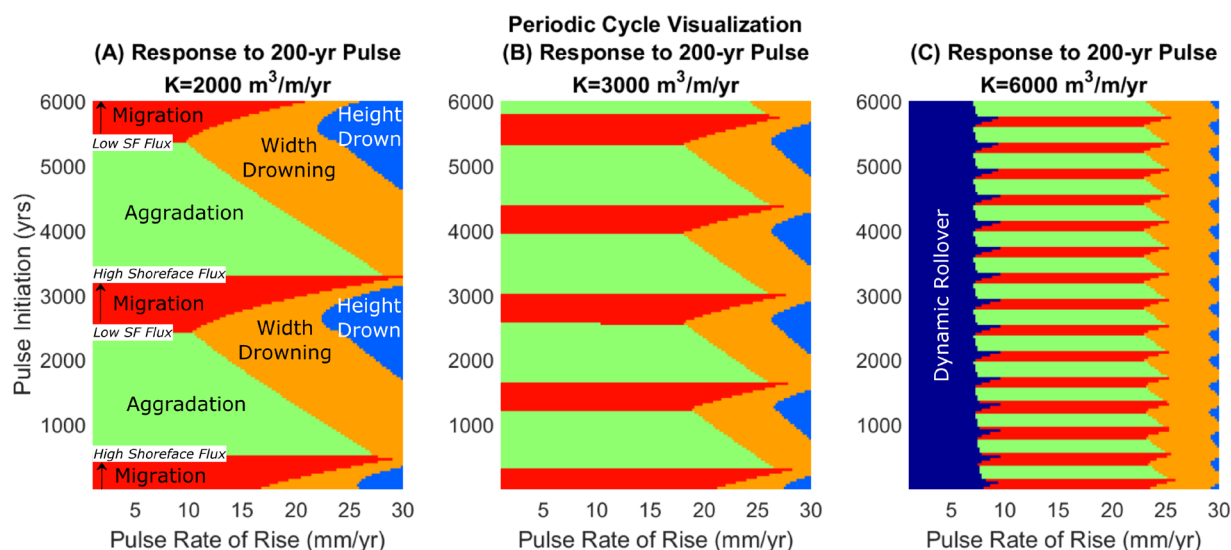


Figure 3.5 – Regime plots depicting the barrier response to a 200-yr sea level pulse, with pulse initiation (relative to start of model run) on the y-axis, and pulse rate of rise on the x-axis. Response shown for barriers with a shoreface response of (A) $2000 \text{ m}^3/\text{m}/\text{yr}$, (B) $3000 \text{ m}^3/\text{m}/\text{yr}$, and (C) $6000 \text{ m}^3/\text{m}/\text{yr}$. Red and green regions occur where remnant barrier deposits are detected and the barrier does not completely drown; red regions correspond with the migrational phase of the periodic cycle, while green regions correspond with the aggradational phase. Dark blue regions highlight dynamic rollover, orange regions highlight width drowning, and light blue regions highlight height drowning. Drowning is least pronounced when the pulse is initiated near the transition from migration (red) to aggradation (green), which corresponds with the timing of maximum landward-directed shoreface fluxes during the periodic cycle. At the highest shoreface response rate ($6000 \text{ m}^3/\text{m}/\text{yr}$), the phase of the periodic cycle exerts relatively little influence on whether the barrier drowns, as autogenic influence is minimized.

A closer examination of the periodic cycle as visualized in Figure 3.5A allows for a regime-based classification of barrier response (Figure 3.6) from the amplitude of deposits as described from profiles in Figure 3.4. Where deposition occurs at $K = 2000 \text{ m}^3/\text{m}/\text{yr}$ it is primarily autogenically-driven, although a region of allogenic influence occurs in the transition

between autogenic deposition/ravinement and width drowning. Where this allogenic influence coincides with aggradation it results in the amplification of autogenic deposits (e.g. Figure 3.4b) and where it occurs with migration it results in ravinement (Figure 3.4C; if the magnitude of the pulse cannot overcome autogenic influence) or ‘emergent’ to ‘large’ allogenic deposits (Figure 3.4D). For the purposes of this classification, emergent allogenic features are defined as deposits formed within the migrational phase that are below the amplitude of autogenic deposits; large allogenic deposits exceed this amplitude.

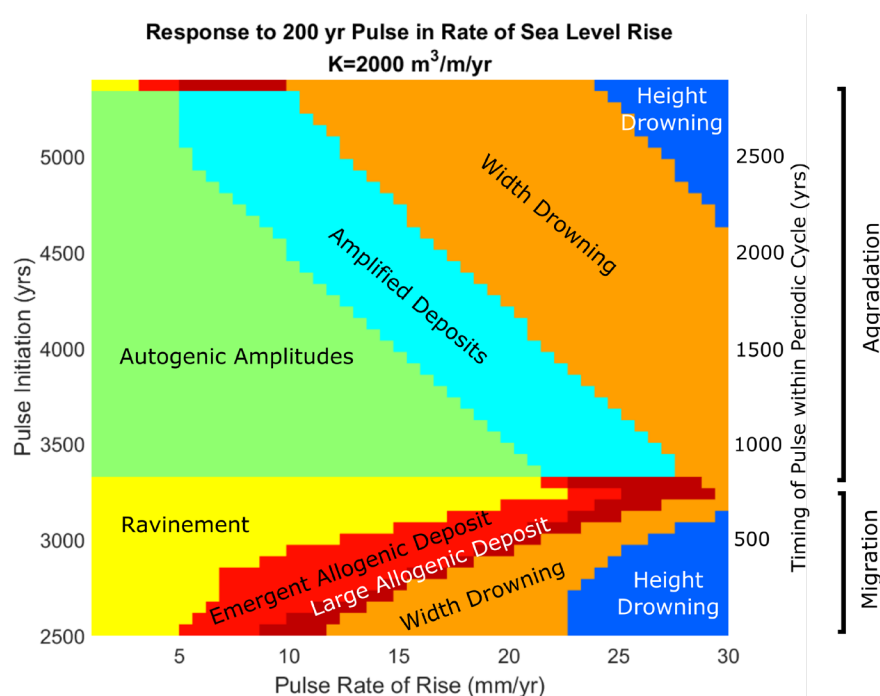


Figure 3.6 – Classification of a full periodic cycle (migration-aggradation) based on the amplitudes of resulting deposits. Allogenic influence from the pulse occurs readily in the transition from autogenic deposition/ravinement to the width drowning regime. During the aggradational phase, pulses can amplify deposits that would already be created during purely periodic retreat. Conversely, in the migrational phase, where ravinement would occur autogenically, emergent allogenic deposits (with amplitudes smaller than autogenic deposits), as well as large allogenic deposits (with amplitudes greater than autogenic deposits) can form.

A comparison of periodic cycles with decreasing autogenic influence (Figure 3.7) shows that as the cycle is shortened, and its corresponding amplitudes reduced, amplification and production of large allogenic deposits from the sea-level pulse become more prominent. At $K =$

6000 m³/m/yr, where the duration of the aggradation/migration phases within the periodic cycle collapse to ~200 years, autogenic deposition ceases entirely. Here, all deposition is dominated by allogenic influence from the sea-level pulse—the largest deposits slightly exceed the amplitude of deposits formed under dominantly autogenic conditions. Additionally, dynamic rollover begins to appear in the regime space, and the barrier becomes unresponsive to lower magnitude pulses (below 7-10 mm/yr).

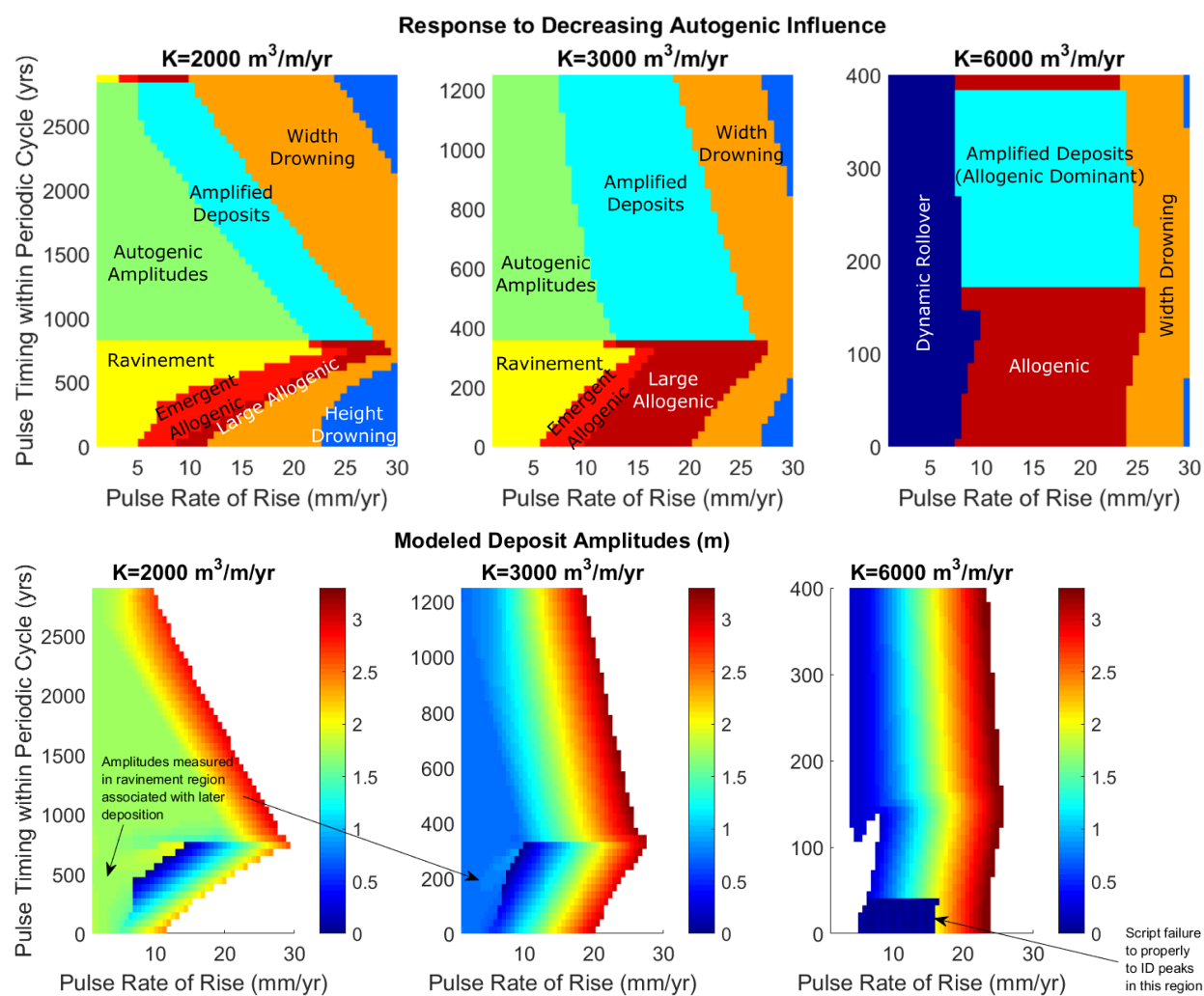


Figure 3.7 – TOP: Classification of a full periodic cycle with decreasing autogenic influence. As shoreface response rate K increases, the periodic cycle shortens, drowning becomes less variable with respect to pulse rate of rise, and amplification and production of allogenic deposits gradually dominate the regime space. At $K=6000$ m³/m/yr, no autogenic deposits are produced, and dynamic rollover begins to dominate the barrier response at low pulse rates or rise. BOTTOM: Corresponding plots of deposit amplitude. White regions indicate to no detection of a deposit or complete drowning of the barrier.

3.5 Discussion: A Complicated Response

As depicted in Figure 3.7, model results suggest barrier island response to a pulse operates along a complex triaxial gradient governed by the pulse magnitude, the timing of the pulse, and the barrier shoreface response rate (or more accurately, lag between shoreface response and overwash). Tuning each parameter independently results in varying degrees of deposition from autogenic/allogenic influence, as well as complete drowning and dynamic rollover. This framework begins to validate the observationally-inspired concept put forward by Rampino and Sanders (1982) that barrier island retreat involves a suite of states between rollover and complete drowning that are capable of producing remnant deposits on the seabed. Moreover, this work shows that the internal dynamics of a barrier can create an autogenic filter that, despite being regularly oscillating with phases of aggradation and migration, produces a complicated response on the seabed.

The rules governing this complicated response within the modeled system share similarities with concepts applied to alluvial-deltaic systems by Jerolmack and Paola (2010) and Li et al. (2016), among others. In particular, as the duration of periodic phases (aggradation/migration) collapse towards the duration of a meltwater/flood pulse, the depositional response of the barrier is progressively dominated by allogenic forcing from sea level. Conversely, for a pulse within the duration of periodic phases, the internal dynamics of the barrier act as an autogenic filter, and only relatively high magnitude pulses produce a depositional response—however, the range of magnitudes where allogenic influence is effective in producing deposition is also variable based on the phasing of the periodic cycle.

While it is possible to model barrier response under autogenic-allogenic interaction, identifying it as a signal in real-world seabed deposits is likely to be difficult based on the similar

ranges of deposit amplitudes produced across the autogenic-allogenic spectrum (Figure 3.7). In particular, this suggests that the autogenics of barrier islands are superficially similar to deltas in the way they shred the signals of allogenic forcing operating on sub-autogenic timescales (Foreman and Straub, 2017). One possibility to interpret the response of the barrier from relict deposits is to utilize, where available, a more continuous record of deposition, with multiple deposits. Figures 3.4B and 3.4D demonstrates that, especially for amplified deposition, pulse interaction can produce a noticeable disruption in amplitude across a series of relict deposits, suggesting autogenic-allogenic interaction could be inferred in cases where periodicity is already suspected—this could be supplemented, where available, by age control to correlate timing with known pulses, as has already been accomplished for some field sites (*e.g.* Mellet & Plater, 2018, especially describing a barrier system that likely drowned during interaction with the 8.2 kyr event rise per Mellet et al., 2012; Mellet et al., 2012b).

Additionally, it may be possible to constrain the potential for past interaction based on calculating the shoreface response rate and maximum overwash rate of the barrier system if a modern analog is available (or a paleobarrier can be reconstructed from relict morphology or other data). This technique, in combination with modeling, could also be applicable to modern barriers to gain insight into future evolution, and could help describe the vulnerability or resilience of specific systems to anthropogenic sea-level rise. As indicated in Figures 3.5, 3.6, and 3.7, periodic barriers are generally more susceptible to drowning during rapid sea-level rise, although in some cases results demonstrate that they could withstand up to 30 mm/yr of rise for two centuries.

3.6 Conclusions

This investigation demonstrates that autogenic periodicity in barrier islands could act to filter the response of transgressive systems to rapid changes in rate of sea-level rise (pulses). For sea-level forcing to exert a dominant control on the depositional response of the system, the duration of a pulse must approach the timescale of phases of aggradation and migration within a barrier's periodic cycle. Alternatively, a pulse of sufficiently high magnitude could induce deposition when none is expected to occur, or result in amplification of autogenic deposits. Taken together, these insights suggest similarities in the ways barriers and alluvial-deltaic systems process external (allogenic) forcing. It is also shown that, across the spectrum of pulse interaction with periodicity, the range of deposit amplitudes varies little, which could complicate interpretation of deposits in the field. However, it could be suggested that in cases where multiple relict deposits are present on the seabed, large deviations in relative amplitude could be attributable to the effects of pulses acting on periodically retreating barriers, especially if age control is available to correlate timing. Insights from this modeling exercise could also be extended to modern barriers experiencing enhanced sea-level rise, providing guidance on the relative vulnerability of barriers to drowning over decadal to centennial scales.

CHAPTER 4 - QUANTIFYING SEDIMENT BUDGET FROM SUBAERIAL BARRIER RIDGE AND SWALE MORPHOLOGY

The contents of this chapter appear in:

Ciarletta, D. J., Shawler, J. L., Tenebruso, C., Hein, C. J. & Lorenzo-Trueba, J. (2019).
Reconstructing Coastal Sediment Budgets from Beach- and Foredune- Ridge Morphology: A
Coupled Field and Modeling Approach. *Journal of Geophysical Research: Earth Surface*.

4.0 Summary

Preserved beach/foredune ridges may serve as proxies for coastal change, reflecting alterations in sea level, wave energy, or past sediment fluxes. In particular, time-varying shoreface sediment budgets have been inferred from the relative size of foredune ridges through application of radiocarbon and optically stimulated luminescence (OSL) dating to these systems over the last decades. However, geochronological control requires extensive field investigation and analysis. Purely field-based studies might also overlook relationships between the mechanics of sediment delivery to the shoreface and foredune ridges, missing insights about sensitivity to changes in sediment budget. In this investigation, a simple geomorphic model of beach/foredune ridge and swale morphology is proposed to quantify the magnitude of changes in cross-shore sediment budget, employing field measurements of ridge volume, ridge spacing, elevation, and shoreline progradation. Model behaviors are constrained by the partitioning of sediment fluxes to the shoreface and foredune ridge, and can be used to reproduce several cross-shore patterns observed in nature. These include regularly spaced ridges ('washboards'), large singular ridges, and wide swales with poorly developed ridges ('flats'). The model is evaluated against well-preserved ridge and swale systems at two sites along the Virginia Eastern Shore (USA): Fishing Point, for which historical records provide a detailed history of shoreline progradation and ridge growth, and Parramore Island, for which a relatively more complex morphology developed over a poorly constrained period of prehistoric growth. Results suggest this new model could be used to infer the sensitivity of field sites around the world to variations in sediment supply.

4.1 Introduction: Ridge and Swale Systems as Records of Past Change

Coastal ridge and swale systems, composed predominantly of relict wave-built beach ridges and/or aeolian foredune ridges, are found in association with progradational shorelines around the world (Tamura, 2012). The morphology of these elongate, shore-parallel to subparallel features preserve paleoenvironmental signatures which have been used to infer changes in shoreline position (Mason et al., 1993), coastal sediment delivery rates and textures (Bristow & Pucillo, 2006; Hein et al., 2016), relative sea level (Billy et al., 2015; Hede et al., 2013; Long et al., 2012), and storm frequency (Buynevich et al., 2004; Costas et al., 2016). Subsequently, ridge proxies could be useful in predicting future changes to the coastal zone in response to autogenic forcings, climate change, and anthropogenic interventions.

The morphology of relict beach/foredune ridges have been used to infer changes in shoreline migration for at least a century (Johnson, 1919). However, whereas modern studies employing historical mapping, beach profiling, LiDAR investigations, and shallow stratigraphy provide insight into the scales and sediment budget contributions of various short-term shoreline processes (Dougherty et al., 2016; Pye and Blott, 2016; Saye et al., 2005; Young et al., 2006), quantifying long-term changes in sediment flux across the Holocene has been constrained by the need for geochronologic control.

Studies of pre-historic spatiotemporal change in regressive coastal systems commonly rely on a combination of radiocarbon dating and optically stimulated luminescence (OSL) to derive geochronology (e.g. Argyilan et al., 2010; Hails, 1968; Oliver et al., 2015; Rhodes, 1980; Rink and Forrest, 2005). Both techniques can be combined with high-resolution topography (*i.e.*, derived from LiDAR or real-time kinematic [RTK] GPS mapping), ground-penetrating radar (GPR) (*e.g.*, Dougherty et al., 2016; Oliver et al., 2017a), and sediment coring to produce

quantitative analyses of sediment flux at a given field site. However, these approaches are expensive, time consuming, and labor intensive.

In contrast, quantitative models of geomorphic change, grounded in field-based conceptual models of geomorphic evolution, present an opportunity for a more rapid and cost-effective approach to reconstructing time-varying controls on coastal change. This investigation uses simple geomorphic relationships, combined with minimal age-control points, to develop a morphological model that applies a cross-shore mass balance approach to an idealized ridge and swale morphology in order to quantify past changes in sediment budget. Application of this model to several test field sites provides insight on the sensitivity of coastal systems to variations in sediment delivery. As a tool, the model could be used to explore how changes in sediment fluxes and accommodation (*e.g.*, sea-level rise or fall) might impact future shoreline response.

For this study, ridge and swale systems composed of shore-parallel relict foredunes are initially considered, and the model is evaluated at two sites along the Eastern Shore of Virginia (USA). One site, Fishing Point (an elongating barrier spit at the southern end of Assateague Island), formed in historical times and allows for the construction of a time-series analysis of sediment inputs based on observations from aerial photos and recent LiDAR data. The other site, Parramore Island, features a prominent ridge and swale system that formed during a period of pre-historic progradation. The model framework at Fishing Point is validated using the short-term time-series, demonstrating the magnitude of past sediment fluxes can be quantified from morphology. Later, the model is applied to Parramore Island, where no time-series data exist and only limited chronological control is available.

4.2 Background: Concept to Quantification

A chief concept of this investigation is that the morphology of a foredune ridge and swale system could be broadly controlled by the partitioning of two main components of the sediment budget: fluxes of sand delivered to the beach and fluxes delivered from the beach to the foredune ridge (Figure 4.1). In the former, fluxes of sand are delivered to the shoreface and beach through cross-shore and longshore transport. This commonly occurs through the landward migration and welding of nearshore bars, for example along beaches fed through inlet-sediment bypassing (FitzGerald 1984; Guadiano & Kana, 2001) and strandplain systems in which sediment is sourced from proximal rivers (Nooren et al, 2017; Psuty, 1965). In the latter, sand is transported by tides, waves, and wind from the beach to the foredune by a variety of shallow subaqueous and subaerial physical mechanisms; as such, transport from beach to foredune requires processes that span the foreshore, backshore, and dune line (Cohn et al., 2019). Recent modeling work also suggests that the density of subaerial vegetation (partly controlled by wave climate) also strongly modulates the morphology of dunes built primarily by aeolian accretion (Vincent & Moore, 2013).

Partly motivating this investigation's approach, field observations suggest that shoreface sediment fluxes needed to grow a beach are roughly an order of magnitude larger than sediment fluxes accumulated in foredunes over comparable timescales. A sampling of global field sites shows that foredunes generally accrete sediment at a rate of $< 20 \text{ m}^3/\text{m}/\text{yr}$ (Appendix Table A4.1). Comparatively, Himmelstoss et al. (2017) report long-term rates of progradation along the United States southeastern Atlantic and Gulf coasts between 8.5 and 33.5 m/yr, which, assuming a characteristic shoreface depth of *ca.* 5 m, would produce net fluxes in the range 43-168 $\text{m}^3/\text{m}/\text{yr}$. The disparity in transport rate may be as easy to explain as the energy applied to move

sand—hydraulic processes are more efficient, with net transport rate decaying rapidly as sand particles move from the subaqueous domain into the intertidal/subaerial domain.

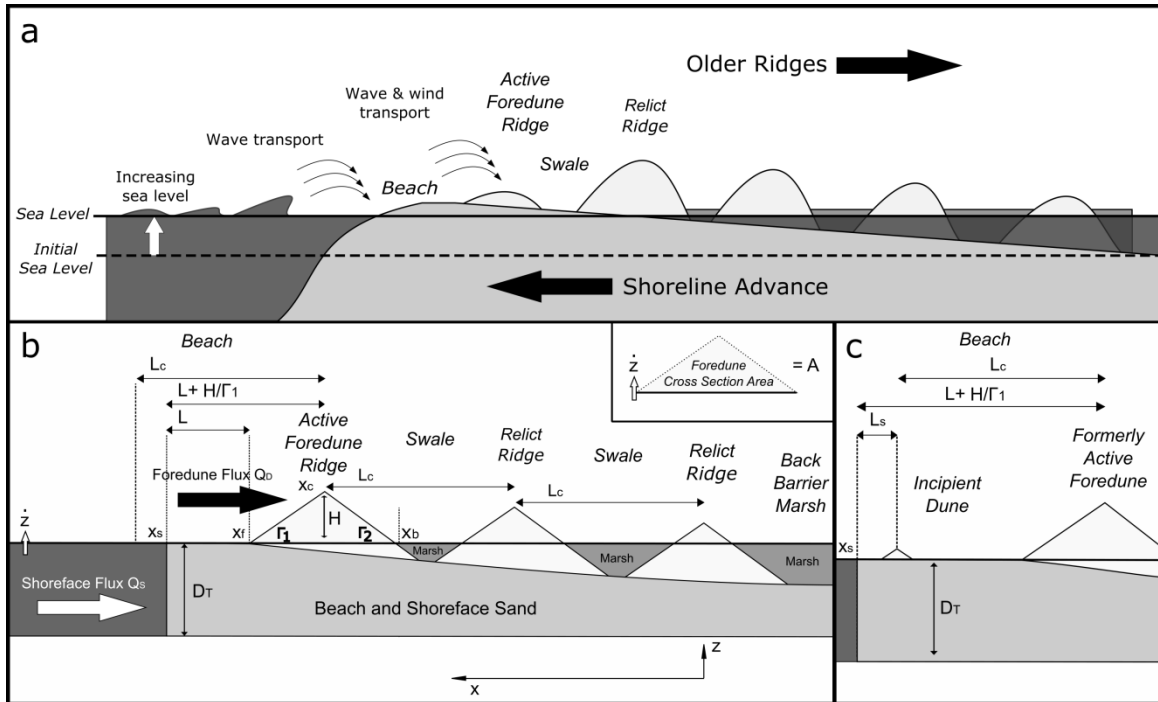


Figure 4.1 – (a) Processes responsible for shoreline progradation. Sand is first transported to the beach (largely through onshore bar migration and contributions from longshore transport) and later transported to the active beach/foredune ridge by aeolian and wave transport. The shoreline advances seaward with time, and new dunes form with a characteristic crest spacing, producing an alternating pattern of ridges and swales. In this example, swales are progressively flooded by rising sea level and experience upland marsh migration from the back-barrier margin. In cases of falling sea level and decreasing shoreface accommodation (also included in model development), this would not occur. (b) Model idealized geometry and processes. (c) Depiction of new dune line emplacement. An incipient foredune forms when the width of the beach and dune flank $L + H/\Gamma_1$ is greater than or equal to the critical ridge spacing plus the setback distance $L_c + L_s$. The crest of the new dune forms at $x_s - L_s$ so that the incipient dune is inland of the shoreline.

Psuty (2004) observes that rapidly prograding beaches with abundant sediment tend to be composed of many low beach ridges, in contrast to slowly growing beaches with limited sediment availability. Conceptually, slowly prograding beaches develop higher foredune ridges due to greater time to accumulate subaerial sediment. Thus, there is an inverse relationship between ridge size and rate of progradation, which is observed at field sites throughout the world (e.g., Bristow & Pucillo, 2006; Nooren et al., 2017; Oliver et al., 2018). While this relationship

has not before been explicitly integrated into numerical models of beach-dune growth, here it is suggested that envisioning the coast as a two-step partitioning provides a relatively simple means to quantitatively implement this inverse relationship. The dissociation of transport in the subaqueous and intertidal/subaerial domains not only matches favorably with the conceptual progradational model of Psuty (2004), but also allows for more diverse ridge morphology within and between individual coastal systems.

This investigation validates such a numerical model, and then applies it, quantifying volume changes in ridge and swale systems through time. Taking a reduced-complexity approach, the model is not intended to directly investigate the physical processes responsible for transporting sediment, focusing instead on the net effect of time-varying sediment fluxes. The framework is specifically built to produce patterns of subaerial ridge and swale morphology from a simplified sediment partitioning perspective, utilizing idealized ridge geometries. The field methods and approach thus follow those of Bristow and Pucillo (2006) and Oliver (2015): LiDAR-derived topography is used to compute subaerial ridge volume, and a combination of sediment coring and GPR is used to measure subsurface volumes. Additionally, as model results are validated against a study site with a comprehensive historical record, the approach of Kraus and Hayashi (2005) is followed in employing aerial photos to construct a time-series analysis of shoreline and ridge-area change.

4.2.1 Development of Ridge Morphology

While it has not before been directly parameterized, a widely observed morphologic characteristic of ridge and swale systems is the systematic spacing of foredune ridges. Nucleation of an incipient foredune occurs through multiple processes (Hesp, 2011; Otvos, 2000) but in many cases is observed to produce a regular pattern (Figure 4.1). In describing the process

driving this periodicity, Johnson (1919) observed that wave-formed platforms could act as regular anchor points for aeolian accumulation, a process later termed “berm-ridge progradation” (Otvos, 2000). Under this process, aeolian-capped, wave-built beach ridges episodically develop upon a substrate provided by the welding of nearshore bars, a process typically associated with inlet sediment bypassing for prograding barrier islands and river mouth strandplain systems (FitzGerald 1984; Noreen et al., 2017).

For barrier islands, nearshore bars—in this case, elongated, inlet-attachment bars—taper downdrift from ebb tidal deltas, moving onshore as large packages of sediment with lengths of 300-1500 m, and widths of 40-300 m (FitzGerald, 1982). As a bar moves up the shoreface, it is subject to increasing subaerial exposure during the tidal cycle, which slows its rate of landward advance and contributes to the production of a swale between the bar and the beach, forming a ridge and runnel-like system—although FitzGerald (1982) emphasizes that these systems are much larger than true ridge and runnel systems and form over longer timescales. Such quasi-cyclic welding of nearshore bars is widely recognized, and occurs on the order of every 4-7 years (Price Inlet, South Carolina [FitzGerald, 1984]) to 8 years (Skallingen, Denmark [Aagaard et al., 2004]), but may be more or less frequent.

The observation that nearshore bars form and migrate onshore at rates which scale as a function of sediment input (FitzGerald, 1982) suggests that ridge spacing itself scales proportionally to the flux of sediment to the beach. As such, ridge spacing is a proxy for the frequency of bar welding, and assuming continued berm-ridge progradation, the production of incipient foredunes. Ridge spacing is therefore parameterized as a measurable component of field morphology which can be used to prompt the formation of an emergent foredune within the model framework. Additionally, as a consequence of the decadal timescales of bar welding, this

constrains the applicability of the current framework to relatively long-term modeling—the *a priori* insights at decadal to centennial scales from conceptual models and observations allow the construction of a reduced order system to coarsely control morphology, approximating the ridge formation processes (French et al., 2016) without incorporating specific wind and wave processes responsible for the growth of individual ridges. Notably, even where berm-ridge progradation is not identified specifically as the process responsible for ridge formation, beach sediment fluxes are hypothesized to dominate the morphological response of ridge systems over similar timescales (Oliver et al., 2017b), which suggests a first-order parameterization of ridge spacing is sufficient for an initial exploration. Walker et al. (2017) similarly suggests that, at the landscape scale, individual events and processes become less important than the ‘broader context’ of beach-dune interlinkage—the focus of parameterization shifts to the patterns of morphology produced from sequences of events and the sum of background processes.

While welding events can trigger new ridge formation, the location of an incipient foredune ridge relative to the shoreline must also be considered, due in part to both the influence of waves and the salt tolerance of pioneering plants, which help stabilize the incipient foredune (Vincent & Moore, 2013). This shoreline setback has been theorized to relate to the cross-shore gradient in plant community that occurs on the beach, with narrower zonation (inversely proportional to wave height, since this acts as a disturbance factor) leading to more stable, linear foredune ridges with plan-view morphology similar to those observed in the Virginia field sites (Figure 4.2; Appendix Figure A4.5).

While it has been shown that the height of purely aeolian foredunes could reflect a steady state condition associated with the local sediment supply regime and the presence/absence of stabilizing vegetation (Vincent & Moore, 2013), a height limitation is not imposed in this

investigation. Instead, ridges are modeled according to Davidson-Arnott et al. (2018), who suggest that dune height is a function of sediment supply, whereby vertical growth rate responds strictly to the size of the ridge. For example, under constant input, the rate of elevation gain decreases for progressively larger ridges, but never results in an equilibrium height. It is observed, however, that the largest ridges along the Virginia coast approach 8 meters, which could suggest a characteristic maximum timescale of formation and/or sediment supply for this region.

4.3 Model Setup and Methods

An idealized geometry is used to model a beach/foredune ridge and swale system (Figure 4.1), simplifying the process of simulating new ridge formation. As the shoreline progrades, it is assumed that foredunes are formed at a regular spacing for morphologically similar ridges. A critical ridge spacing L_C is applied to define the cross-shore distance threshold at which the beach has grown too far from a given foredune ridge for that ridge to receive sediment, thereby halting its growth and initiating formation of a new ridge. It is also assumed that development of this new foredune does not occur directly on the shoreline, requiring a setback distance L_S per the discussion of Vinent and Moore (2013).

Based on the idealized geometry depicted in Figure 4.1b, the evolution of the ridge and swale system is fundamentally described by two state variables: the shoreline location x_s , and the cross-sectional foredune volume A . The change in these boundaries is described through their modification by shoreface sediment fluxes delivered to the beach Q_S , and fluxes of sand from the beach to the foredune Q_D .

First, the relationship between the aforementioned fluxes and the location of the shoreline is expressed as:

$$\frac{dx_s}{dt} = \frac{Q_s}{D_T} - \frac{Q_D}{D_T} - \frac{L \cdot \dot{z}}{D_T} \quad (1)$$

in which $L = x_s - x_f$ is the cross-shore width of the beach, or the distance between the shoreline and the foredune front toe (Figure 4.1b). Q_s/D_T and Q_D/D_T are the sediment delivery to the beach and the foredune divided by the depth of the shoreface, and $L \cdot \dot{z}/D_T$ is the loss of beach volume to vertical aggradation as a function of sea-level rise \dot{z} . Although falling sea level is not used in this investigation's field-model comparison, the framework is designed to account for different regional settings, and in this case $L \cdot \dot{z}/D_T$ responds by creating negative accommodation at the beach, extending the shoreline.

Beach-to-dune fluxes grow the cross-sectional volume A of the active foredune ridge, while rising (falling) sea level simultaneously reduces (increases) subaerial volume storage, yielding the following relationship:

$$\frac{dA}{dt} = Q_D - (x_f - x_b) \cdot \dot{z} \quad (2)$$

in which Q_D is sediment input from the beach and $(x_f - x_b) \cdot \dot{z}$ is the loss/gain in subaerial volume due to the effect of sea-level change (x_b is the location of the foredune back toe).

The cross-sectional volume A of the foredune ridge, modified by sea-level rise, and the front and back slopes Γ_1 and Γ_2 are used to solve for the position of the front and back foredune toes x_f , and x_b using geometric relationships. For initial model simulations, a triangular foredune profile is assumed (although more complex geometries could be used):

$$x_f = x_c + \frac{H}{\Gamma_1} \quad (3)$$

$$x_b = x_c - \frac{H}{\Gamma_2} \quad (4)$$

where x_c is the location of the foredune crest, and the height of the foredune is computed as $H = [2 \cdot A / (1/\Gamma_1 + 1/\Gamma_2)]^{1/2}$.

The crest position x_c of a new, incipient foredune ridge relative to the previous ridge crest is given by the critical ridge spacing L_C . When the width of the beach plus the width of the foredune front flank $L + H/\Gamma_1$ is greater than or equal to the critical ridge spacing plus the setback distance $L_C + L_S$ a new foredune will form at $x_s - L_S$ (Figure 4.1c). Over time, the horizontal position of the foredune ridge crest can be approximated by the following relationship:

$$x_c = (n - 1) \cdot L_C \quad (5)$$

where n is the ridge number, increasing in the seaward direction (newer ridges). The position of the first (oldest) ridge is given at $x_c = 0$.

Equations (1) to (5) are solved using the Euler method and a time step Δt of 0.1 yrs over decades to centuries. A full list of the state variables are included in Table 4.1, while input parameters and descriptions, including a range of explored values, are shown in Table 4.2. The idealized starting dune and beach geometry is given by initial shoreline and dune crest locations x_s and x_c , dune volume A , and shoreface depth D_T . The beach has a flat slope and maintains

elevation with sea level Z . The active foredune is also considered to have constant front and back flank slopes Γ_1 and Γ_2 , which define the ridge shape. Additionally, for the purposes of field comparison, total subaerial volume is computed as the profile area of ridges above sea level Z .

Table 4.1 – State Variables

Symbol	Units	Description
t	T	Time
x_s	L	Shoreline Position
x_f	L	Foredune Front Toe Location
x_b	L	Foredune Back Toe Location
x_c	L	Foredune Crest Location
A	L ³ /L	Dune Cross-Section Volume (Area)
Z	L/T	Sea Level

Table 4.2 – Model Input Parameters

Symbol	Description / Unit Type	Fishing Point (Figs 6,7)	Parramore Island (Figs 8,9)
Q_s	Shoreface Flux	134 m ³ /m/yr*	1.6 to 15 m ³ /m/yr*
Q_D	Foredune Flux	13 m ³ /m/yr	0.7 m ³ /m/yr
L_C	Critical Ridge Spacing	109 m	117 m
L_S	New Foredune Shoreline Setback	5 m	5 m
Γ_1, Γ_2	Foredune Front/Back Flank Slopes	0.05 m/m	0.065 m/m
D_T	Depth of Shoreface	5 m	5 m
\dot{Z}	Rate of Sea-Level Rise	2 mm/yr	1 mm/yr

*Fishing Point sediment fluxes are derived from time-series analysis of shoreline and subaerial elevation change; Parramore Island fluxes are derived from morphological calibration. See sections 4.4.1 and 4.5.1 for additional input parameter discussion.

4.3.1 Exploration of Model Behaviors

Based on the theoretical framework of Psuty (2004) and a variety of field observations (Bristow & Pucillo, 2006; Nooren et al., 2017), the end-members of ridge and swale systems can be conceptualized under different sediment-input regimes. The fastest rates of progradation—relatively high beach flux and low foredune flux—should lead to numerous, low-elevation ridges or open sand flats. Conversely, the slowest rates of progradation—low beach flux and high foredune flux—should result in the formation of fewer, prominent ridges or a monolithic foredune. Additionally, observations of coastal systems such as Fishing Point (Figure 4.2) indicate that regularly repeating ridges of moderate elevation or ‘washboards’ should occur

between the aforementioned endmembers. Thus, in order to classify ridges in the field, and using the modeling framework, morphological members are categorized according to Figure 4.3.

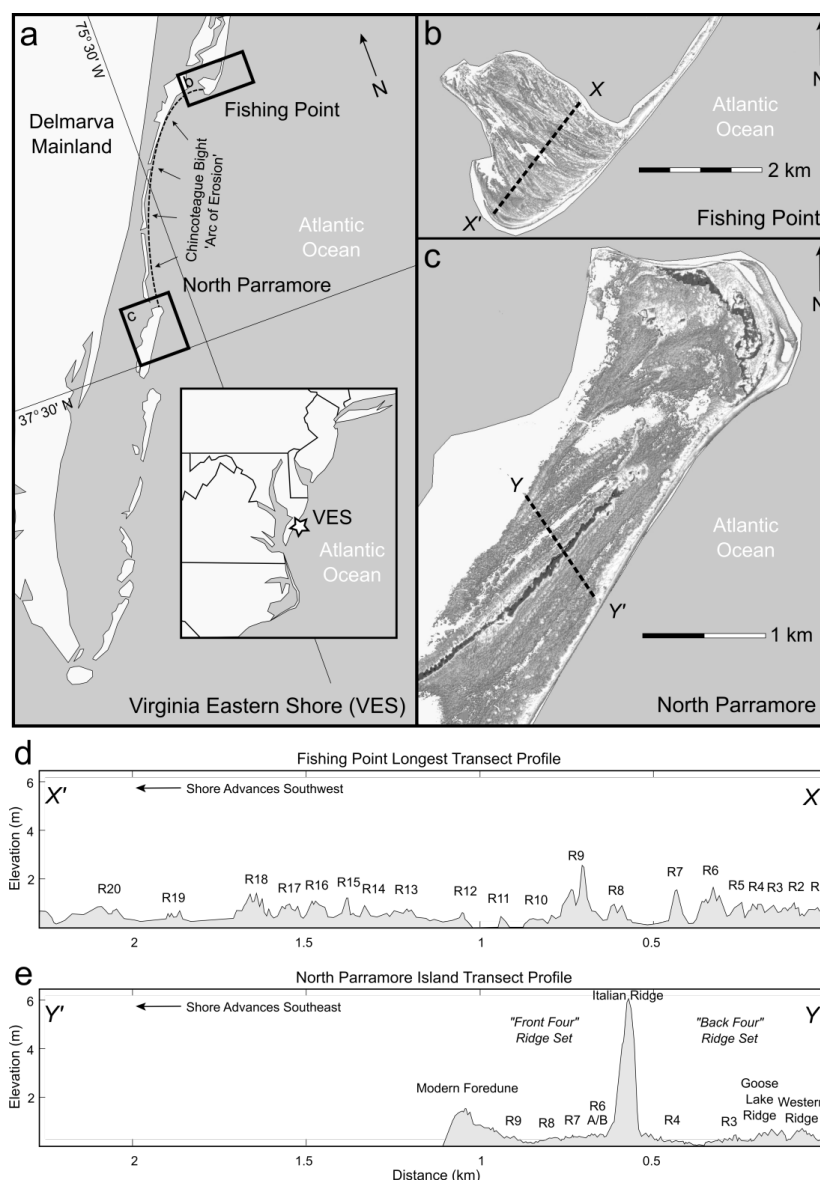


Figure 4.2 – (a) Map overview of the Virginia Eastern Shore (VES), at the southern end of the Delmarva Peninsula on the United States Atlantic coast. (b) Hillshaded LiDAR-derived digital elevation models of Fishing Point and (c) North Parramore Island, showing orientation of ridge and swale systems. Highest elevations on Fishing Point are > 3 m, while some points on North Parramore reach > 7 m above mean higher high water (MHHW). (d) Ridge-perpendicular transects of Fishing Point and (e) Parramore Island showing elevation profiles referenced to MHHW. Individual ridges are numbered from landward to seaward, unless otherwise named.

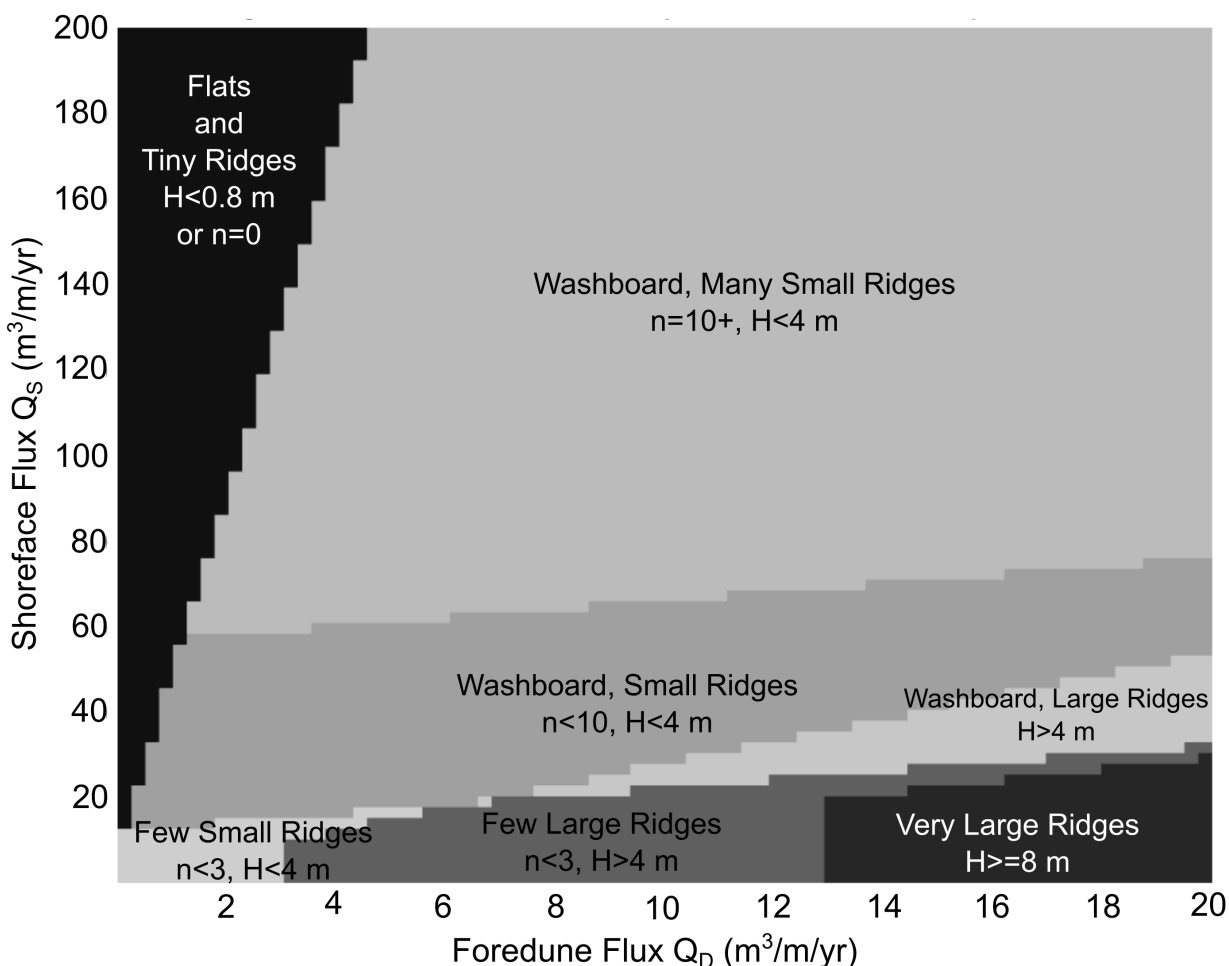


Figure 4.3 – Regime plot showing the types of subaerial ridge and swale patterns modeled over the timescale of Fishing Point (100 years) for combinations of shoreface fluxes Q_S and foredune fluxes Q_D . The characterization of ridge heights is based on the tallest ridges observed in the Virginia system (8 m). The rate of rise was set to 2 mm/yr, and the critical ridge spacing was 109 m. To distinguish patterns, n =number of ridges and H =height of ridge.

In order to explore endmember ridge morphologies in the context of input fluxes, differences in the magnitude of Q_S versus Q_D are considered from natural systems. Based on the work of Himmelstoss et al. (2017), Q_S values fall within the range 0-200 $\text{m}^3/\text{m}/\text{yr}$. Additionally, Q_D values occur within the range 0-20 $\text{m}^3/\text{m}/\text{yr}$, as determined from a global compilation of foredune accretion rates (Appendix Table A4.1).

Within the modeled input space, washboards can be broadly created when Q_S is approximately an order of magnitude larger than Q_D (Figure 4.4a). Modulating this sediment-

input regime by increasing Q_S by another order of magnitude yields sand flats and tiny ridges (Figure 4.4b). Such morphologies are readily observable in the field: central Parramore Island contains a large swale-like structure approximately 0.7 km wide (Raff et al., 2018), and in Sandy Hook (New Jersey, USA), both wide, inter-ridge swales and sand flats that extend up to 400 m in width are present (National Park Service, 2016). Conversely, reducing Q_S to within the same order of magnitude as Q_D yields relatively large ridges (Figure 4.4c); this morphology mimics that of the 7+ m high Italian Ridge located on northern Parramore Island (Figure 4.2c/e).

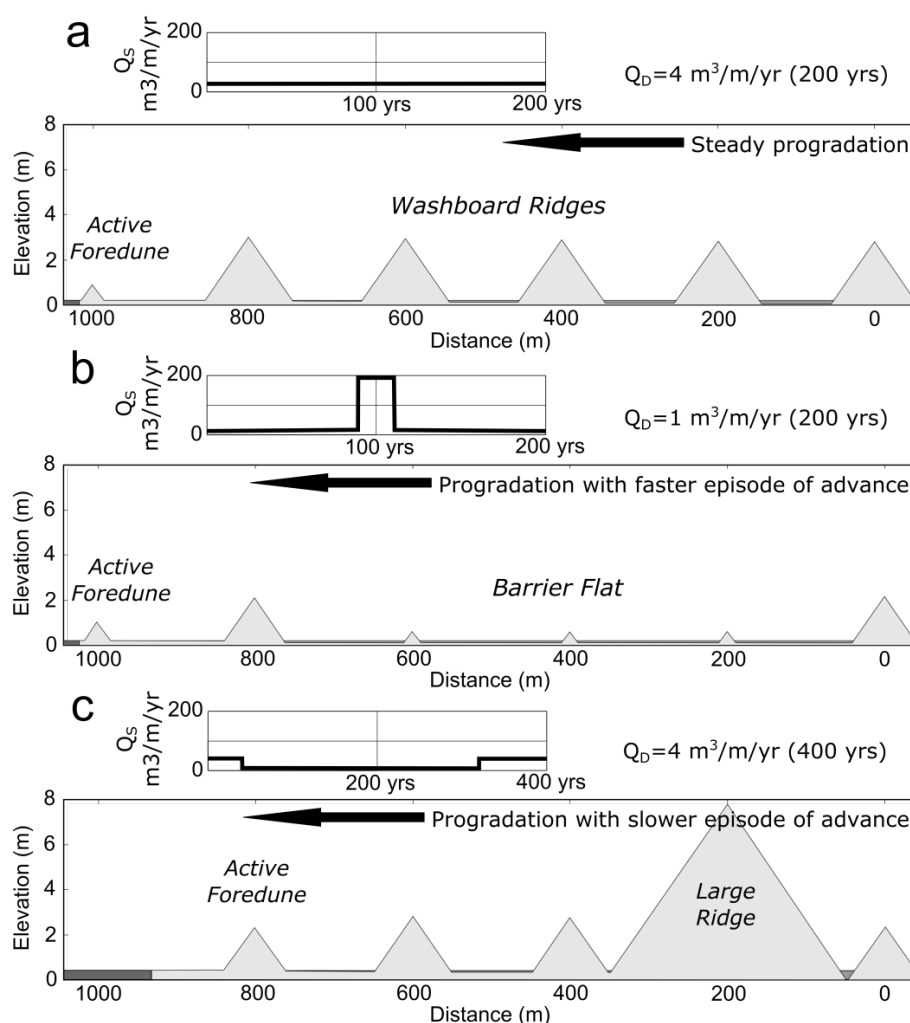


Figure 4.4 – Modeled pattern of cross-shore changes in ridge geometry resulting from adjustments in the rate of progradation by modulating Q_S . (a) Washboard pattern of regularly spaced ridges, with steady Q_S . (b) Episode of fast progradation that suppresses ridge height and results in a wide flat on the barrier platform (c) Sustained episode of slow progradation, allowing time to build a large, complex ridge. For all cases, $L_C = 200 \text{ m}$, $L_S = 5 \text{ m}$, with rate of rise of 1 mm/yr.

4.3.2 Field Comparison

The sediment budget history of a set of beach and foredune ridges is modeled as a series of morphological patterns with distinct flux regimes, generating ridge sets with characteristics that can be compared with measurements of field sites. Specifically, measurements readily captured by the modeling framework include the subaerial volume of ridges, the number of ridges formed during progradation of the shoreline by a given distance (a function of ridge spacing), and the height of ridges. These are characteristics readily measurable using LiDAR data and other geophysical approaches. In this study, elevation profiles are measured perpendicular to the ridge system at the two Virginia field sites using the 2016 CoNED (Coastal National Elevation Database) LiDAR digital elevation model (Appendix Figure A4.1; A4.2). Ridges in these systems do not have uniform crests as a result of erosion/reworking by waves, wind, and vegetation, and/or incomplete initial amalgamation (Raff et al., 2018). As such, they commonly display mottled surfaces consistent with vegetation-induced nebkha (coppice dunes), wave-induced washarounds, or mounds formed through a combination of processes. To account for this alongshore variation, ridge crests are delineated in plan-view using high-resolution LiDAR-derived elevation maps (*e.g.*, Appendix Figure A4.15). Furthermore, to make a comparison with the two-dimensional model, elevation profiles are averaged every 10 to 20 m across a 100 m wide (alongshore) swath to produce a profile that reflects a mean cross-shore ridge structure along the study transects (Figure 4.2d/e). Critical ridge spacing L_C is measured by taking the average crest-to-crest spacing from the mean profile.

To correlate LiDAR-derived elevations and subaerial ridge volumes with model outcomes, the lowest elevation of swales is used as a common point of reference. LiDAR measurements along the Virginia barrier islands indicate that the base of swales, and in particular

of those now flooded by rising sea level, are at an elevation of approximately mean higher high water (MHHW) for both Parramore Island and Fishing Point (Appendix Table A4.2). This elevation corresponds to the tidal inundation boundary that NOAA uses to map the marsh-upland transition (NOAA 2017), and has been used in GIS-based studies to approximate the limit of upland marsh migration (Archbald, 2010).

Finally, in determining the setback distance of incipient foredune ridges for the model simulations, it is noted in Vinent and Moore (2013) that foredune height scales in proportion to setback; ridges become capable of growing (initially) larger as the beach area grows in conjunction with increasing aeolian sand fetch. For this investigation, $L_S=5$ m is used, as Vinent and Moore (2013) show that a setback of 10 m for a reasonable range of shear stress values produces a ridge approximately 1-2 meters in height—double the height of the lowest ridges observed at field sites.

4.4 Model Validation: Analysis of the Growth of Fishing Point, Virginia

To validate the model framework, the historical record available from Fishing Point is used to conduct a time-series analysis of Q_S and Q_D , and supply these directly to the model. This allows a comparison of morphological characteristics from modeled cross-sections directly to field observations. A subsequent sensitivity analysis of morphological characteristics based on mean fluxes through time for Fishing Point demonstrates that an average long-term sediment budget can be determined based on measurements of field characteristics alone. In section 4.5, this insight is used to derive Q_S and Q_D for morphological patterns of ridges at Parramore Island, where construction of a time series of ridge development is not possible from existing data.

4.4.1 Fishing Point Overview

Fishing Point (Figure 4.2b/d) is a southward-prograding spit constructed at the southernmost point of Assateague Island. It receives sediment through southerly longshore transport at a rate of $0.16\text{--}1.1 \times 10^6 \text{ m}^3/\text{yr}$ (Finkelstein, 1983; Headland et al., 1987; Moffat & Nichol, 1986). Coast and Geodetic survey charts (Appendix Figure A4.3; A4.4) indicate that its subaerial growth initiated sometime after the mid-1850s, although formation of the recurved spit end, and associated coast-perpendicular ridge development, did not begin until the early 20th century. Between 1908 and the present, Fishing Point prograded nearly 2.5 km through the amalgamation of at least twenty distinguishable foredune ridges (Appendix Table A4.3, Appendix Figure A4.5). The upper surface of ridges tends to be irregular, likely as a result of incomplete amalgamation or modification by waves and vegetation.

Survey charts show former seabed depths in the area of Fishing Point were generally around 5 m, providing an estimate of the modern shoreface thickness. Likewise, a sediment core approximately located at the 1902 shoreline of the spit (Halsey, 1978) indicates that barrier sands are ~5 m thick. Based on LiDAR and aerial images (Figure 4.2, Appendix Figure A4.5), the overall ridge morphology is relatively regular, with ridges averaging 1 m in height and with an average crest spacing L_C of 109 m. Generally, ridges are symmetric, with front and back slopes near 0.05 m/m (Appendix Figure A4.6). Total subaerial cross-sectional volume through the longest ridge-perpendicular transect is $1300 \text{ m}^3/\text{m}$.

Fishing Point experienced a mean, long-term rate of progradation (southerly elongation) of ~24 m/yr, with a corresponding beach sediment flux of ~120 $\text{m}^3/\text{m}/\text{yr}$ (Appendix Figure A4.7). However, the maximum progradation rate estimated from Landsat imagery and nautical charts over the last 35 years is 41.8 m/yr, and possibly higher in recent years. This increase in

progradation may be related to a shift in sediment depocenter along the Fishing Point shoreline (Hein et al., 2019) and/or beach nourishment on the northern end of Assateague Island, ongoing biannually since 2002 and supplemented by berm reconstruction approximately every four years (Smith et al., 2016). Nourishment volume lost to longshore transport updrift of Fishing Point totals almost 380,000 m³/yr (Smith et al., 2016). If that updrift volume is completely distributed over the actively prograding face of the southern-most part of the spit (~1.5 km alongshore), the theoretical modern progradation rate is 51 m/yr, not considering additional inputs (e.g., cross-shore fluxes from the shallow shelf). Presumably, some portion of this missing volume is also bypassed across Chincoteague Inlet to islands further downdrift.

4.4.2 Deriving Input Fluxes from the Historical Record

In model simulations, sediment fluxes to the beach Q_S and the foredune Q_D during the historical period of growth of Fishing Point are given as time-varying input parameters which are derived from historical imagery. Q_S values are computed using a 95-year (1919–2014) record of digitized former shorelines. By overlaying shoreline locations on the cross-ridge elevation profile (Appendix Figure A4.11), it is possible to divide the profile into intervals of sediment delivery, and calculate a time-averaged shoreface flux (Figure 4.5a).

Determining foredune fluxes Q_D requires a means by which to separate foredune ridge sand from beach sand. If minimal impact from sea-level rise is assumed, the simplest solution is to use MHHW as a threshold elevation between the two units. However, foredune emplacement, driven by a complex interplay of wave and aeolian transport, lags the advance of the shoreline. As a result, changes in subaerial volume cannot be calculated directly from sediment delivery to the beach.

To compute foredune fluxes through time, a timeline of foredune emplacement is developed independent of changes in shoreline position. Historic aerial photos are used to determine the first known date individual ridges or sets of ridges became relict; that is, when they are no longer adjacent to the beach or substantially accreting. High-resolution aerial photos extending back to 1958 provide nearly six decades of observations on which to develop a progression of ridge abandonment (Appendix Figure A4.5) and a corresponding quantification of subaerial volumetric growth based on the transect elevation profile (Appendix Figure A4.12). Foredune fluxes are then calculated over a 58-year period ending in 2016 (Figure 4.5b).

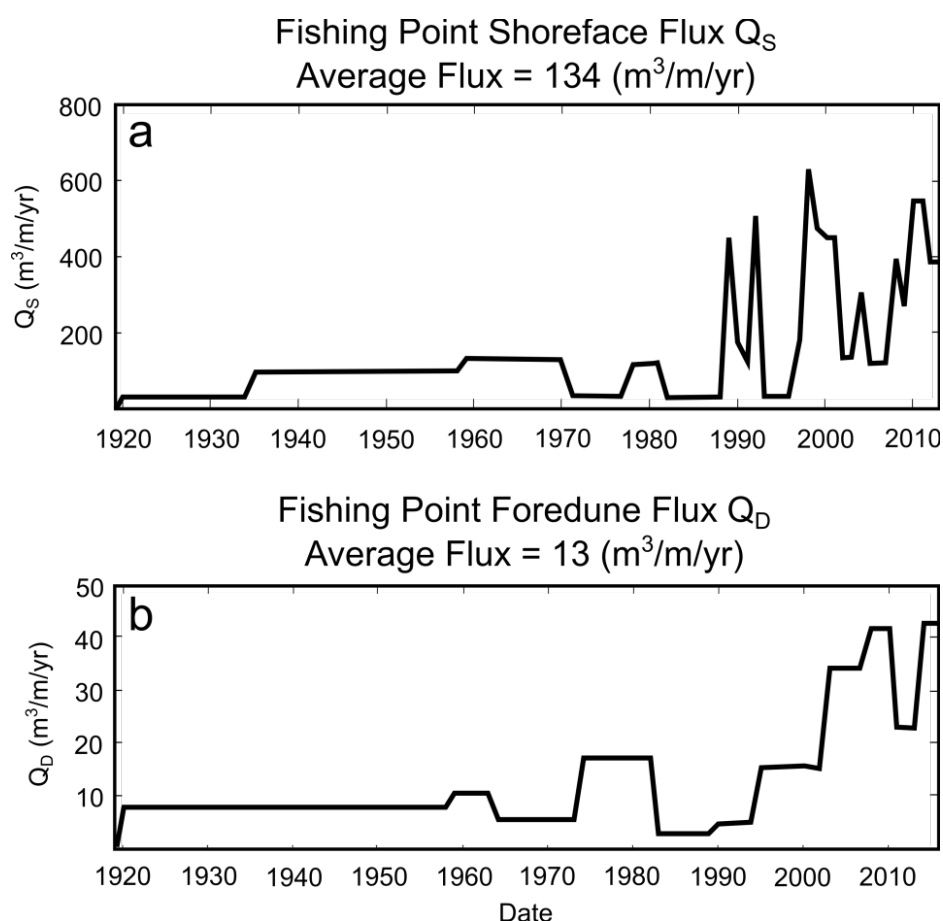


Figure 4.5 – (a) Calculated shoreline fluxes for the Fishing Point transect for 1919–2013. The average flux for this period is 134 $\text{m}^3/\text{m}/\text{yr}$. (b) Calculated foredune fluxes for the Fishing Point transect for 1958–2016. The average flux for this period is 13 $\text{m}^3/\text{m}/\text{yr}$.

4.4.3 Modeled Fluxes and Morphology

The growth of Fishing Point was evaluated in the model framework using a time series of input fluxes derived from the historical record and compared to field observations using average ridge height, ridge cross-sectional volume, and number of ridges within the distance prograded by the shoreline (Table 4.3, Appendix Table A4.3). Over 95 years, the model produced washboard-like morphology with characteristics measured to within the same order of magnitude as field estimates (Figure 4.6b). The greatest discrepancy between modeled morphology and field measurements occurs for dune height: the model produces ridges approximately 50% taller than those measured from LiDAR (Table 4.3).

Table 4.3 – Modeled vs. Field Measurements

Parameter	Field	Model	Diff. Field - Model	% Diff. to Field
<i>Fishing Point Time Series</i>				
Total Cross Section Volume (m ³ /m)	1295	1073	222	-16.2%
Average Ridge Height (m ³ /m)	1	1.5	-0.5	+50%
Distance Prograded (m)	2290	2181	109	-5%
Number of Ridges	20	20	0	0%
<i>Fishing Point Average Fluxes</i>				
Total Cross Section Volume (m ³ /m)	1295	1214	82	-6%
Average Ridge Height (m ³ /m)	1	1.6	0.6	+60%
Distance Prograded (m)	2290	2237	53	-9%
Number of Ridges	20	21	-1	+5%
<i>North Parramore “Back Four” (200 years)</i>				
Total Cross Section Volume (m ³ /m)	140	133	7	-5%
Average Ridge Height (m ³ /m)	0.6	1.3	-0.7	+110%
Distance Prograded (m)	500	483	17	-3%
Number of Ridges	4	4	0	0%

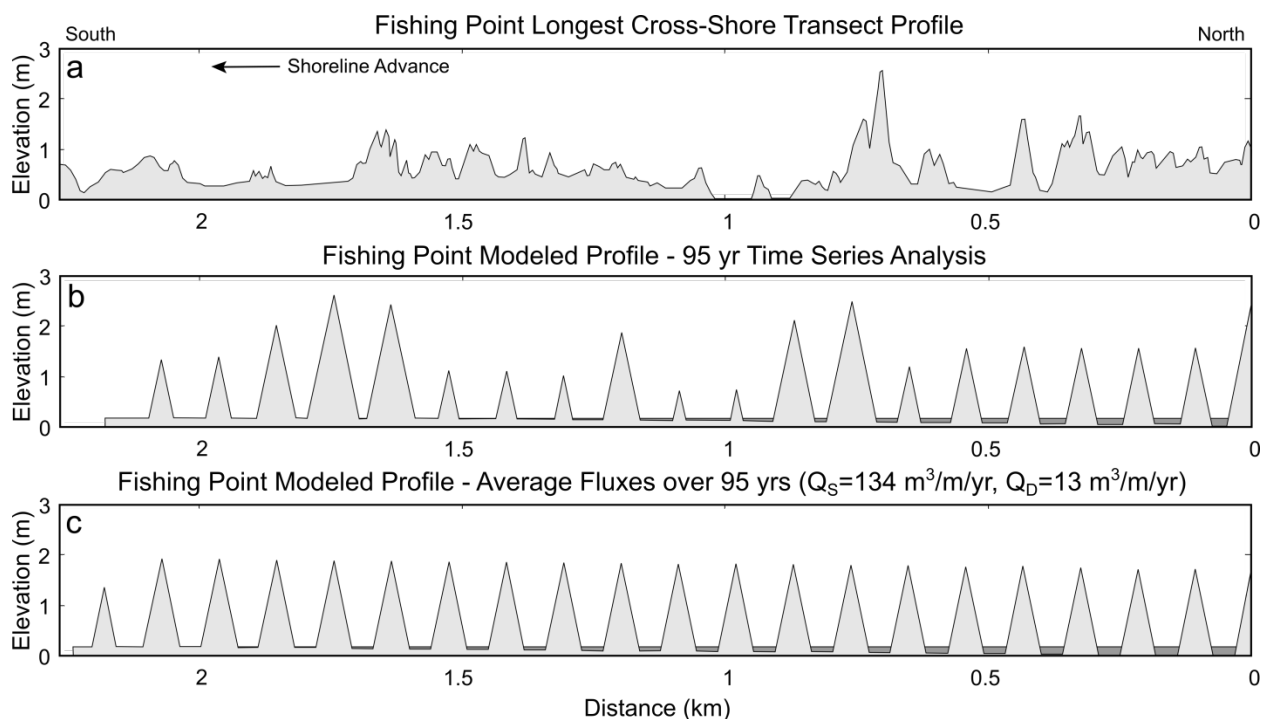


Figure 4.6 – (a) Elevation cross section of Fishing Point along its widest dimension measured from LiDAR data. (b) Modeled profile of Fishing Point using a time series of shoreface and foredune fluxes derived from the historical record. While the average height of the modeled profile is 50% taller than the field average, remaining parameters are within 20% of field measurements (Table 3). (c) Modeled geomorphological profile of Fishing Point using a time-invariant shoreface flux Q_S of $134 \text{ m}^3/\text{m}/\text{yr}$ and a foredune flux Q_D of $13 \text{ m}^3/\text{m}/\text{yr}$, the long-term average flux values derived from the historical record.

A sensitivity analysis of the input flux space was also undertaken (Figure 4.7), allowing a range of average fluxes that produce a more generalized washboard pattern to be constrained (Figure 4.6c). Actual measurements of morphologic characteristics are highlighted as key contours and are used to construct a morphological calibration plot (Figure 4.7e), which identifies a region of similarity where flux combinations generally reproduce measurements from the field. For Fishing Point, average historical Q_S and Q_D values occur within this region of fluxes, near the contour for subaerial ridge volume. Comparison of modeled average height and spacing values (Figure 4.6c) to remote observations (Table 4.3) produces results similar to the time-series model-field comparisons, including the discrepancy in ridge height. While the model does not fully capture real-world ridge heights, it reasonably reproduces the overall sediment balance, as well as the partitioning between subaerial and subsurface volumes.

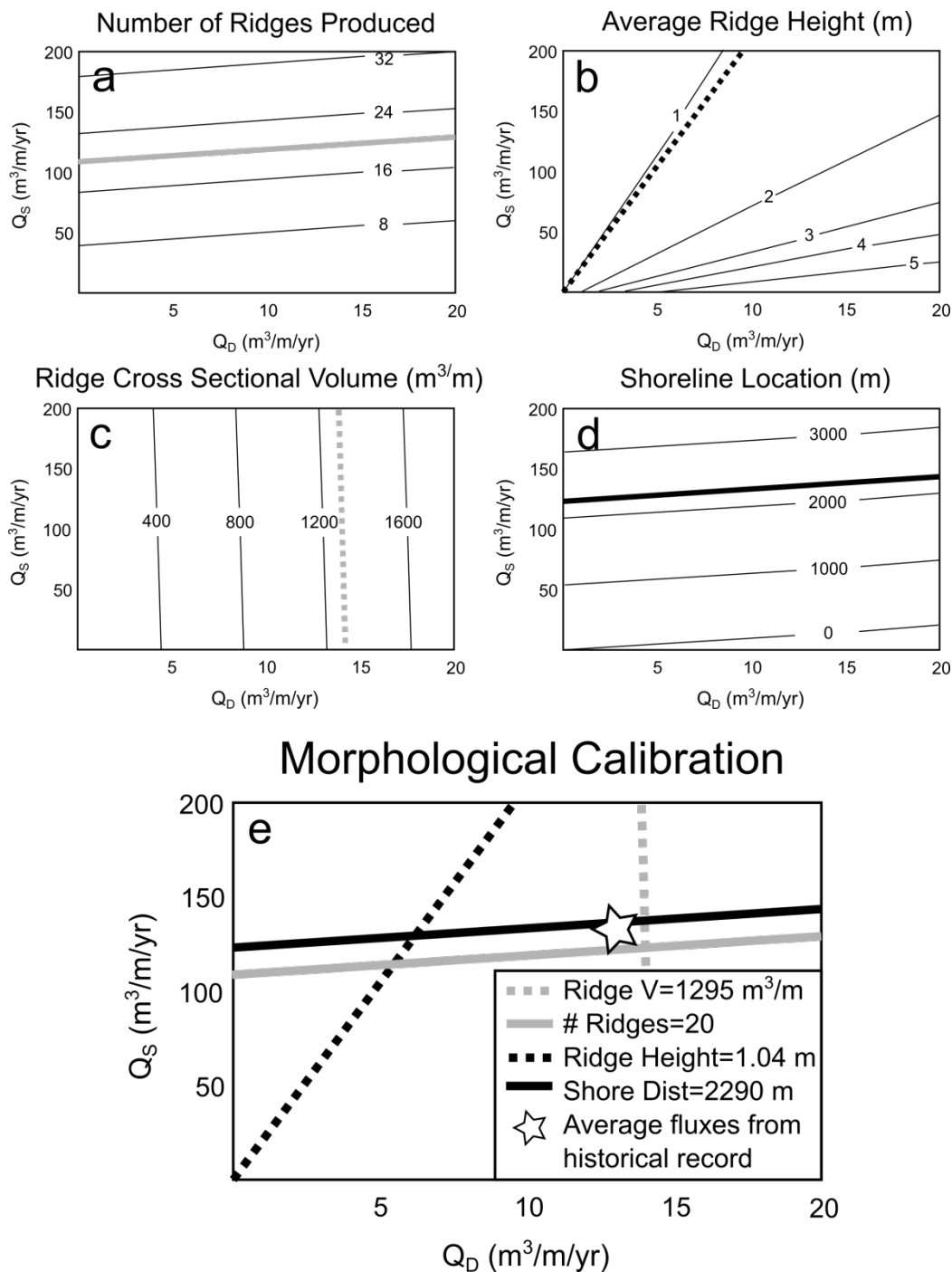


Figure 4.7 – Sensitivity plots of (a) number of ridges produced, (b) average ridge height, (c) cross-sectional dune volume, and (d) final shoreline location, as a function of input-flux combinations. Bolded contours represent measurements of the four morphologic parameters obtained from the field at Fishing Point. (e) A morphological calibration in which the area bound by the intersection of the four parameter lines—the *region of similarity*—indicates the range of flux combinations that produce results similar to field measurements.

4.5 Model Application: Reconstructing the Growth of Parramore Island, Virginia

Field-based model validation demonstrates that use of characteristics of beach/foredune ridge morphology may allow for the reconstruction of long-term shoreface sediment budgets, and notably, the magnitude of time-varying sediment fluxes. To evaluate the capabilities of the model, it is next applied to an investigation of Parramore Island. A limited chronology based on OSL and radiocarbon dating is used to constrain the development of the complex foredune ridge system on the northern half of the island. Then, using morphological characteristics observed in the field, the model is used to calibrate the range of input Q_S and Q_D values for sections of the ridge and swale complex and apply this to simulate development of a cross-island, two-dimensional morphological profile for field comparison.

4.5.1 Parramore Island Overview

Parramore Island (Figure 4.2c/e) is 11 km long and located ~36 km south of Fishing Point. It is a historically rotational (undergoing erosion of its southern end and progradation at its northern end), mixed-energy barrier island that, prior to the early 20th century, maintained a drumstick-like shape (McBride et al, 2015, Deaton et al., 2017). Humans have never occupied the island continuously, and it has existed in a near-natural state since it was first documented (Rice et al., 1976).

Northern Parramore Island contains two sets of northeast- to southwest- striking, low-relief washboard ridges (the “Back Four” and “Front Four” ridges) that flank a large, central ridge (Italian Ridge). Whereas the average elevation of northern Parramore is ~1.1 m (MHHW), the maximum elevation along Italian Ridge is > 7 m (Figure 4.2, Appendix Table A4.4). Remaining ridges reach generally no more than 60 cm in elevation. Despite hummocky topography, the low washboard ridges have an average profile that is triangular and slightly

asymmetric. The westernmost “Western Ridge” is the best preserved, with a front slope of 0.012 m/m and a back slope of 0.018 m/m (Appendix Figure A4.8). The slopes of Italian Ridge are an order of magnitude steeper, at 0.125 m/m and 0.11 m/m (Appendix Figure A4.9). In the modeling exercise, a mean slope for Parramore Island is set at 0.065 m/m, which attempts to account for the difference in slope between Italian Ridge and its smaller counterparts (Appendix Figure A4.13 depicts a sensitivity analysis of ridge height as a function of slope and shoreface accommodation). Regressive barrier island sands beneath the ridges extend to 4.5-5.0 m below MHHW, and the underlying transgressive surface is nearly horizontal from the modern foredune to west of Italian Ridge, located about 600 m landward (Raff et al., 2018).

Though once transgressive, landward migration of Parramore Island ended ~1000 years ago, and has been followed by a period of slow progradation lasting at the northern end of the island until the mid-1950s (Raff et al., 2018). Italian Ridge was dated with OSL to about 200 years ago (this likely represents the time at which this former foredune became inactive [Raff et al., 2018]), and historical maps indicate that the northern Parramore shoreline reached its maximum seaward position by the late 1800s (Rice et al., 1976).

4.5.2 Modeled Fluxes and Morphology

Parramore Island presents an opportunity to apply the model to a site with a poorly constrained pre-historic record of growth to explore Q_S and Q_D flux combinations that reproduce patterns of observed ridge morphology. Due to the location of age control points, the growth of the “Back Four” washboard ridges and Italian Ridge are considered, which together developed over a period of ~800 years from the inception of Western Ridge (1000 C.E.) to the abandonment of Italian Ridge (1800 C.E.). The initiation of growth for Italian Ridge, a timestamp which would constrain the period of formation of the “Back Four”, is unknown, but

an informed guess is possible. The western four ridges are morphologically similar to the eastern (seaward) four ridges, which developed over a period spanning at least the mid-1700s to the early 20th century (Rice et al., 1976). This morphological resemblance suggests a similarity in formation processes and time; from this a period of growth of *ca.* 200 years is estimated for the development of the “Back Four” ridges. An upper limit of 600 years is applied as a maximum period of growth.

Assuming a 200-year period of development, the “Back Four” washboard was evaluated in the model framework using field-derived morphological characteristics (Table 4.3). From morphological calibration plots (Figure 4.8), a Q_S and Q_D flux combination ($Q_S = 13 \text{ m}^3/\text{m/yr}$ and $Q_D = 0.7 \text{ m}^3/\text{m/yr}$) was selected that adequately reproduced subaerial volume, distance prograded, and number of ridges produced. The morphological characteristics of the washboard ridge system resulting from this flux combination are within 5% of bounds from field measurements, except for average ridge height (Table 4.3).

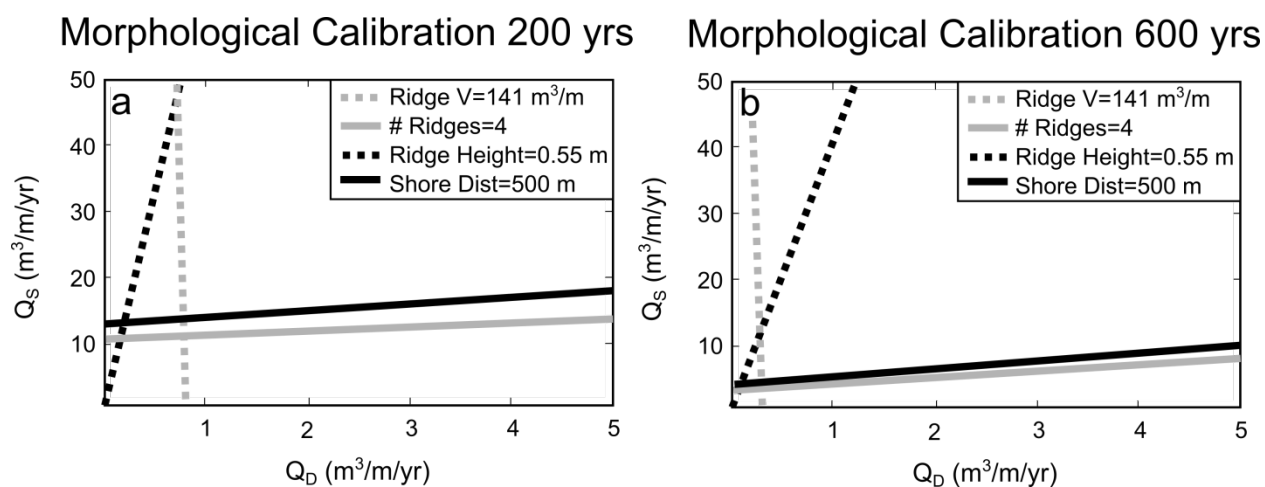


Figure 4.8 – Evaluation of the “Back Four” ridges of North Parramore Island using morphological calibration plots to constrain the balance of Q_S and Q_D fluxes consistent with field sites parameters over timescales of (a) 200 years and (b) 600 years. The area bound by the intersection of the four parameter lines—the *region of similarity*—indicates the range of flux combinations that produce results similar to the field.

Calibration plots (Figure 4.8) show the range of shoreface flux Q_S and foredune flux Q_D combinations that produce results consistent with the morphology of the western and eastern washboard ridge sets on Parramore Island are an order of magnitude smaller than those determined for Fishing Point. This result implies the shoreface flux must be even smaller to create the 7 m tall Italian Ridge. Using a constant Q_D of $0.7 \text{ m}^3/\text{m}/\text{yr}$, and conserving all other input parameters, an attempt was made to reconstruct the full profile of north Parramore Island, allotting 200 years to build the “Back Four” washboard ridges, 600 years to build Italian Ridge, and another 200 years to build the “Front Four” washboard ridges. The model best reproduced the morphology of Italian Ridge when Q_S was reduced by an order of magnitude, to $1.6 \text{ m}^3/\text{m}/\text{yr}$. The “Front Four” ridges were then approximated with Q_S values returned to $15 \text{ m}^3/\text{m}/\text{yr}$ (Figure 4.9).

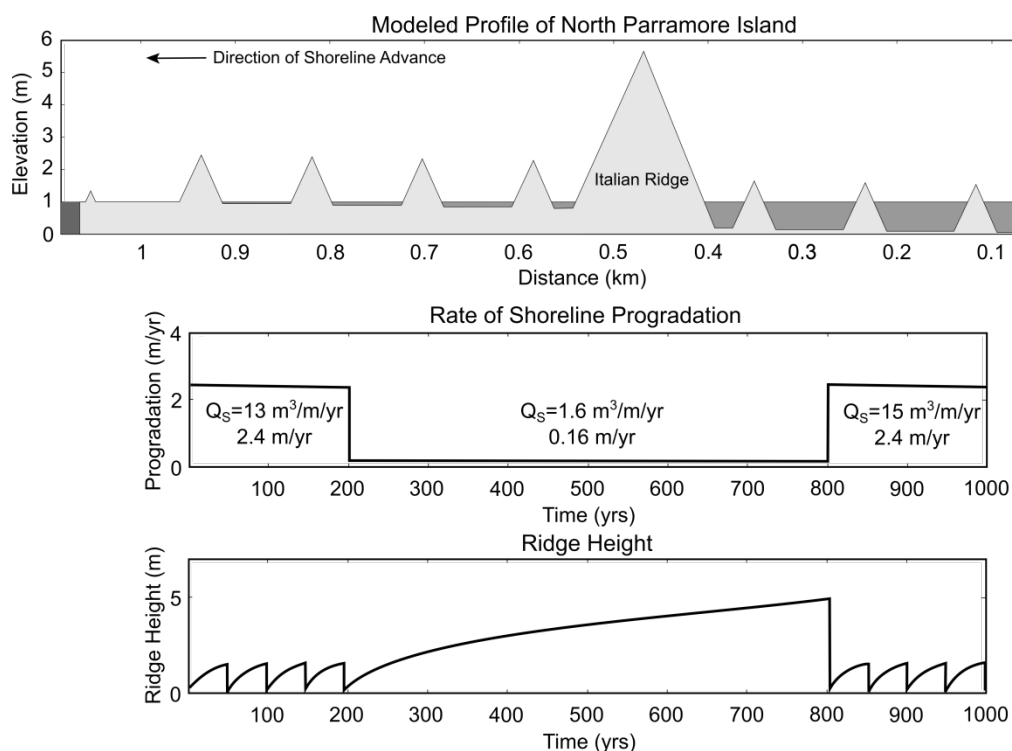


Figure 4.9 – (a) Modeled geomorphological profile of North Parramore Island using a shoreline flux Q_S of $13 \text{ m}^3/\text{m}/\text{yr}$ for 200 years, $1.6 \text{ m}^3/\text{m}/\text{yr}$ for 600 years, and $15 \text{ m}^3/\text{m}/\text{yr}$ for the last 200 years—with a constant foredune flux Q_D of $0.7 \text{ m}^3/\text{m}/\text{yr}$. Changes in (b) rate of shoreline progradation and (c) ridge height are shown for the 1000 yr run time of the model.

Historically, the average progradation rate of north Parramore Island was 1.9 m/yr from 1852 to 1955 (Rice et al., 1976); this closely matches the progradation rate (2.4 m/yr) given by the model (Figure 4.9b). However, this investigation does not account for the increased rate of sea-level rise since the late 1800s: tide gauges in the vicinity of the Delmarva Peninsula indicate the current rate of rise is between 3 and 5 mm/yr (Boon and Mitchell, 2015). Instead, the model applies the long-term pre-industrial estimate of 1.0 mm/yr (Engelhart and Horton, 2012) as a constant rate throughout the period of development of Parramore Island. This difference may partially account for the faster (by 0.5 m/yr) rate of progradation reproduced by the model, as overall vertical accommodation available in the modeled ridge system is $\sim 30\text{-}50\text{ m}^3/\text{m}$ less than that created by sea-level rise in the real-world system (See Appendix Figure A4.14 for additional sea-level sensitivity analysis).

One component not captured by the model is the development of the modern transgressive foredune ($\sim 1.6\text{ m}$ elevation), which on northern Parramore has formed over the last ~ 70 years. While the model does not capture transgression, Psuty (2004) shows that transgressive foredunes probably occur only for beaches undergoing relatively slow erosion: the landward transport of sediment has to outpace losses on the seaward edge, otherwise the foredune quickly erodes. As a consequence, transgressive foredunes should (hypothetically) not exist under input conditions which differ significantly from those which occur under static or slow shoreline progradation. Coincidentally, the height of the transgressive foredune in the modern Parramore system roughly agrees with model predictions for seventy years of ridge growth.

For Italian Ridge, it is possible that long-term progradation was interrupted by one or more periods of beach erosion and foredune transgression, but sediment input at the beach during such a period may well have been within the same order of magnitude as modeled values. (There

is presently no evidence to indicate this in GPR data or historical mapping [Raff et al., 2018], although more detailed investigation may prove otherwise.) The plan-view morphology (Figure 4.2c) also suggests such erosion probably did not occur over long timescales, because the orientation of the ridge axis is effectively parallel with the ridges landward of Italian Ridge, a feature not shared with the sub-parallel modern transgressive foredune. Changes in the orientation of transgressive foredunes (relative to relict ridges) are common along other beach-ridge plains (Oliver et al., 2017a; Psuty, 2004), including on nearby Assateague Island. Only the northern and southern ends of Italian Ridge are shifted out of alignment with adjacent ridges, likely as a result of erosion associated with inlet activity (Raff et al., 2018).

4.6 Discussion

4.6.1 Parramore Island

The planar, near-horizontal transgressive surface upon which Parramore Island prograded makes it an ideal site to record externally mediated changes in shoreface sediment fluxes, as accommodation effects such as growth into an offshore-deepening basin (*e.g.*, Bristow & Pucillo, 2006) or into an infilling bay (*e.g.*, Hein et al., 2016) are minimal. Hence, the rate of progradation of this barrier island should reflect only the rate of sea-level rise and net (longshore and cross-shore inputs minus long-term erosion) external sediment fluxes. Assuming long-term (multi-decadal through centennial) shoreface sediment fluxes are primarily derived from sediment delivered through the southerly longshore transport system, then changes in the progradation rate of northern Parramore Island—and by extension, changes in the morphology of associated foredune ridges—reflect changes in the rate of allogenic sediment delivery. Along the Virginia barrier islands, longshore sediment fluxes are controlled by such factors as updrift inlet configurations and sediment-bypassing processes (FitzGerald, 1984), sediment trapping in flood-

tidal deltas associated with ephemeral inlets (Seminack and McBride, 2015), variations in ebb-tidal delta storage (Fenster et al., 2016), and disruptions in sediment supply associated with the growth and erosion of updrift spits and islands (McBride et al., 2015; Raff et al., 2018). For example, Fishing Point itself—located updrift of the mixed-energy barrier islands to the south—traps sand at a rate of up to $1.1 \times 10^6 \text{ m}^3/\text{yr}$ (Moffat & Nichol, 1986), removing it from the longshore transport system. Without this substantial sediment sink, an additional $\sim 11.6 \text{ m}^3/\text{m}/\text{yr}$ of sand could be distributed to the shoreface of all islands to the south ($\sim 95 \text{ km}$ of beach). This flux is significant: this investigation shows that the net growth of Parramore Island has been slow, on the order of a few meters per year over the last thousand years, and operating on a net cross-shore sediment budget of $15 \text{ m}^3/\text{m}/\text{yr}$ or less.

The results of this study suggest Parramore Island is a naturally marginal system (only barely maintaining a state of progradation given historical sediment fluxes and rates of sea-level rise), and therefore particularly vulnerable to changes in sediment fluxes consistent with the magnitude of trapping at Fishing Point. This investigation supports the hypothesis proposed by Raff et al. (2018) that the Virginia barriers are subject to rapid state transitions (between net erosion, progradation, and migration) resulting from downdrift-cascading sediment supply deficits.

4.6.2 Broader Application

Globally, beach/foredune ridge systems are diverse and complex. Some have morphologies similar to Fishing Point, characterized primarily by repeating sets of low-elevation ridges (*e.g.*, Samsø, North Sea [Hede et al., 2015]; Pinheira, Brazil [Hein et al., 2013]), or are more characteristic of Parramore Island, dominated by low-elevation ridges with rare, much higher individual ridges (*e.g.*, Miquelon-Langlade, France [Billy et al., 2014]; Seven Mile Beach,

Australia [Oliver et al., 2017a]). Application of the model to each of these progradational systems could allow for quantification of sediment-flux conditions associated with their development, potentially providing insights on sensitivity to future environmental change.

In particular, this investigation's findings may be most applicable to strandplains, broad accumulations of sediment formed as beach and foredune ridges oriented approximately parallel to the coastline (Roy et al., 1994). These are typically characterized by long-term, continuous progradation of successive ridges and swales. As compared with beach/foredune ridge systems on barrier islands, strandplain ridge systems are less likely to be punctuated by inlet activity, and are particularly common in regions of stable or falling sea level (Tamura, 2012). Variability in progradation rates observed across strandplain systems has been attributed to differences in coastal slope, sediment supply, accommodation, wave energy, and sea-level history (Choi et al., 2014); the model used here could provide quantitative insight into the role of each of these. For instance, the punctuated growth of strandplain systems like Seven Mile Beach, Australia has been linked with variations in shoreface fluxes driven by possible changes in the rate of sea-level rise (Oliver et al., 2017a). A similar deceleration in shoreline growth at Pedro Beach, Australia may be linked to changes in accommodation (Oliver et al., 2018). A possible concern is that the rates of strandplain progradation (0.4–1.8 m/yr [Bristow and Pucillo, 2006], [Brooke et al., 2008], [Hein et al., 2016]) are generally lower than those observed in the barrier island study sites. However, as demonstrated through application to Parramore Island, the model can be used at sites undergoing slower progradation (*i.e.*, 0.16 m/yr; $Q_S = 1.6$ m/yr), particularly if corresponding foredune fluxes are also low (*i.e.*, $Q_D = 0.7$ m/yr). Furthermore, strandplains can experience episodes of progradation similar to those demonstrated in the initial validation of the model (*e.g.*, ~7.8 m/yr; Bristow and Pucillo, 2006).

4.6.3 Considerations and Future Work

The model used in this investigation partitions subaerial sediment volume into idealized ridge geometries, and so does not yet capture impacts associated with vegetation or erosional reworking. As such, field calibration requires an assumption of a high degree of preservation of ridge morphologies. For example, segmentation of foredune ridges by former inlets further south along Parramore Island (Raff et al., 2018) renders that portion of the island ridge system unsuitable for model application. However, this investigation demonstrates that through averaging of elevations of ridge transects across an alongshore swath, it is possible to adequately reconstruct topographic profiles of even moderately degraded ridges. Specifically, this investigation suggests the number of topographic profiles used to develop an alongshore-average profile should scale with ridge slopes: broad, gently sloping ridges (northern Parramore) require fewer profiles to integrate than steeper, more discrete ridges (Fishing Point).

Among the field parameters used to perform morphological calibrations, this investigation's implementation of ridge height could be further refined. For example, an average, site-wide ridge slope for Fishing Point and Parramore Island is used to inform model geometry, and results generally overestimate height. Examining a sensitivity analysis of modeled ridge heights versus slope (Appendix Figure A4.13) shows that, in the example of the Parramore Island 'Back Four' ridges, using an island-averaged slope (0.065 m/m) could produce ridges slightly more than 0.5 meters taller than would be produced by more exact slope measurements of specific ridges. While this is a small deviation, it is within the same magnitude as the actual ridge heights, which suggests the triangular idealization of ridge geometry is less a source of discrepancy than choice of slope. However, for sustained washboard patterns with a larger number of ridges (*e.g.* Fishing Point), this outcome could present challenges if ridge slope varies

considerably from ridge-to-ridge. One possibility is that, because the foredune ridges along Fishing Point are more spatially discrete than those on Parramore, deviations in ridge slope occur more readily from wind/wave reworking during and following ridge formation.

Finally, the model can be reconfigured in a variety of ways to account for other subaerial and subaqueous processes/geologic controls. For the field sites evaluated in this study, a constant seabed elevation and rate of sea-level rise are employed, but the model is already built to investigate changes in accommodation through, for example, non-uniform offshore slopes (growth into deep basins or shallowing bays) or alterations in the rate and/or direction of sea-level change (Appendix Figure A4.14). It can thus be readily applied to the many well-studied beach/foredune ridge plains formed in regimes of sea-level fall (*e.g.*, Bristow and Pucillo, 2006; Hein et al., 2013, 2016; Oliver et al., 2017a). Future extensions could also include grain-size partitioning, stochastic storm/episodic erosion, and conversion of prograded ridges to transgressive dunes—potentially important considerations discussed by Billy et al. (2014) and Oliver et al. (2017a), among others.

4.7 Conclusions

This investigation demonstrates a simple framework to quantify the magnitude of changes in cross-shore sediment budget for prograding beach/foredune ridge systems by making use of the morphology of subaerial ridge and swale complexes. Within the model, the development of ridge and swale morphology is constrained by fluxes of sediment to both the foredune ridge system and the shoreface. Partitioning of these fluxes gives rise to cross-shore morphologies defined as flats, washboards, and large ridges. This framework is used to perform a morphological calibration on these patterns at field sites along the northern Virginia Atlantic coast, employing field and remote measurements of subaerial ridge volume, spacing (number of

ridges), ridge height, shoreline progradation distance, and geochronology to derive time-varying net sediment budgets.

Initial results offer insight into the development of the Virginia barrier islands, suggesting that a marginal sediment budget could influence historical state shifts of islands between relative stability/progradation and rapid erosion. Moreover, the model could provide an intuitive means to explore the sediment supply history of strandplains and prograding barrier systems around the world, especially with future model extension. The model is envisioned to add perspective in existing investigations where geochronological control is limited, as well as enable insights into accommodation effects, notably those arising from changes in the rate of sea-level rise and the presence of variable offshore bathymetry.

CONCLUDING SYNTHESIS AND FUTURE WORK

The investigations undertaken in this compendium suggest barrier island systems, already known to be highly dynamic, may be capable of much more diverse behaviors than presently accounted for in current literature. Modeling results demonstrate that transgressive barrier islands could undergo internally-driven long-term changes in geometry that lead to periodic backstepping and production of relict deposits on the shelf seabed. These results are correlated with deposits in nature, suggesting periodic retreat could plausibly explain the production of drowned barriers that formed during the late Pleistocene and early Holocene. Moreover, modeling of barriers subjected to a rapid increase in rate of sea-level rise demonstrates that autogenic periodicity could strongly modulate the effects of external, environmental forcing—in some cases potentially rendering barriers more vulnerable to complete drowning. These efforts support the need to interpret past barrier behavior to better understand the behavior of modern barriers, which are likely to respond to anthropogenically enhanced sea-level rise in ways which have not been observed historically.

In the subaerial domain, modeling the morphology of prograding barrier ridge and swale systems offers a technique to compute long-term changes in the magnitude of beach sediment budget through time. At validation sites along the Virginia Atlantic coast, this framework has been employed to demonstrate that historical oscillations between erosion, stability, and progradation across the island chain could be driven in part by marginal sediment supply. Similar insights could be gleaned from field sites around the world, including at strandplains, where the record of progradation preserved in ridge morphology may actually be more complete than in comparable barrier island systems. As with modeling of transgressive barriers, understanding past changes in sediment budget will allow the sensitivity of barrier systems to future change to

be explored, furthering the ability to understand how barriers may respond to anthropogenic disruption.

While the aforementioned insights are intriguing and add to the body of recent literature expanding the knowledge of barrier behavior, the works described here are far from finished. Exploration of the continental shelf seabed will undoubtedly recover more overstepped barrier islands, which will continue to call into question the paradigms of steady-state retreat, as well as provide new field evidence to model and explore the behavior of pre-historic transgressive barriers. Additionally, work with the cross-shore model of ridge and swale morphology is intended to be expanded to account for transgression, which may allow for more complex surface morphologies to be modeled. In its current form, the model can already account for variable (rising and falling) sea level, as well as variable offshore bathymetry, which could allow it to be employed in other parts of the world where these conditions exist. Even in Virginia, where initial validation was undertaken, the model could be applied to portions of this system where offshore deepening and progradation over sand shoals is known or suspected to have occurred—exploration of these topographic forcings may reveal expressions in ridge morphology that could be used to infer the presence of seabed features buried during progradation.

The combined efforts in both transgressive barrier modeling and quantifying sediment budget from subaerial ridge and swale morphology are ultimately intended to benefit future coastal management. Insights from drowned deposits will allow managers to anticipate changes in the behavior of barriers that have not been witnessed over previous centuries, and time-variable sediment budgets produced from relict dune ridge morphology will provide baselines to model future changes in sediment delivery (and system sensitivity to change) from rising sea-

level, as well as other human interventions. Moreover, the ridge and swale model is intended to be used as an interactive tool, and was made publicly available through an online repository. A basic graphical user interface has already been built to control the model's input parameters, which is eventually intended to be upgraded and re-configured to serve the specific needs of stakeholders/managers.

Latest version of the cross-shore ridge and swale model:

<https://github.com/ciarletd/Beach-and-Foredune-Ridge>

The cross-shore ridge and swale model described in this investigation is archived under DOI 10.5281/zenodo.2575699.

REFERENCES

- Aagaard, T., Davidson-Arnott, R., Greenwood, B., & Nielsen, J. (2004). Sediment supply from shoreface to dunes: linking sediment transport measurements and long-term morphological evolution. *Geomorphology*, 60(1-2), 205-224.
- Archbald, G. (2010). Merging tidal datums and LIDAR elevation for species distribution modeling in South San Francisco Bay. Report prepared for the South Bay Salt Pond Restoration Project, Alviso, CA.
- Argyilan, E. P., Forman, S. L., & Thompson, T. A. (2010). Variability of Lake Michigan water level during the past 1000 years reconstructed through optical dating of a coastal strandplain. *The Holocene*, 20(5), 723-731.
- Ashton, A.D., Nienhuis, J., & Ells, K. (2016). On a neck, on a spit: controls on the shape of free spits. *Earth Surface Dynamics*, 4(1), 193.
- Billy, J., Robin, N., Hein, C. J., Certain, R., & FitzGerald, D. M. (2014). Internal architecture of mixed sand-and-gravel beach ridges: Miquelon-Langlade Barrier, NW Atlantic. *Marine Geology*, 357, 53-71.
- Boon, J. D., & Mitchell, M. (2015). Nonlinear change in sea level observed at North American tide stations. *Journal of Coastal Research*, 31(6), 1295-1305.
- Bristow, C. S., & Pucillo, K. (2006). Quantifying rates of coastal progradation from sediment volume using GPR and OSL: the Holocene fill of Guichen Bay, south-east South Australia. *Sedimentology*, 53(4), 769-788.
- Buynevich, I. V., FitzGerald, D. M., & van Heteren, S. (2004). Sedimentary records of intense storms in Holocene barrier sequences, Maine, USA. *Marine Geology*, 210(1-4), 135-148.
- Cattaneo, A., & Steel, R. J. (2003). Transgressive deposits: a review of their variability, *Earth-Science Reviews*, 62(3), 187-228.
- Choi, K. H., Choi, J. H., & Kim, J. W. (2014). Reconstruction of Holocene coastal progradation on the east coast of Korea based on OSL dating and GPR surveys of beach-foredune ridges. *The Holocene*, 24(1), 24-34.
- Cohn, N., Hoonhout, B. M., Goldstein, E. B., De Vries, S., Moore, L. J., Durán Vinent, O., & Ruggiero, P. (2019). Exploring Marine and Aeolian Controls on Coastal Foredune Growth Using a Coupled Numerical Model. *Journal of Marine Science and Engineering*, 7(1), 13.
- Cohn, N., Ruggiero, P., de Vries, S., & Kaminsky, G. M. (2018). New insights on coastal foredune growth: the relative contributions of marine and aeolian processes. *Geophysical Research Letters*.

Cooper, J. A. G., Green, A. N., Meireles, R. P., Klein, A. H., Souza, J., & Toldo, E. E. (2016). Sandy barrier overstepping and preservation linked to rapid sea level rise and geological setting. *Marine Geology*, 382, 80-91.

Costas, S., Ferreira, Ó., Plomaritis, T. A., & Leorri, E. (2016). Coastal barrier stratigraphy for Holocene high-resolution sea-level reconstruction. *Scientific reports*, 6, 38726.

Davidson-Arnott, R. G., Hesp, P., Ollerhead, J., Walker, I., Bauer, B., Delgado-Fernandez, I., & Smyth, T. (2018). Sediment budget controls on foredune height: Comparing simulation model results with field data. *Earth Surface Processes and Landforms*, 43(9). 1798-1810.

Davidson-Arnott, R. G., & Law, M. N. (1996). Measurement and prediction of long-term sediment supply to coastal foredunes. *Journal of Coastal Research*, 654-663.

Deaton, C. D., Hein, C. J., & Kirwan, M. L. (2017). Barrier island migration dominates ecogeomorphic feedbacks and drives salt marsh loss along the Virginia Atlantic Coast, USA. *Geology*, 45(2). 123-126.

De Falco, G., Antonioli, F., Fontolan, G., Presti, V.L., Simeone, S., & Tonielli, R. (2015). Early cementation and accommodation space dictate the evolution of an overstepping barrier system during the Holocene, *Marine Geology*, 369, 52-66.

Del Angel, D. (2012). *Dune-beach morphodynamic interaction along a semi-arid, wave dominated barrier island: South Padre Island, Texas* (Dissertation). Texas A&M University–Corpus Christi, TX, USA.

De Vries, S., Southgate, H. N., Kanning, W., & Ranasinghe, R. (2012). Dune behavior and aeolian transport on decadal timescales. *Coastal Engineering*, 67, 41-53.

Donoghue, J.F. (2011). Sea level history of the northern Gulf of Mexico coast and sea level rise scenarios for the near future. *Climatic Change*, 107(1-2), 17.

Dougherty, A. J., Choi, J. H., & Dosseto, A. (2016). Prograded barriers+ GPR+ OSL= insight on coastal change over intermediate spatial and temporal scales. *Journal of Coastal Research*, 75(sp1). 368-372.

Engelhart, S. E., & Horton, B. P. (2012). Holocene sea level database for the Atlantic coast of the United States. *Quaternary Science Reviews*, 54, 12-25.

Feagin, R. A., Smith, W. K., Psuty, N. P., Young, D. R., Martínez, M. L., Carter, G. A., ... & Koske, R. E. (2010). Barrier islands: coupling anthropogenic stability with ecological sustainability. *Journal of Coastal Research*, 26(6), 987-992.

Fenster, M. S., Dolan, R., & Smith, J. J. (2016). Grain-size distributions and coastal morphodynamics along the southern Maryland and Virginia barrier islands. *Sedimentology*, 63(4). 809-823.

- Finkelstein, K. (1983). Cape formation as a cause of erosion on adjacent shorelines. In *Coastal Zone'83* (pp. 620-640). ASCE.
- FitzGerald, D. M. (1982). Sediment bypassing at mixed energy tidal inlets. In *Coastal Engineering 1982* (pp. 1094-1118).
- FitzGerald, D. M. (1984). Interactions between the ebb-tidal delta and landward shoreline: Price Inlet, South Carolina. *Journal of Sedimentary Research*, 54(4).
- Forbes, D. L., Taylor, R. B., Orford, J. D., Carter, R. W. G., & Shaw, J. (1991). Gravel-barrier migration and overstepping, *Marine Geology*, 97(3-4), 305-313.
- Foreman, B. Z., & Straub, K. M. (2017). Autogenic geomorphic processes determine the resolution and fidelity of terrestrial paleoclimate records. *Science advances*, 3(9), e1700683.
- French, J., Payo, A., Murray, B., Orford, J., Eliot, M., & Cowell, P. (2016). Appropriate complexity for the prediction of coastal and estuarine geomorphic behaviour at decadal to centennial scales. *Geomorphology*, 256, 3-16.
- Gedan, K. B., Kirwan, M.L., Wolanski, E., Barbier, E B., & Silliman, B.R. (2011). The present and future role of coastal wetland vegetation in protecting shorelines: answering recent challenges to the paradigm. *Climatic Change*, 106(1), 7-29.
- Gilbert, G. K. (1885). *The topographic features of lake shores*. US Government Printing Office.
- Green, A. N., Cooper, J. A. G., & Salzmann, L. (2018). The role of shelf morphology and antecedent setting in the preservation of palaeo-shoreline (beachrock and aeolianite) sequences: the SE African shelf. *Geo-Marine Letters*, 38(1), 5-18.
- Guadiano, D. J., and T. W. Kana. (2001). Shoal bypassing in mixed energy inlets: geomorphic variables and empirical predictions for nine South Carolina inlets. *Journal of Coastal Research* 17, 280–291.
- Hails, J. R. (1968). The late Quaternary history of part of the mid-north coast, New South Wales, Australia. *Transactions of the Institute of British Geographers*, 133-149.
- Hajek, E.A., & Straub, K.M. (2017). Autogenic sedimentation in clastic stratigraphy, *Annual Review of Earth and Planetary Sciences*, 45(1).
- Halsey, S. D., (1978). *Late Quaternary geologic history and morphologic development of the barrier island system along the Delmarva Peninsula of the mid-Atlantic Bight* (Dissertation). University of Delaware, Newark, Delaware, 592 pp.
- Headland, J. R., Vallianos, L., and Sheldon, J. G. (1987). Coastal processes at Wallops Island, Virginia, in *Proceedings, Coastal Sediments '87*, New Orleans, Louisiana, 12–14 May 1987: New York, American Society of Civil Engineers, p. 1305–1320.

- Hede, M. U., Bendixen, M., Clemmensen, L. B., Kroon, A., & Nielsen, L. (2013). Joint interpretation of beach-ridge architecture and coastal topography show the validity of sea-level markers observed in ground-penetrating radar data. *The Holocene*, 23(9), 1238-1246.
- Hein, C. J., FitzGerald, D. M., de Souza, L. H., Georgiou, I. Y., Buynevich, I. V., Klein, A. H. Da F., J. T. De Menezes, Clearly, W.J., & Sclaro, T. L. (2016). Complex coastal change in response to autogenic basin infilling: An example from a sub-tropical Holocene strandplain. *Sedimentology*, 63(6), 1362-1395.
- Hein, C. J., Shawler, J. L., De Camargo, J. M., Klein A. H.D.F, Tenebruso, C., & Fenster, M. S. (2019). The Role of Coastal Sediment sinks in Modifying Longshore Sand Fluxes: Examples from the Coasts of Southern Brazil and the Mid-Atlantic, USA. In *The Proceedings of the Coastal Sediments 2019*, World Scientific Pub Co Inc, San Diego, USA.
- Hesp, P. (2011). Dune Coasts. In: Wolanski E and McLusky DS (eds.) *Treatise on Estuarine and Coastal Science*, Vol 3, pp. 193–221. Waltham: Academic Press.
- Hijma, M. P., & Cohen, K. M. (2010). Timing and magnitude of the sea-level jump precluding the 8200 yr event. *Geology*, 38(3), 275-278.
- Himmelstoss, E.A., Kratzmann, M.G., and Thieler, E.R. (2017). National assessment of shoreline change—Summary statistics for updated vector shorelines and associated shoreline change data for the Gulf of Mexico and Southeast Atlantic coasts: U.S. Geological Survey Open-File Report 2017–1015, 8 p.
- Hoonhout, B., & de Vries, S. (2017). Aeolian sediment supply at a mega nourishment. *Coastal Engineering*, 123, 11-20.
- Houston, J. R. (2008). The economic value of beaches: a 2008 update. *Shore and beach*, 76(3), 22-26.
- Jerolmack, D. J., & Paola, C. (2010). Shredding of environmental signals by sediment transport. *Geophysical Research Letters*, 37(19).
- Johnson, D. W. (1919). *Shore processes and shoreline development*. John Wiley & Sons, Incorporated.
- Kaczkowski, H. L., Kana, T. W., Traynum, S. B., & Visser, R. (2017). Beach-fill equilibration and dune growth at two large-scale nourishment sites. *Ocean Dynamics*, 68(9), 1191-1206.
- Kim, W., Petter, A., Straub, K., & Mohrig, D. (2014). Investigating the autogenic process response to allogenic forcing, in Martinius, A., et al., eds., *From Depositional Systems to Sedimentary Successions on the Norwegian Continental Margin*: Hoboken, NJ, USA, IAS Special Publication 46, p. 127-138.

- Kraus, N. C., & Hayashi, K. (2005). Numerical morphologic model of barrier island breaching. In *Coastal Engineering 2004: (In 4 Volumes)* (pp. 2120-2132).
- Lawrence, T., Long, A. J., Gehrels, W. R., Jackson, L. P., & Smith, D. E. (2016). Relative sea-level data from southwest Scotland constrain meltwater-driven sea-level jumps prior to the 8.2 kyr BP event. *Quaternary science reviews*, *151*, 292-308.
- Lazarus, E., Harley, M. D., Blenkinsopp, C. E., & Turner, I. L. (2019). Environmental signal shredding on sandy coastlines. *Earth Surface Dynamics*, *7*, 77-86.
- Li, Q., Yu, L., & Straub, K.M. (2016). Storage thresholds for relative sea level signals in the stratigraphic record, *Geology*, *44*(3), 179-182.
- Liu, J. P., & Milliman, J. D. (2004). Reconsidering melt-water pulses 1A and 1B: global impacts of rapid sea-level rise. *Journal of Ocean University of China*, *3*(2), 183-190.
- Locker, S.D., Hine, A.C., & Brooks, G.R. (2003). Regional stratigraphic framework linking continental shelf and coastal sedimentary deposits of west-central Florida, *Marine Geology*, *200*(1), 351-378.
- Locker, S.D., Hine, A.C., Tedesco, L.P., & Shinn, E.A. (1996). Magnitude and timing of episodic sea level rise during the last deglaciation. *Geology*, *24*(9), 827-830.
- Long, A. J., Strzelecki, M. C., Lloyd, J. M., & Bryant, C. L. (2012). Dating High Arctic Holocene relative sea level changes using juvenile articulated marine shells in raised beaches. *Quaternary Science Reviews*, *48*, 61-66.
- Lorenzo-Trueba, J., & Ashton, A. D. (2014). Rollover, drowning, and discontinuous retreat: Distinct modes of barrier response to sea-level rise arising from a simple morphodynamic model. *Journal of Geophysical Research: Earth Surface*, *119*(4), 779-801.
- Martínez, M. L., Intralawan, A., Vázquez, G., Pérez-Maqueo, O., Sutton, P., & Landgrave, R. (2007). The coasts of our world: Ecological, economic and social importance. *Ecological economics*, *63*(2-3), 254-272.
- Mason, O. K. (1993). The geoarchaeology of beach ridges and cheniers: studies of coastal evolution using archaeological data. *Journal of Coastal Research*, *9*(1), 126-146.
- McBride, R. A., Fenster, M. S., Seminack, C. T., Richardson, T. M., Sepanik, J. M., Hanley, J. T., Bundick, J. A., and Tedder, E. (2015). Holocene barrier-island geology and morphodynamics of the Maryland and Virginia open-ocean coasts: Fenwick, Assateague, Chincoteague, Wallops, Cedar, and Parramore Islands, in Brezinski, D. K., Halka, J. P., and Ortt, R. A., Jr., eds., *Tripping from the Fall Line: Field Excursions for the GSA Annual Meeting, Baltimore, 2015: Geological Society of America Field Guide 40*, p. 309–424.

- McNamara, D. E., & Lazarus, E. D. (2018). Barrier islands as coupled human–landscape systems. In *Barrier Dynamics and Response to Changing Climate* (pp. 363-383). Springer, Cham.
- Mellett, C.L., Hodgson, D.M., Lang, A., Mauz, B., Selby, I., & Plater, A.J. (2012). Preservation of a drowned gravel barrier complex: A landscape evolution study from the north-eastern English Channel, *Marine Geology*, 315, 115-131.
- Mellett, C. L., & Plater, A. J. (2018). Drowned barriers as archives of coastal-response to sea-level rise. In *Barrier Dynamics and Response to Changing Climate* (pp. 57-89). Springer, Cham.
- Moffatt and Nichol, Engineers (1986). Wallops Island shore protection study: NASA/Goddard Space Flight Facility, Wallops Island, Virginia, 86 p. with appendices.
- National Park Service (2016). Digital Pre-Hurricane Sandy Geomorphological-GIS Map of the Gateway National Recreation Area: Sandy Hook, Jamaica Bay and Staten Island Units, New Jersey and New York (NPS, GRD, GRI, GATE, GATE digital map) adapted from a Rutgers University Institute of Marine and Coastal Sciences unpublished digital data by Psuty, N.P., McLoughlin, S.M., Schmelz, W. and Spahn, A. (2014). *NPS Geologic Resources Inventory Program*. <https://irma.nps.gov/DataStore/Reference/Profile/2233886>
- NOAA (2010). “What percentage of the American population lives near the coast?” National Oceanic and Atmospheric Administration. National Ocean Service website: <https://oceanservice.noaa.gov/facts/population.html>
- NOAA (2017). *Method Description: Detailed Method for Mapping Sea Level Rise Marsh Migration*. NOAA Office for Coastal Management, January, 2017. <https://coast.noaa.gov/data/digitalcoast/pdf/slr-marsh-migration-methods.pdf>
- NOAA (2018). Wachapreague, Virginia – Station ID: 8631044. *NOAA Tides and Currents*. <https://tidesandcurrents.noaa.gov/stationhome.html?id=8631044>
- Nordfjord, S., Goff, J.A., Austin, J.A., & Duncan, L.S. (2009). Shallow stratigraphy and complex transgressive ravinement on the New Jersey middle and outer continental shelf, *Marine Geology*, 266(1), 232-243.
- Nooren, K., Hoek, W. Z., Winkels, T., Huizinga, A., Van der Plicht, H., Van Dam, R. L., ... & Wallinga, J. (2017). The Usumacinta–Grijalva beach-ridge plain in southern Mexico: a high-resolution archive of river discharge and precipitation. *Earth Surface Dynamics*, 5(3). 529.
- Oliver, T. S., Dougherty, A. J., Gliganic, L. A., & Woodroffe, C. D. (2015). Towards more robust chronologies of coastal progradation: optically stimulated luminescence ages for the coastal plain at Moruya, south-eastern Australia. *The Holocene*, 25(3). 536-546.

- Oliver, T. S., Donaldson, P., Sharples, C., Roach, M., & Woodroffe, C. D. (2017a). Punctuated progradation of the Seven Mile Beach Holocene barrier system, southeastern Tasmania. *Marine Geology*, 386, 76-87.
- Oliver, T. S. N., Tamura, T., Hudson, J. P., & Woodroffe, C. D. (2017b). Integrating millennial and interdecadal shoreline changes: Morpho-sedimentary investigation of two prograded barriers in southeastern Australia. *Geomorphology*, 288, 129-147.
- Oliver, T. S., Tamura, T., Short, A. D., & Woodroffe, C. D. (2018). Rapid shoreline progradation followed by vertical foredune building at Pedro Beach, southeastern Australia. *Earth Surface Processes and Landforms*.
- Ortiz, A. C., & Ashton, A. D. (2016). Exploring shoreface dynamics and a mechanistic explanation for a morphodynamic depth of closure. *Journal of Geophysical Research: Earth Surface*, 121(2), 442-464.
- Otvos, E. G. (2000). Beach ridges—definitions and significance. *Geomorphology*, 32(1), 83-108.
- Pendleton, L., Donato, D.C., Murray, B.C., Crooks, S., Jenkins, W.A., Sifleet, S., ... & Megonigal, P. (2012). Estimating global “blue carbon” emissions from conversion and degradation of vegetated coastal ecosystems. *PLoS one*, 7(9), e43542.
- Pilkey, O. H., Cooper, J. A. G., & Lewis, D. A. (2009). Global distribution and geomorphology of fetch-limited barrier islands. *Journal of Coastal Research*, 819-837.
- Pilkey, O. H., & Fraser, M. E. (2003). *A celebration of the world's barrier islands*. Columbia University Press.
- Pretorius, L., Green, A., & Cooper, A. (2016). Submerged shoreline preservation and ravinement during rapid postglacial sea level rise and subsequent "slowstand", *Geological Society of America Bulletin*, 128(7-8), 1059-1069.
- Psuty, N. P. (1965). Beach-ridge development in Tabasco, Mexico 1. *Annals of the Association of American Geographers*, 55(1), 112-124.
- Psuty, N. P. (1988). Sediment budget and dune/beach interaction. *Journal of Coastal Research*, (3), 1-4.
- Psuty, N. P. (2004). *The Coastal Fore-dune: A Morphological Basis for Regional Coastal Dune Development*. In: Martinez, M. and N. P. Psuty, editors, *Coastal Dunes: Ecology and Conservation*, Springer-Verlag: Berlin, pp. 11-27.
- Pye, K., & Blott, S. J. (2016). Assessment of beach and dune erosion and accretion using LiDAR: impact of the stormy 2013–14 winter and longer term trends on the Sefton Coast, UK. *Geomorphology*, 266, 146-167.

Raff, J. L., Shawler, J. L., Ciarletta, D. J., Hein, E. A., Lorenzo-Trueba, J., & Hein, C. J. (2018). Insights into barrier-island stability derived from transgressive/regressive state changes of Parramore Island, Virginia. *Marine Geology*, 403, 1-19.

Rampino, M. R., & Sanders, J. E. (1980). Holocene transgression in south-central Long Island, New York. *Journal of Sedimentary Research*, 50(4), 1063-1079.

Rampino, M. R., & Sanders, J. E. (1981). Evolution of the barrier islands of southern Long Island, New York. *Sedimentology*, 28(1), 37-47.

Rampino, M. R., & Sanders, J. E. (1982). Holocene transgression in south-central Long Island, New York: reply. *Journal of Sedimentary Research*, 52(3).

Rampino, M. R., & Sanders, J. E. (1983). Barrier island evolution in response to sea-level rise: reply. *Journal of Sedimentary Research*, 53(3).

Rhodes, E. G. (1980). *Modes of Holocene coastal progradation: Gulf of Carpentaria* (Thesis). Australian National University, Canberra.

Rice, T. E., Niedoroda, A. W., & Pratt, A. P. (1976). The coastal processes and geology: Virginia Barrier Islands, in: Ecosystem Description: Virginia Coast Reserve Study. pp. 107–384. *The Nature Conservancy*, Arlington, VA, USA.

Rink, W. J., & Forrest, B. (2005). Dating evidence for the accretion history of beach ridges on Cape Canaveral and Merritt Island, Florida, USA. *Journal of Coastal Research*, 1000-1008.

Roy, P. S., Cowell, P. J., Ferland, M. A., & Thom, B. G. (1994). Wave dominated coasts. In: Carter RWG and Woodroffe CD (eds) *Coastal Evolution: Late Quaternary Shoreline Morphodynamics*. Cambridge: Cambridge University Press, pp. 121–186.

Ruggiero, P., Mull, J., Zarnetske, P., Hacker, S., & Seabloom, E. (2011). Interannual to decadal foredune evolution. In *The Proceedings of the Coastal Sediments 2011: In 3 Volumes* (pp. 698-711).

Saye, S. E., Van der Wal, D., Pye, K., & Blott, S. J. (2005). Beach–dune morphological relationships and erosion/accretion: an investigation at five sites in England and Wales using LIDAR data. *Geomorphology*, 72(1). 128-155.

Seminack, C. T., & McBride, R. A. (2015). Geomorphic history and diagnostic features of former tidal inlets along Assateague Island, Maryland-Virginia: A life-cycle model for inlets along a wave dominated barrier islands. *Shore and Beach*, 83, 3-24.

Smith, E. R., Reed, J. C., & Delwiche, I. L. (2016). *The Atlantic Coast of Maryland, Sediment Budget Update: Tier 2, Assateague Island and Ocean City Inlet*. ERDC/CHL CHETN-XIV-48. US Army Engineer Research and Development Center, Vicksburg, MS, USA.

- Stouthamer, E., & Berendsen, H. J. (2007). Avulsion: the relative roles of autogenic and allogenic processes. *Sedimentary Geology*, 198(3-4), 309-325.
- Stutz, M. L., & Pilkey, O. H. (2011). Open-ocean barrier islands: global influence of climatic, oceanographic, and depositional settings. *Journal of Coastal Research*, 27(2), 207-222.
- Swift, D.J. (1975). Barrier-island genesis: evidence from the central Atlantic shelf, eastern USA, *Sedimentary Geology*, 14(1), 1-43.
- Tamura, T. (2012). Beach ridges and prograded beach deposits as palaeoenvironment records. *Earth-Science Reviews*, 114(3-4). 279-297.
- Theuerkauf, E. J., & Rodriguez, A. B. (2017). Placing barrier-island transgression in a blue-carbon context. *Earth's Future*, 5(7), 789-810.
- Vinent O. D., & Moore, L. J. (2013). Vegetation controls on the maximum size of coastal dunes. *Proceedings of the National Academy of Sciences*, 110(43). 17217-17222.
- Walker, I. J., Davidson-Arnott, R. G., Bauer, B. O., Hesp, P. A., Delgado-Fernandez, I., Ollerhead, J., & Smyth, T. A. (2017). Scale-dependent perspectives on the geomorphology and evolution of beach-dune systems. *Earth-Science Reviews*, 171, 220-253.
- Young, A. P., & Ashford, S. A. (2006). Application of airborne LIDAR for seacliff volumetric change and beach-sediment budget contributions. *Journal of Coastal Research*, 307-318.
- Zhang, K., & Leatherman, S. (2011). Barrier island population along the US Atlantic and Gulf Coasts. *Journal of Coastal Research*, 27(2), 356-363.

APPENDICES

Chapter 1 Appendix

Model Sensitivity to Input Parameters

The following plots depict modeled wavelength and volume of deposits produced by autogenic partial overstepping for different environmental input parameters: a) the shoreface response rate K , b) equilibrium barrier width W_e , c) equilibrium barrier height H_e , d) shoreface toe depth D_t , and e) maximum overwash rate $Q_{OW,max}$. Figure A1.1, below, shows the baseline scenario for this study, the input parameters for which can be found in the Table 1.2. In each output (Figures A4.1 to A4.11), only one parameter is adjusted from the baseline scenario.

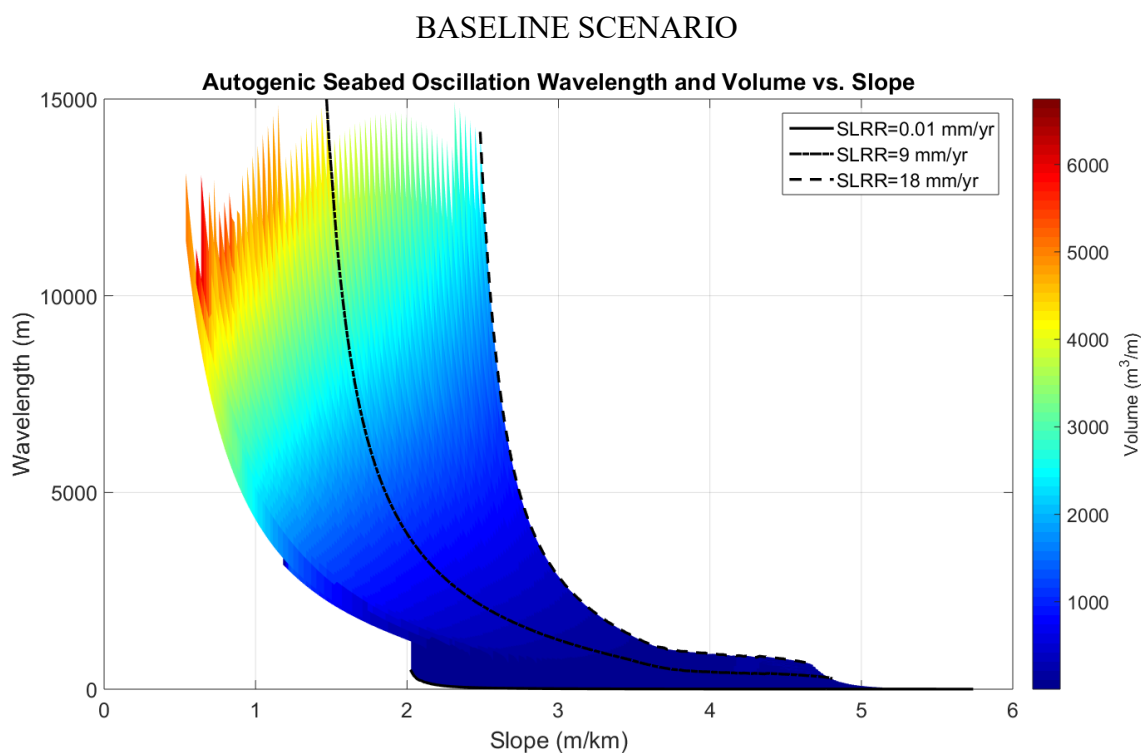


Figure A1.1 – Modeled remnant seabed oscillation wavelength and volume produced by a barrier undergoing periodic retreat under the baseline scenario, with $K=2000 \text{ m}^3/\text{m}/\text{yr}$, $W_e=800 \text{ m}$, $H_e=2 \text{ m}$, $D_T=15 \text{ m}$, and $Q_{OW,max}=100 \text{ m}^3/\text{m}/\text{yr}$ (for other values see Appendix).

SHOREFACE RESPONSE RATE

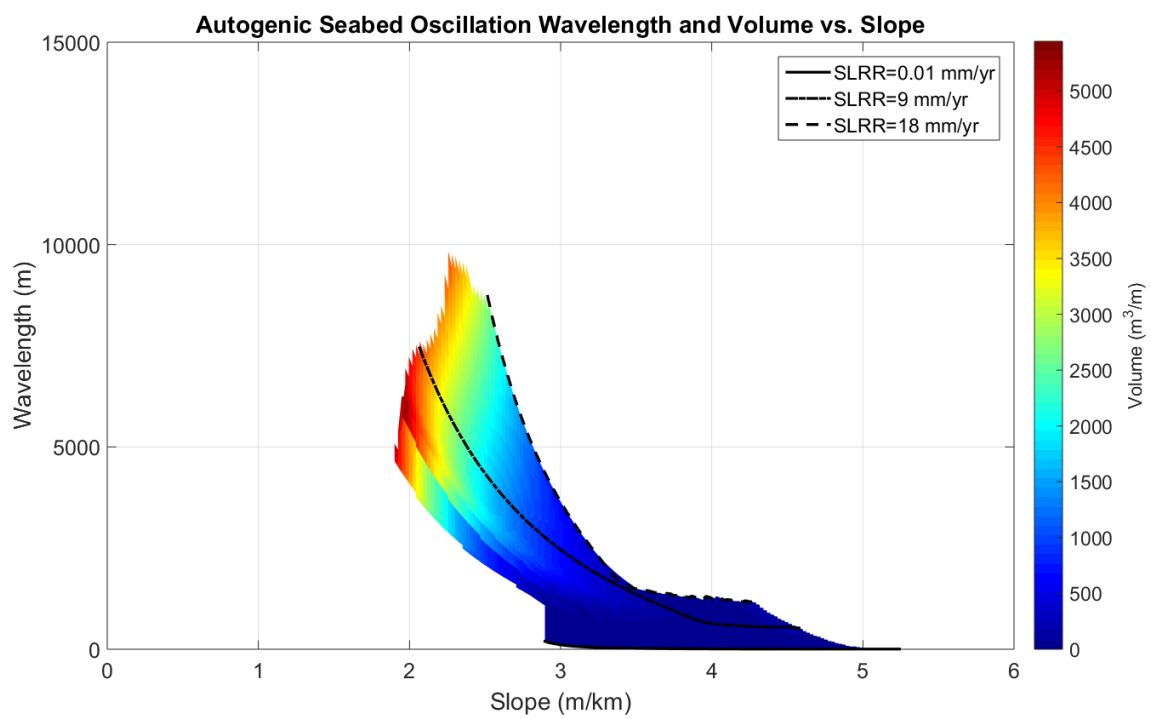


Figure A1.2 – Model results for a slower shoreface response rate $K=1000 \text{ m}^3/\text{m}/\text{yr}$. Baseline scenario: $K=2000 \text{ m}^3/\text{m}/\text{yr}$.

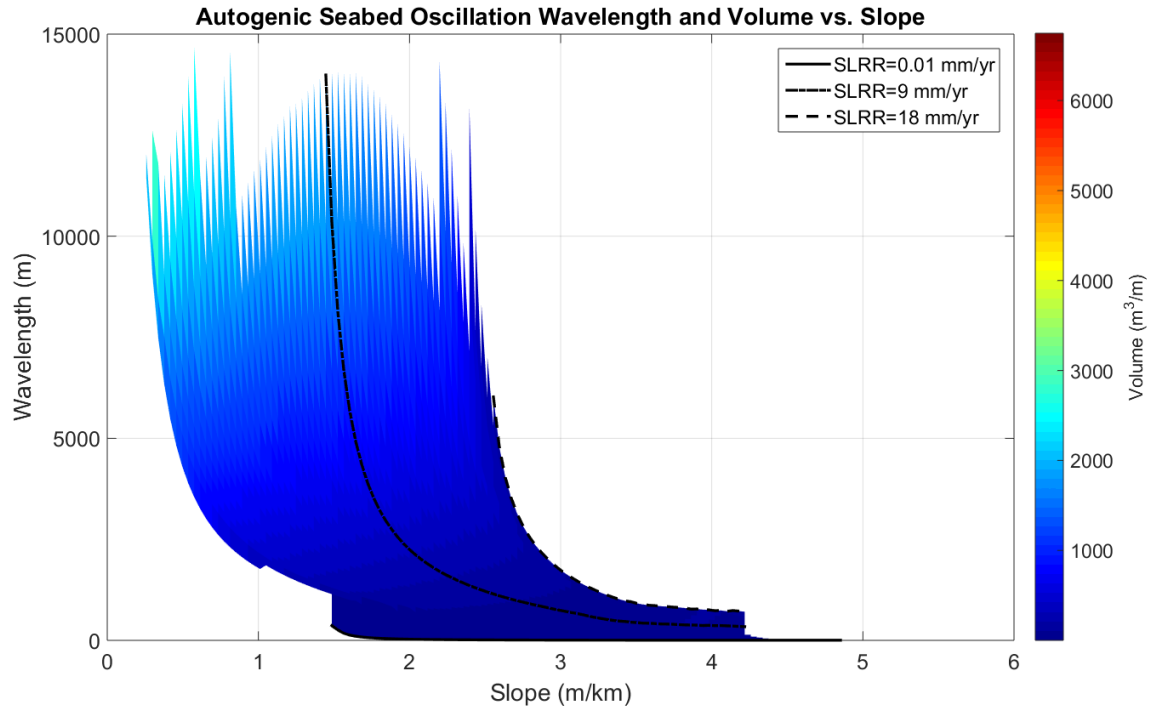


Figure A1.3 – Model results for a faster shoreface response rate $K=3000 \text{ m}^3/\text{m}/\text{yr}$. Baseline scenario: $K=2000 \text{ m}^3/\text{m}/\text{yr}$.

EQUILIBRIUM WIDTH

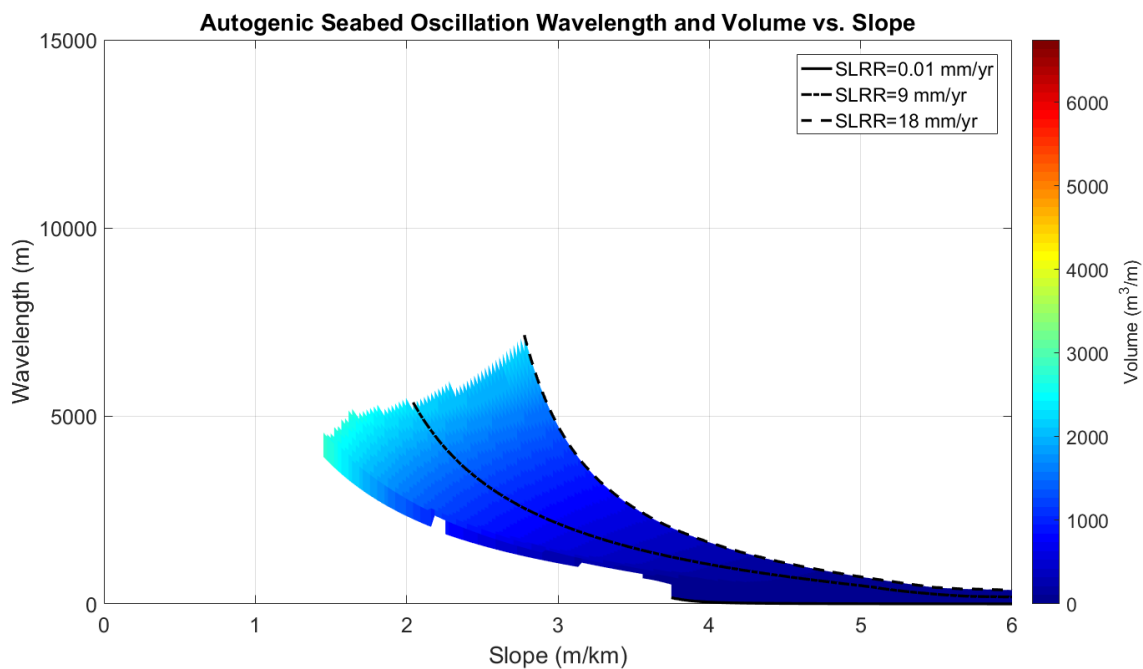


Figure A1.4 – Model results for a narrower equilibrium barrier width $W_e=400$ m. Baseline scenario: $W_e=800$ m.

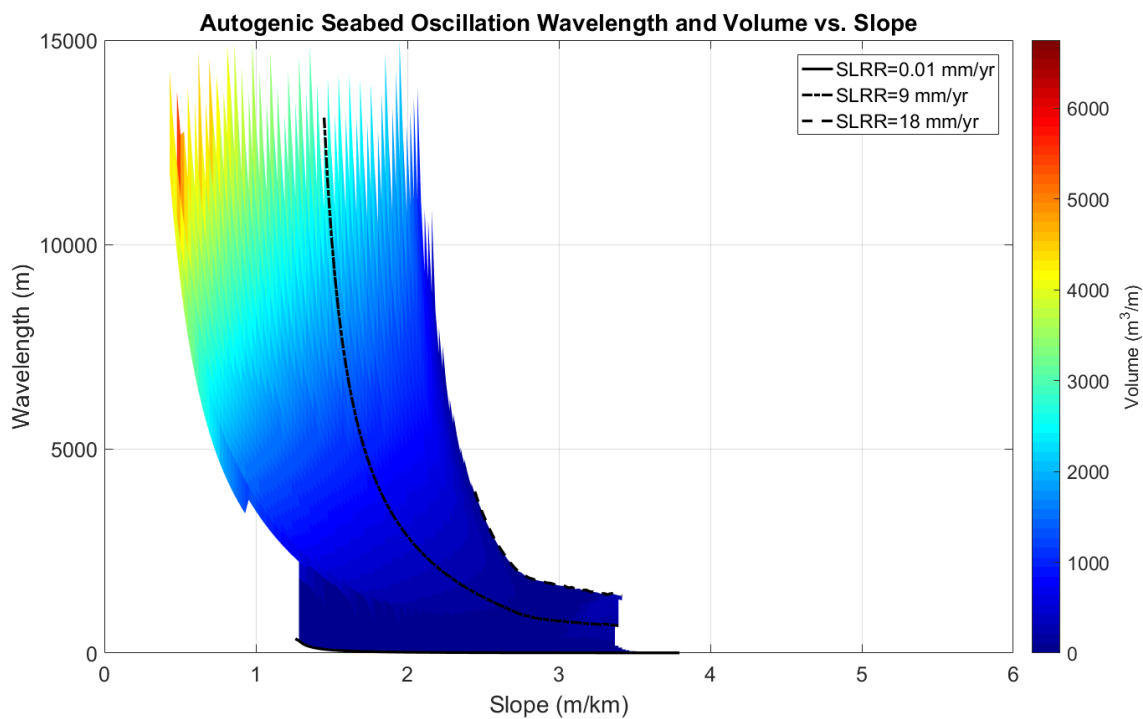


Figure A1.5 – Model results for a wider equilibrium barrier width $W_e=1200$ m. Baseline scenario: $W_e=800$ m.

EQUILIBRIUM HEIGHT

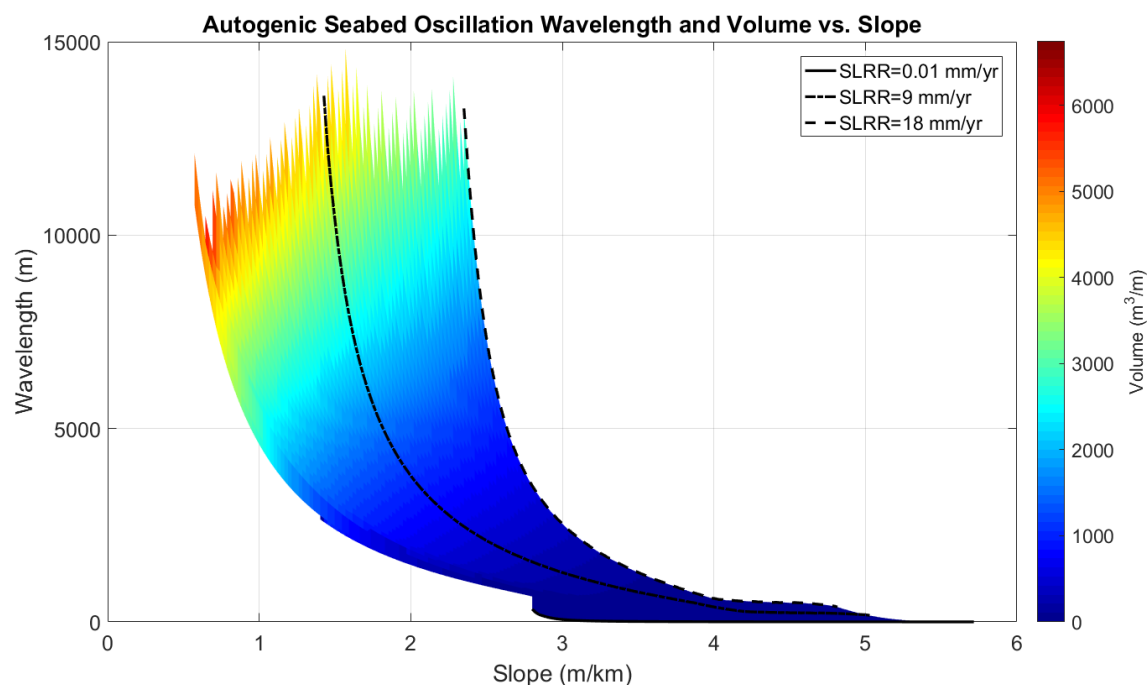


Figure A1.6 – Model results for a shorter equilibrium barrier height $H_e=1$ m. Baseline scenario: $H_e=2$ m.

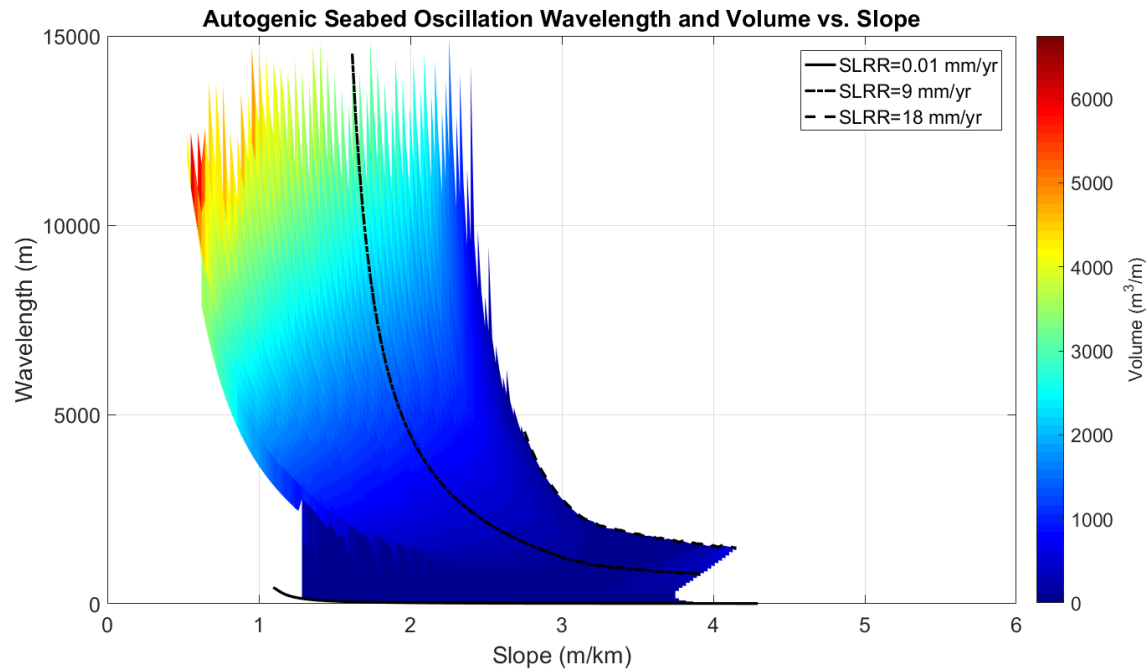


Figure A1.7 – Model results for a taller equilibrium barrier height $H_e=4$ m. Baseline scenario: $H_e=2$ m.

SHOREFACE TOE DEPTH

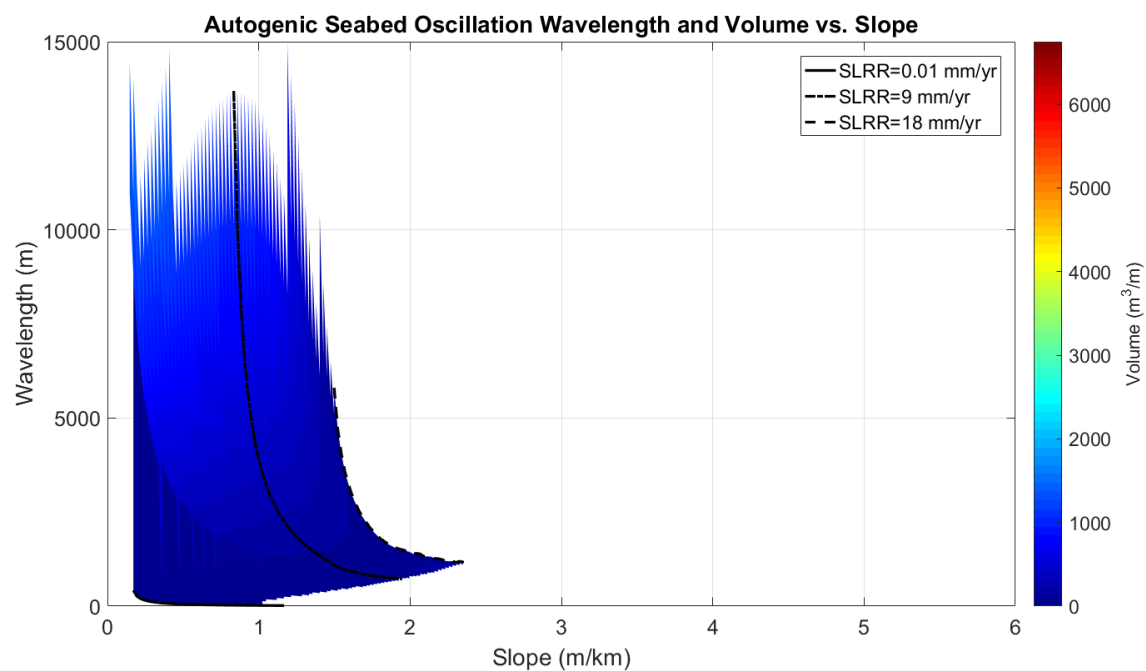


Figure A1.8 – Model results for a shallower shoreface toe depth $D_f=7.5$ m. Baseline scenario: $D_f=15$ m.

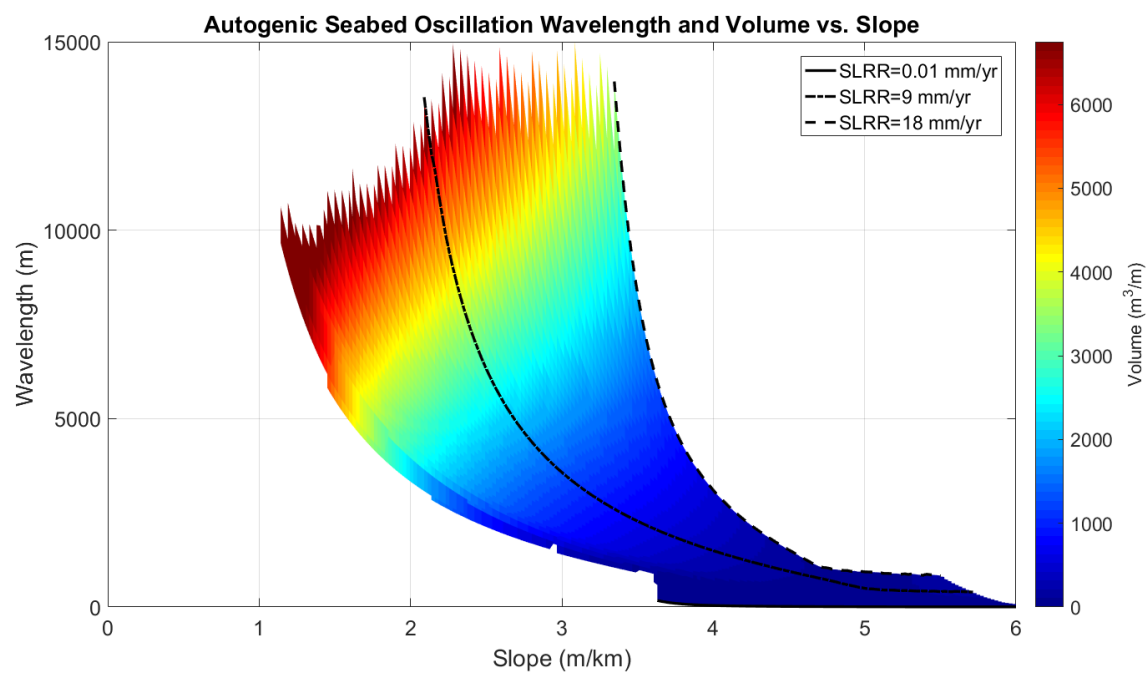


Figure A1.9 – Model results for a deeper shoreface toe depth $D_f=22.5$ m. Baseline scenario: $D_f=15$ m.

MAXIMUM OVERWASH RATE

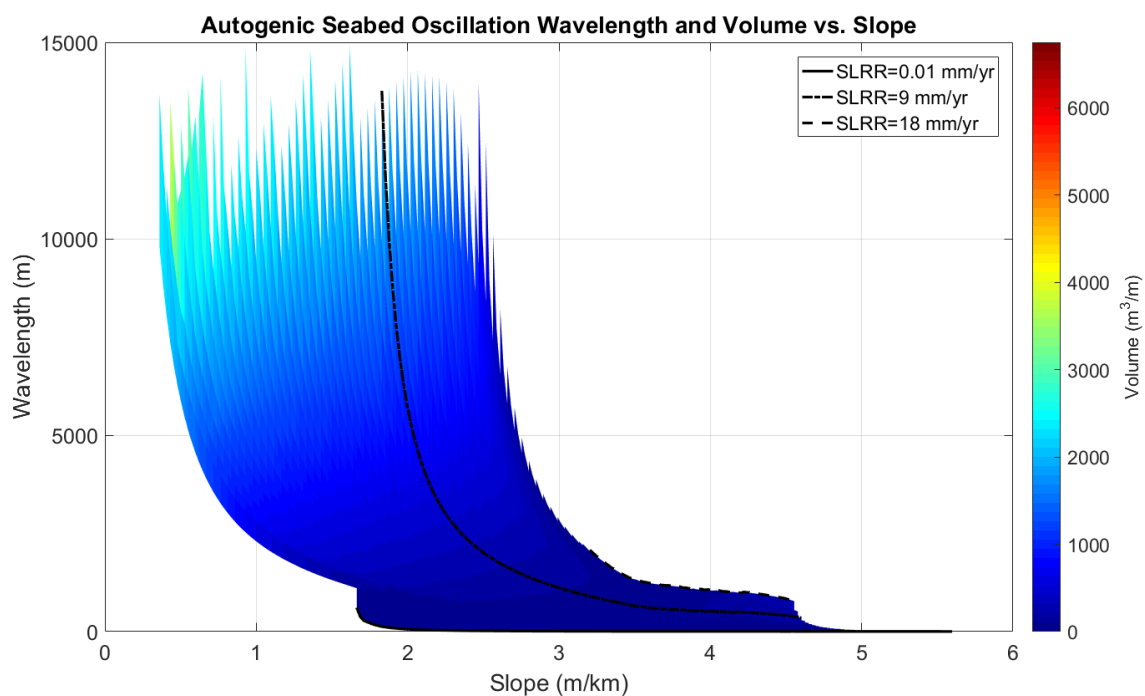


Figure A1.10 – Model results for a decreased maximum overwash rate $Q_{OW,max}=75 m^3/m/yr$. Baseline scenario: $Q_{OW,max}=100 m^3/m/yr$.

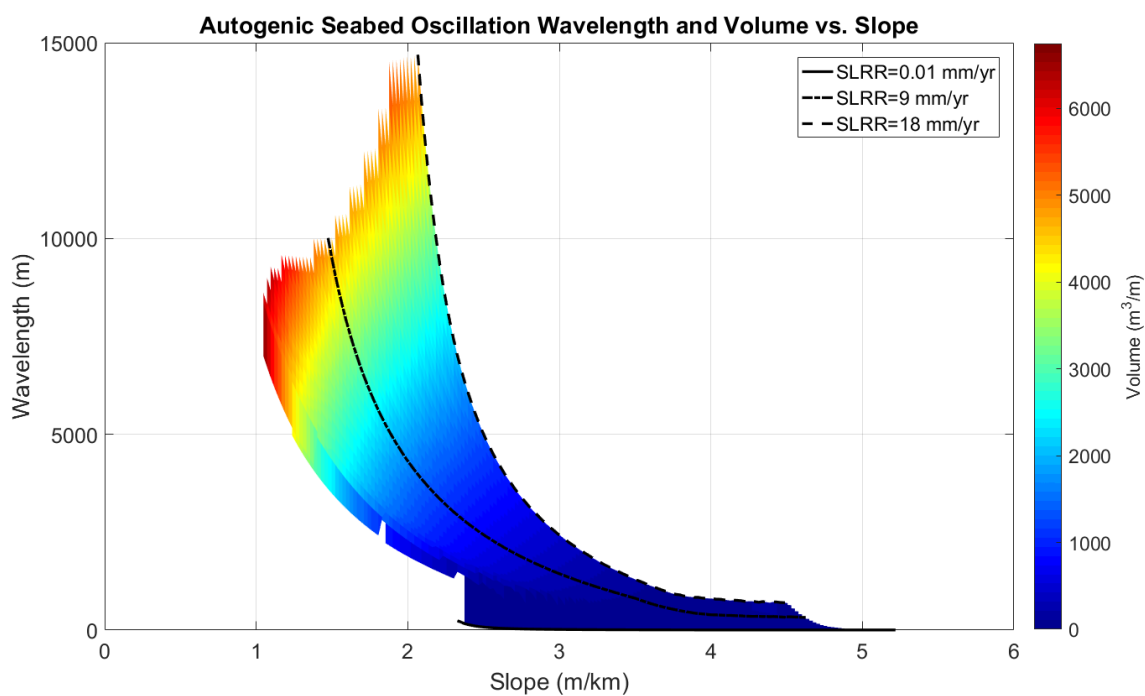


Figure A1.11 – Model results for an increased maximum overwash rate $Q_{OW,max}=125 m^3/m/yr$. Baseline scenario: $Q_{OW,max}=100 m^3/m/yr$.

Chapter 4 Appendix

Tables

Table A4.1 – Rates of Observed Foredune Growth

Location	Timeframe	Average Dune Growth (m ³ /m/yr)	Study
Long Point Spit, Lake Erie, Ontario, Canada	1986–1992	2.6–10.3	Davidson-Arnott & Law (1996)
Skallingen Barrier, Denmark	1996–1999	~5.0	Aagaard et al. (2004)
Holland (Hoek van Holland to Den-Helder), Netherlands	1965–2010	0.0–40.0	de Vries et al. (2012)
Southampton, Long Island, NY, USA	2013–2016	8.8	Kaczkowski et al. (2017)
Between Rotterdam and Schevenigen, Netherlands	2012–2015	14.0–19.0	Hoonhout & de Vries (2017)
South Padre Island, TX, USA	2000–2005	3.5	Del Angel (2012)
Long Beach, WA, USA	1997–2010	7.0	Ruggiero et al. (2011)
Clatsop Plains, OR, USA	1997–2010	6.0	Ruggiero et al. (2011)

Table A4.2 – Sta. 8631044
Wachapreauge, VA
V. datums referenced to NAVD88

STND	-1.51 m
MSL	-0.11 m
MHW	0.47 m
MHHW	0.57 m

Local vertical datums at the Wachapreauge tide gauge, referenced to NAVD88: STND=Station Datum, MSL=Mean Sea Level, MHW=Mean High Water, MHHW=Mean Higher-High Water (NOAA, 2018). The elevation of swale floors that have experienced upland marsh migration is ~0.6 m, which corresponds with MHHW.

Table A4.3 – Fishing Point Ridge Heights

Ridge	Raw Height (m)	Adjusted H (m)
1	1.76	1.16
2	1.59	0.99
3	1.49	0.89
4	1.52	0.92
5	1.59	0.99
6	2.26	1.66
7	2.14	1.54
8	1.57	0.97
9	3.10	2.50
10	1.10	0.50
11	1.02	0.42
12	1.17	0.57
13	1.28	0.68
14	1.46	0.86
15	1.80	1.20
16	1.69	1.09
17	1.54	0.94
18	1.97	1.37
19	1.24	0.64
20	1.46	0.86
AVERAGE	1.64	1.04

Average heights of delineated ridges for Fishing Point, arranged from north to south. Raw heights are NAVD88 derived from LiDAR, while adjusted heights are referenced to the swale floor elevation, which corresponds to MHHW on the Wachapreauge, VA tide station (+0.6 m NAVD88).

Table A4.4 – North Parramore Ridge Heights

Ridge	Raw Height (m)	Adjusted H (m)
Western Ridge	1.34	0.74
Goose Lake Ridge	1.32	0.72
3	1.07	0.47
4	0.85	0.25
Italian Ridge	6.70	6.10
6ab	1.12	0.52
7	1.05	0.45
8	0.94	0.34
9	1.02	0.42
AVERAGE	1.71	1.11
AVG Back Four	1.15	0.55
AVG Front Four	1.03	0.43

Average heights of delineated dune ridges are shown for North Parramore Island, arranged from west to east. Raw heights are NAVD88 derived from LiDAR, while adjusted heights are referenced to the swale floor elevation, which corresponds to MHHW on the Wachapreauge tide station (+0.6 m NAVD88).

Figures

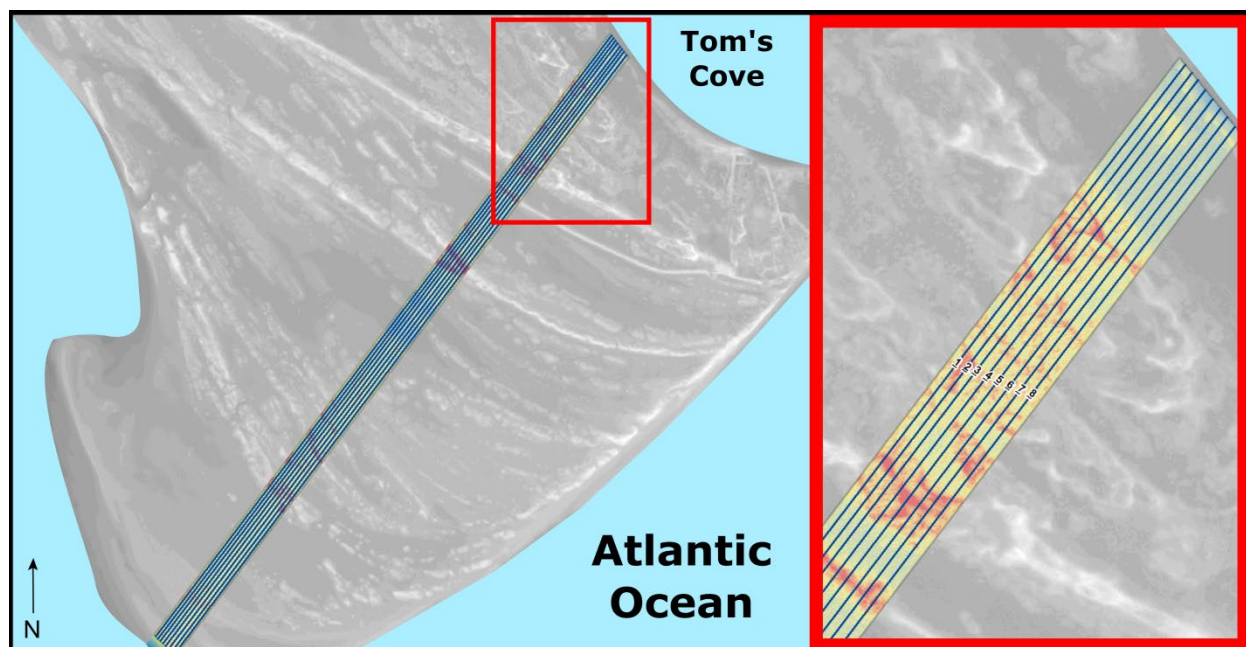


Figure A4.1 – Plan view of study area on Fishing Point, at the southern end of Assateague Island in Virginia. Background image is CoNED (Coastal National Elevation Database) LiDAR derived elevation. The rectangular boxed area represents the ridge perpendicular transect swath, and blue lines represent individual transect profiles used to produce an average elevation profile (Figure 2). Inset with red border shows zoomed in region of transect area adjacent to Tom’s Cove, at the most ‘landward’ section of the swath. Eight individual transect slices were utilized to produce Fishing Point’s average profile, as the narrowness of the ridges required additional resolution to properly visualize.

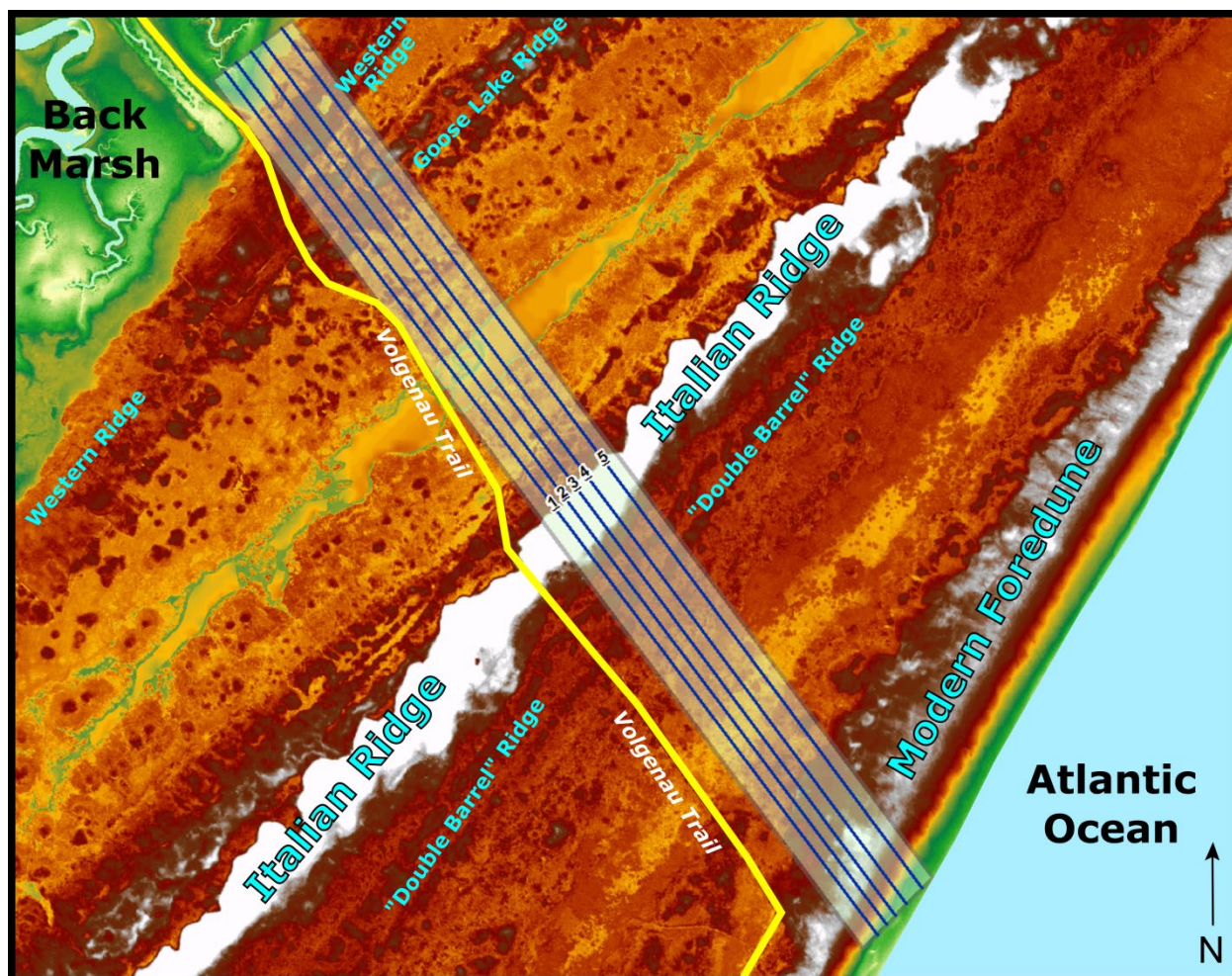


Figure A4.2 – Plan view of study area on north Parramore Island, Virginia, with 2016 CoNED (Coastal National Elevation Database) LiDAR derived elevation. The gray boxed area represents the ridge perpendicular transect swath, and blue lines represent five individual transect profiles used to produce an average elevation profile (Figure 2).

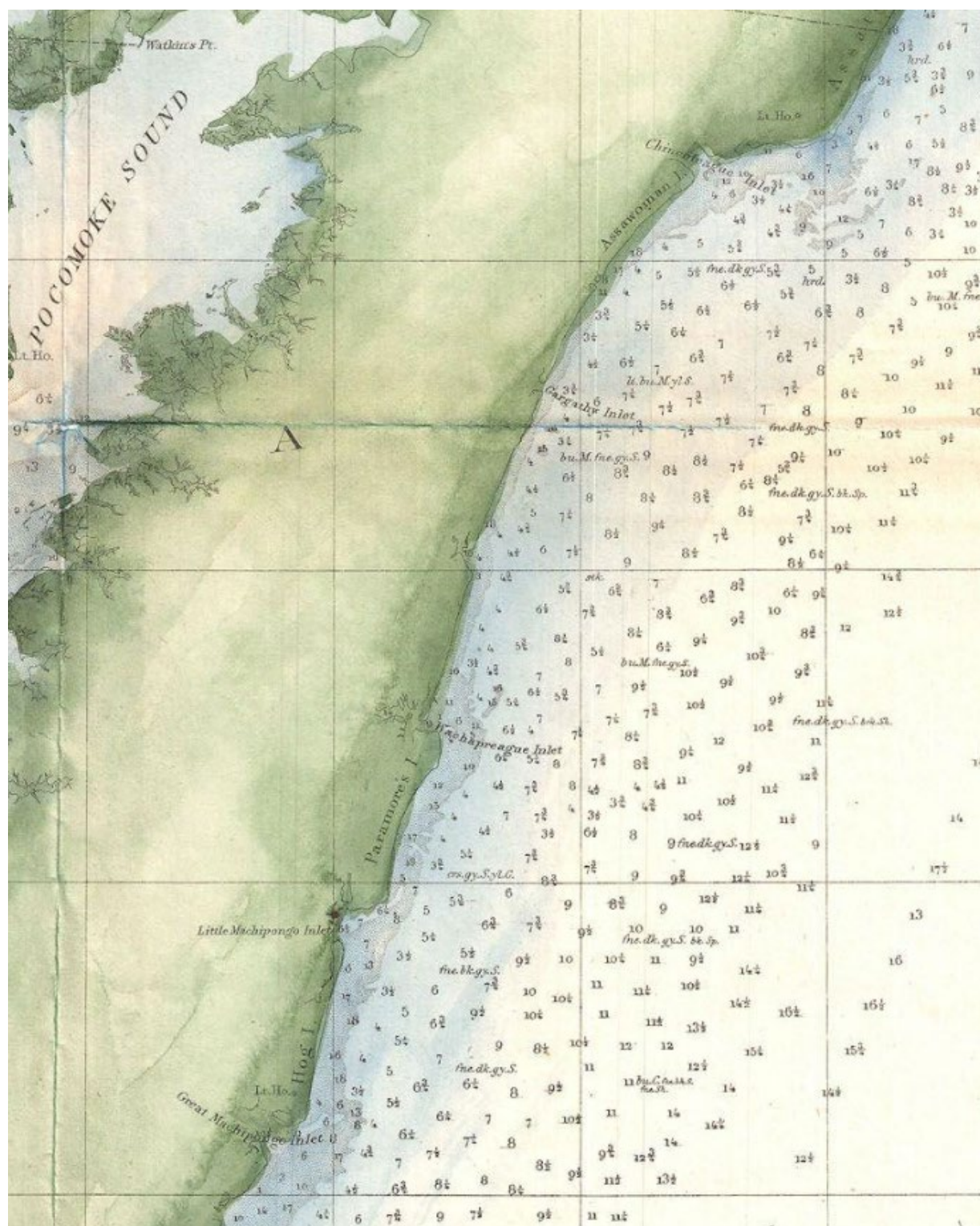


Figure A4.3 – Clip from the Office of Coast Survey *Preliminary Chart of Delaware and Chesapeake Bays and Sea Coast From Cape Henlopen to Cape Charles*, series 1855. Fishing Point, which has yet to form, would eventually exist northeast of Chincoteague Inlet in the north, where shoals are indicated. Parramore Island (center, bottom) shown with seaward bulging southern shoreline. Depths greater than 20 feet are displayed in fathoms.

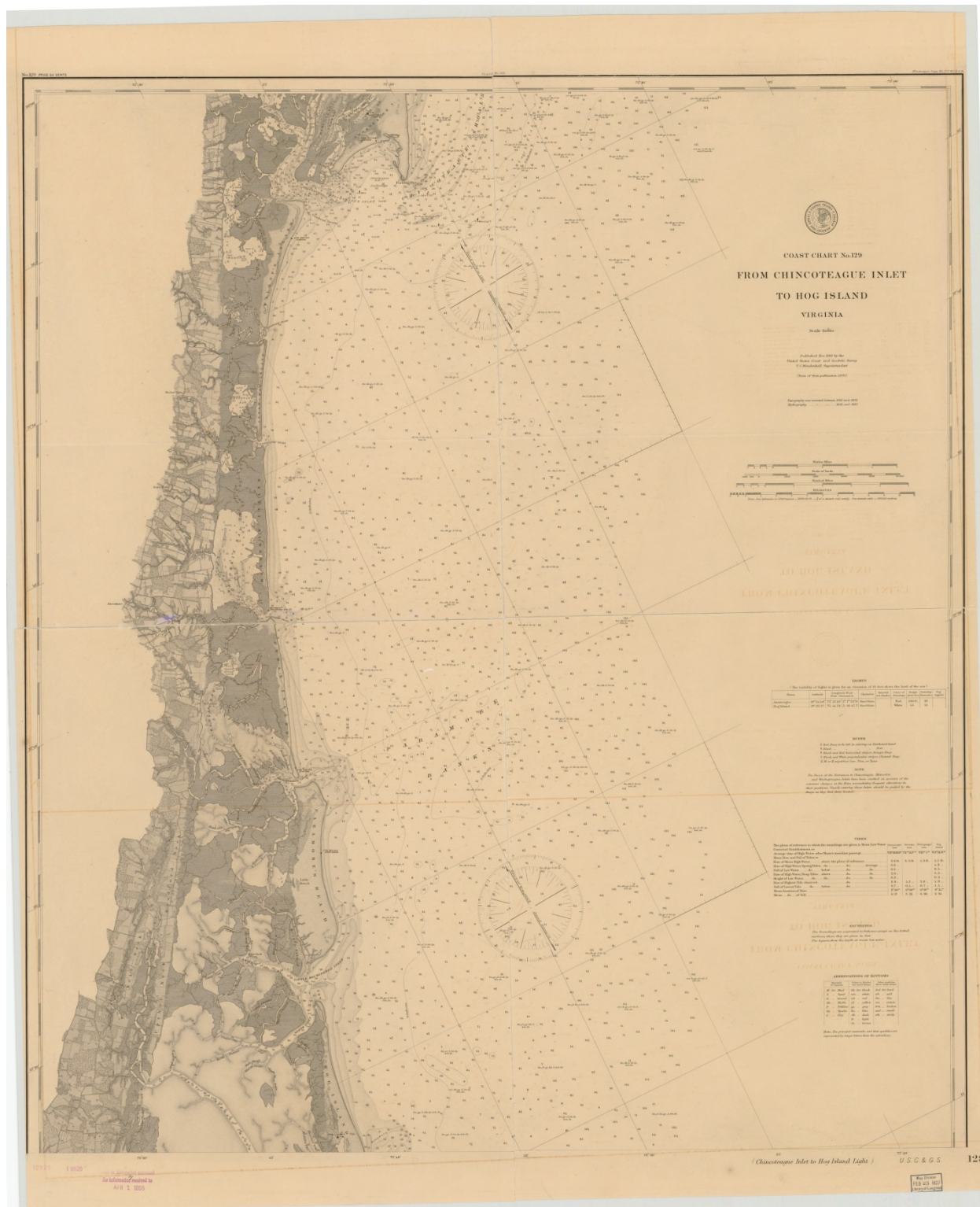


Figure A4.4 – Office of Coast Survey nautical chart *From Chincoteague Inlet to Hog Island Virginia*, series 1895, 4th Edition. Fishing Point charted as an emerging feature in the north. Parramore Island (2nd island to bottom) shown near its maximum state of progradation.

Progression of Ridge Abandonment

Image: March, 2013



Figure A4.5 – Aerial photo of Fishing Point showing progression of dune ridge abandonment along the cross-shore transect through time. 2013 image selected as base due to high resolution and contrast. Map data: Google, USDA Farm Service Agency.

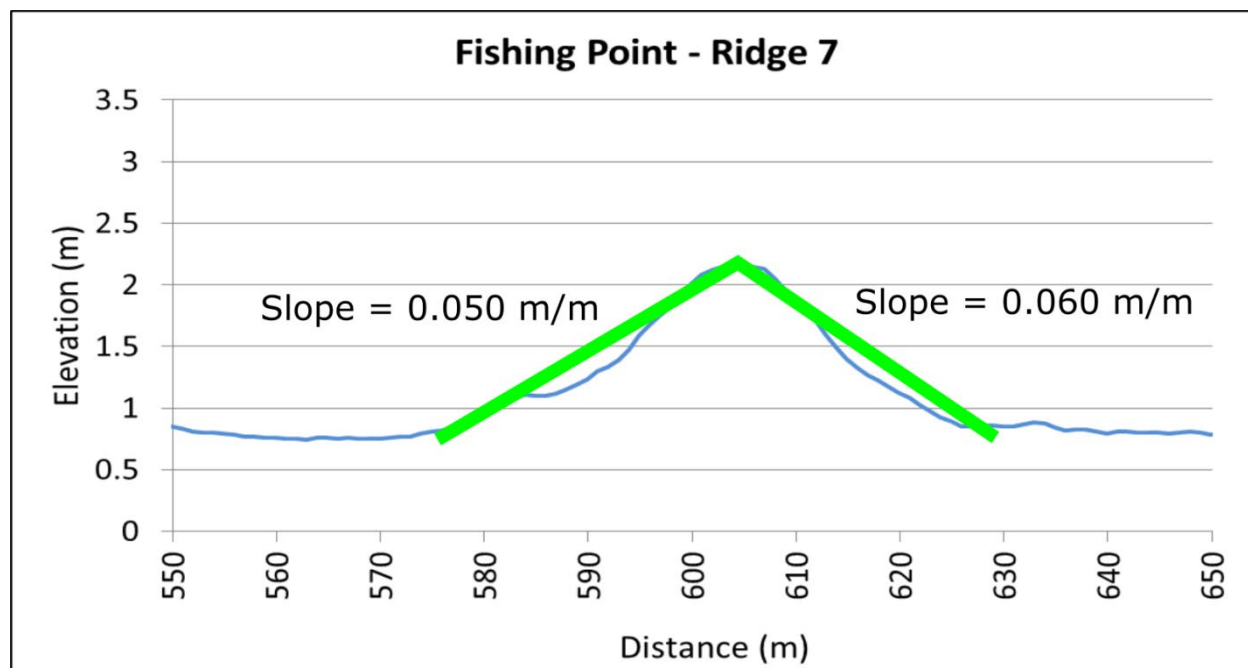


Figure A4.6 – Detailed cross section of Fishing Point Ridge #7, depicting slope of dune flanks. Elevation relative to NAVD88 is shown on the y axis, while the x axis indicates cross shore distance increasing in the seaward direction (south).

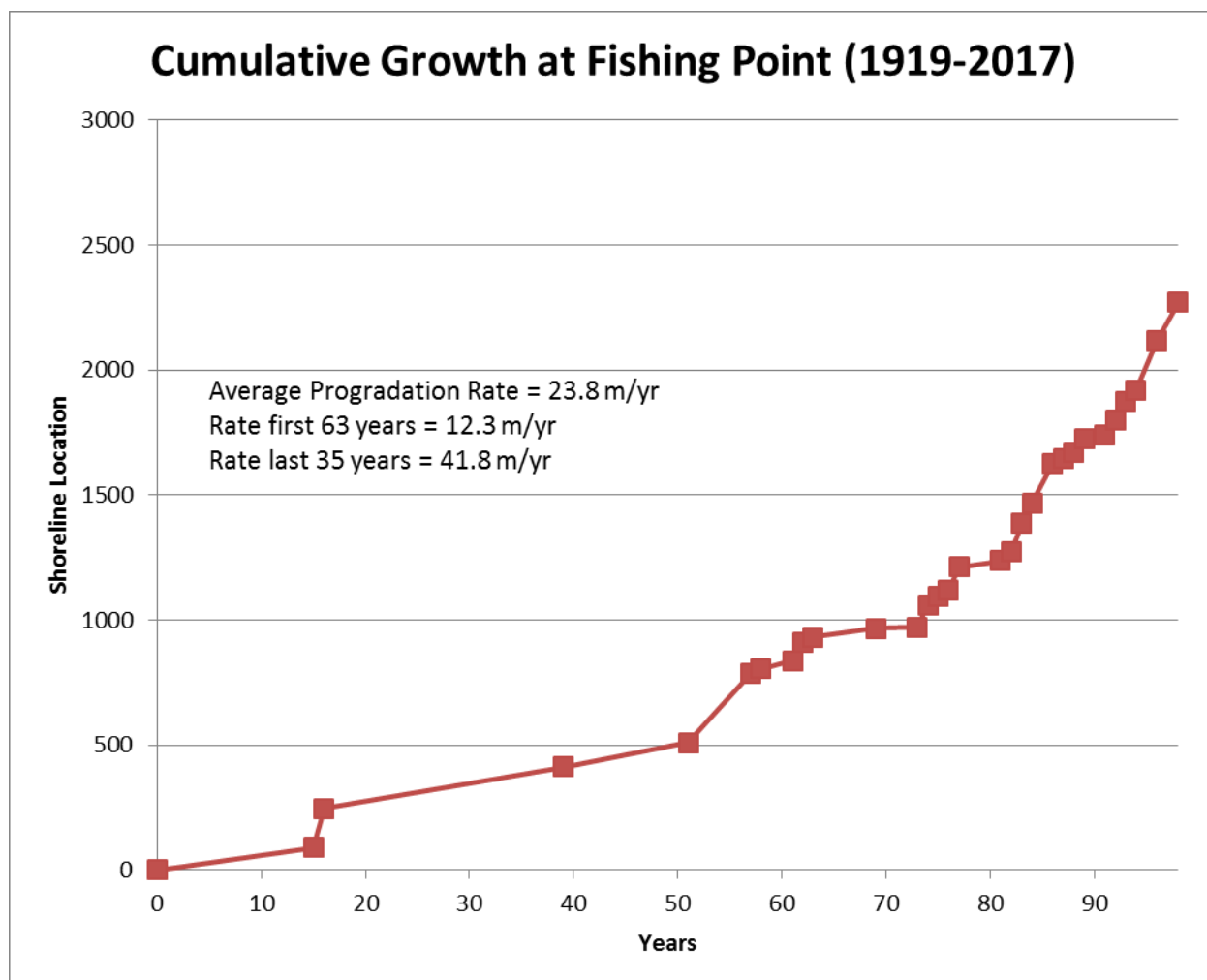


Figure A4.7 – Cumulative shoreline growth along the longest ridge-perpendicular transect of Fishing Point, from 1919 to 2017. From 1919 to 1982, the rate of shoreline advance averaged 12.3 m/yr. After 1982, progradation accelerated to 41.8 m/yr.

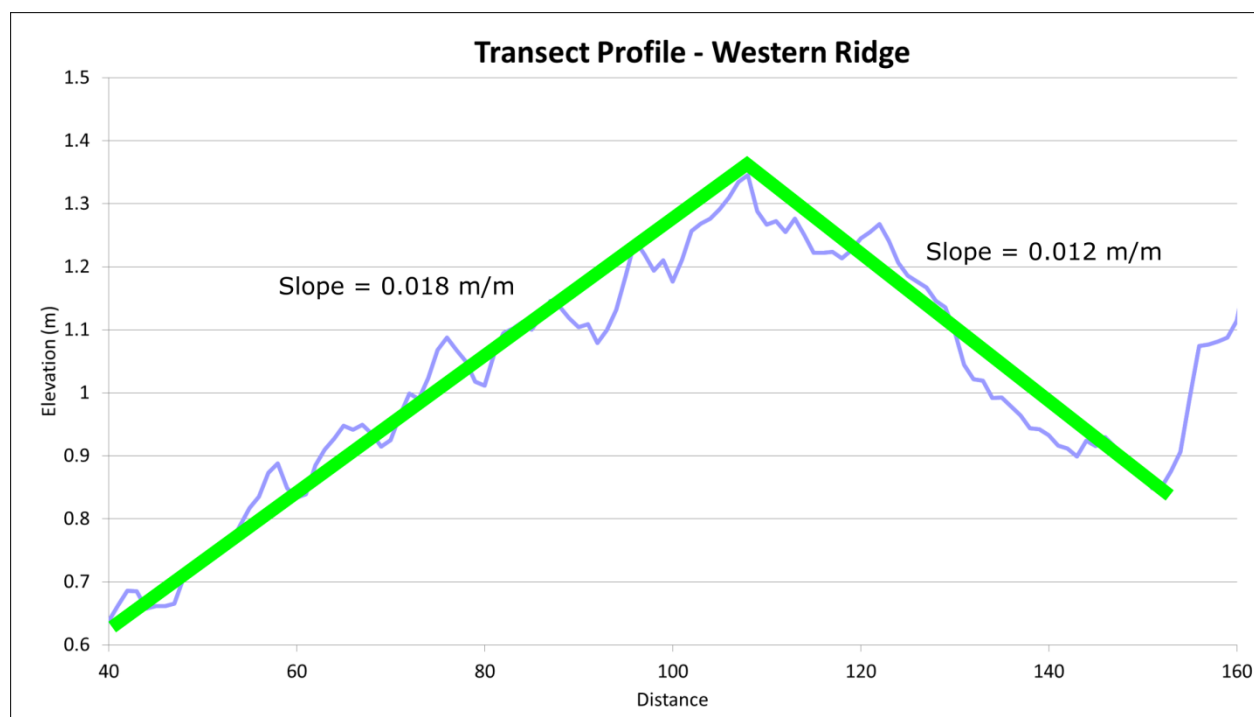


Figure A4.8 – Detailed cross section of Western Ridge, depicting slope of dune flanks. Elevation relative to NAVD88 is shown on the y axis, while the x axis indicates cross shore distance increasing in the seaward direction (east).

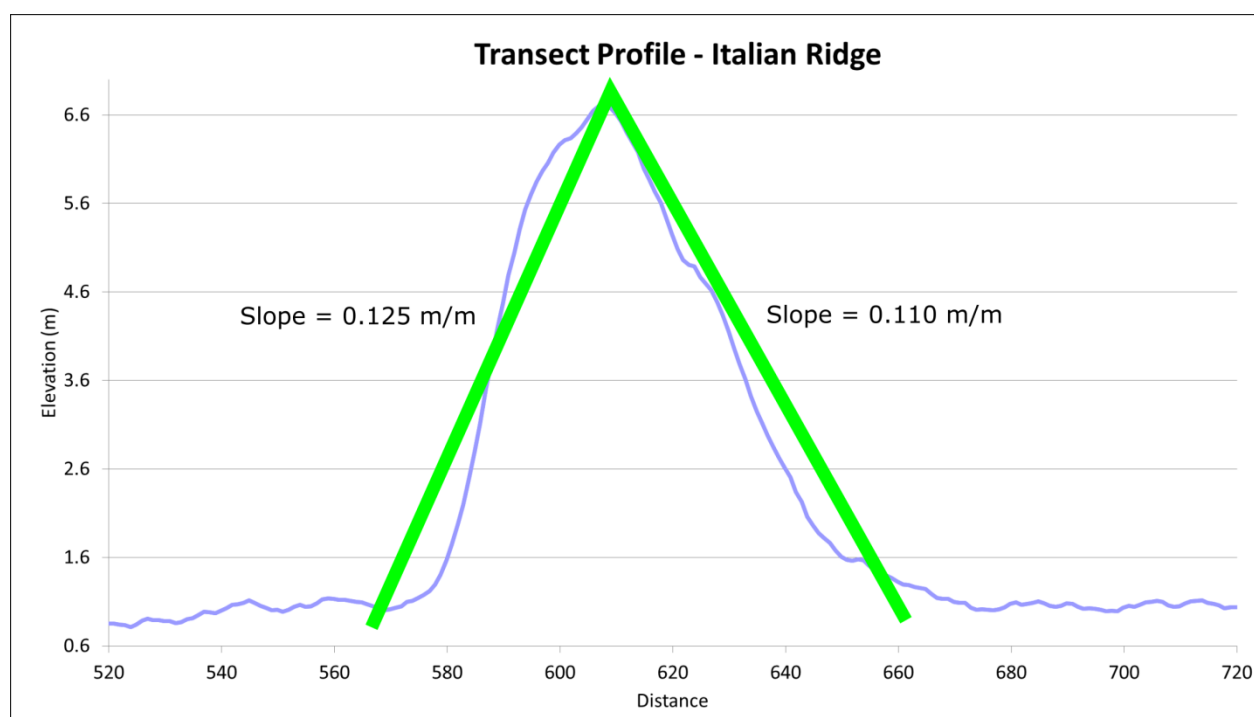


Figure A4.9 – Detailed cross section of Italian Ridge, depicting slope of dune flanks. Elevation relative to NAVD88 is shown on the y axis, while the x axis indicates cross shore distance increasing in the seaward direction (east).

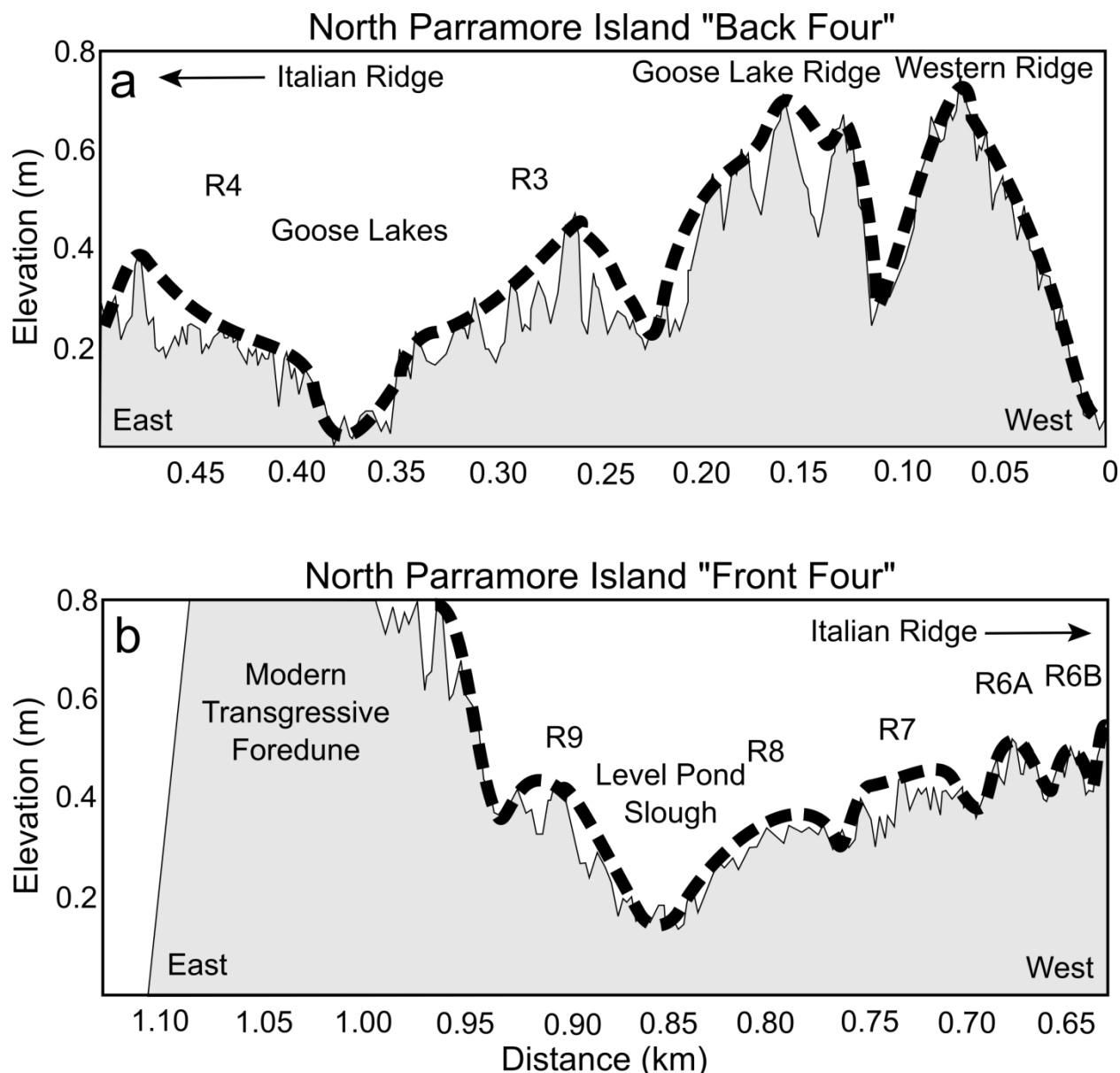


Figure A4.10 – Elevation cross section of the (a) “Back Four” and (b) “Front Four” ridges west and east of Italian Ridge, respectively, with distance increasing in the seaward direction. The dashed line is a subjective impression of what the ridges might look like with ideal preservation (in reality, ridges have an irregular profile, presumably due to post-abandonment erosion and local vegetation effects). For example, Goose Lake Ridge appears to have 4 ridges crests in the profile, but these are actually surface variations generated by hummocky topography that are apparent in planar view. Ridges are numbered from landward to seaward, with the most substantial ridges, Western Ridge (R1) and Goose Lake Ridge (R2) annotated.

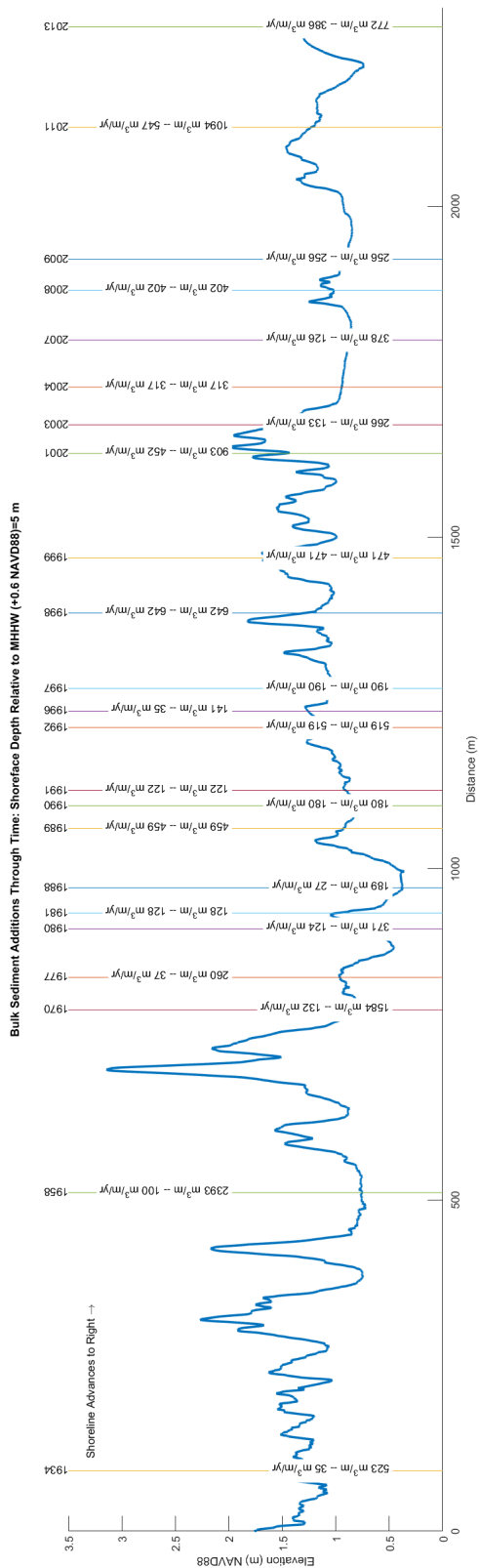


Figure A4.11 – Elevation profile of Fishing Point transect overlain with former shoreline locations. The bulk sediment additions to the system are shown for each advance in shoreline location, calculated by computing the cross section volume under the elevation profile plus the shoreface depth.

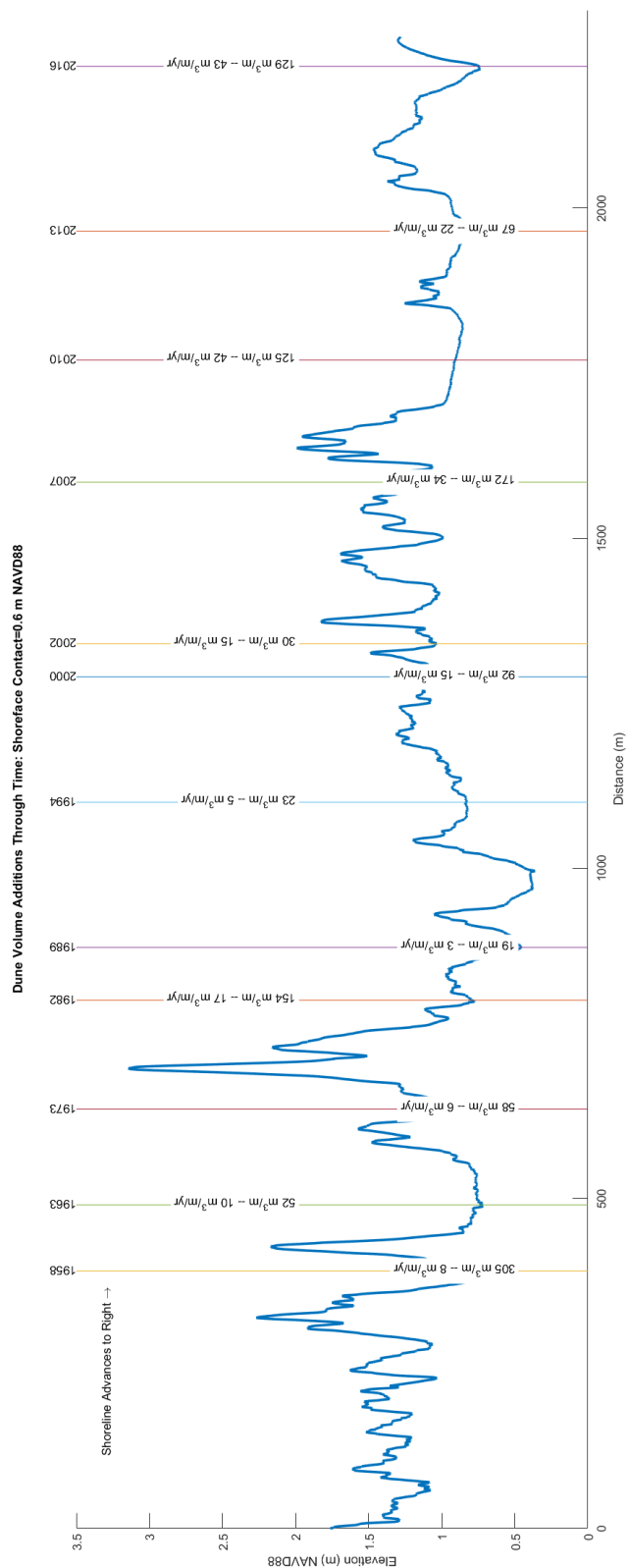


Figure A4.12 – Elevation profile of Fishing Point transect overlain with locations marking the dates when ridges or sets of ridges became relict. Dune volume additions with the progression of ridge inactivity are calculated by computing the cross section volume under the elevation profile to MHHW.

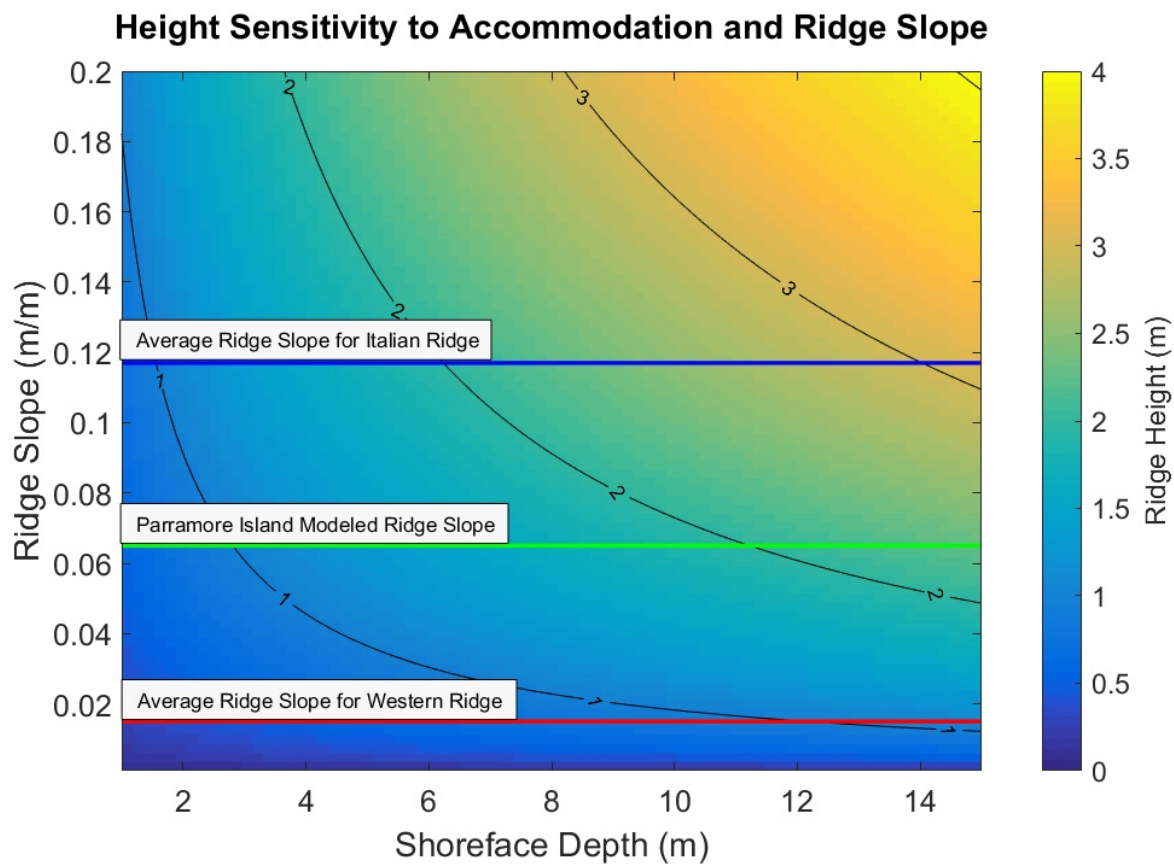


Figure A4.13 – Ridge height sensitivity to ridge slope and shoreface depth (accommodation) after 200 years, using $L_S = 5$ m, $L_c = 117$ m, $Q_S = 15$ m³/m/yr, and $Q_D = 0.7$ m³/m/yr. The average ridge slope for Western Ridge, Parramore Island (red) is 0.015 m/m, and the average ridge slope for Italian Ridge, Parramore Island (blue) is 0.117 m/m.

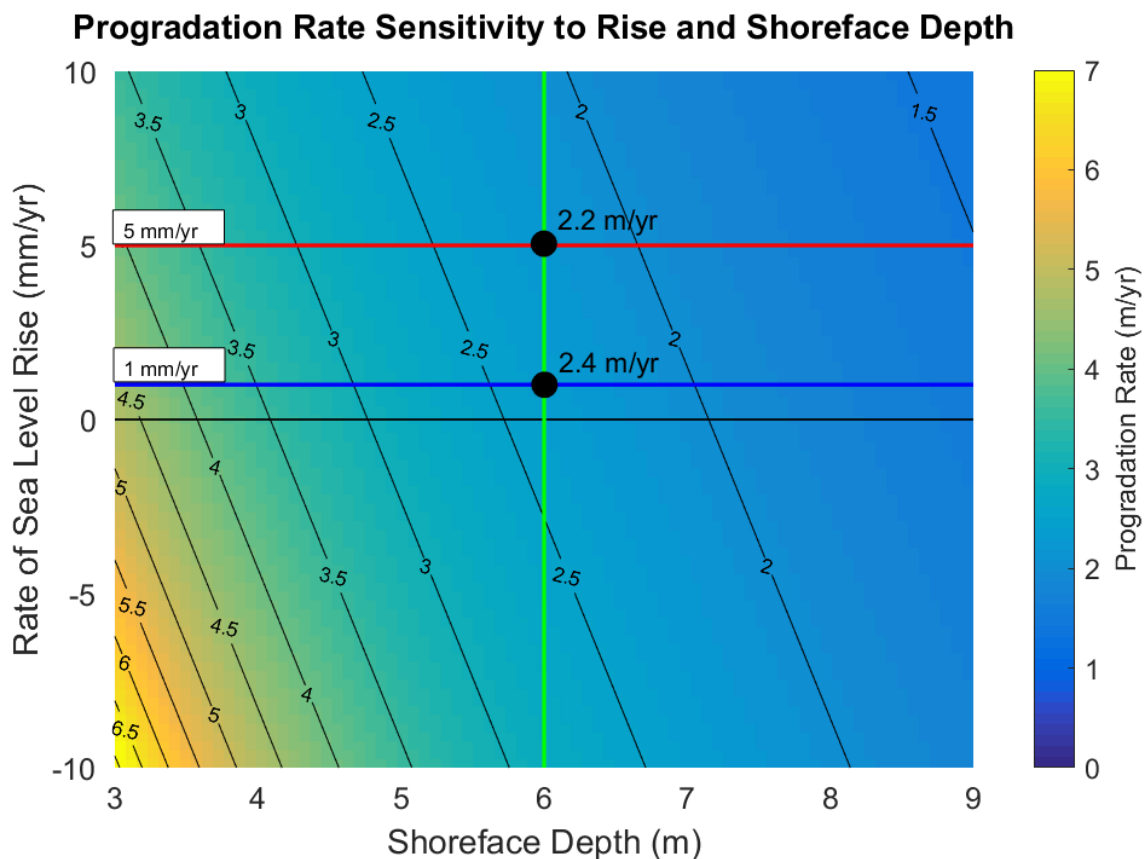


Figure A4.14 – Progradation rate sensitivity to rate of sea-level rise and shoreface depth (accommodation) after 100 years, using $L_S = 5$ m, $L_C = 117$ m, $Q_S = 15$ m³/m/yr, and $Q_D = 0.7$ m³/m/yr. The progradation rate of Parramore Island is plotted as modeled in Figure 9b from 900 to 1000 years, with a sea-level rise rate of 1 mm/yr (blue) at a shoreface depth of 6 meters (green). The rate of progradation is also plotted at 5 mm/yr (red), demonstrating a 0.2 m/yr decrease in progradation rate.

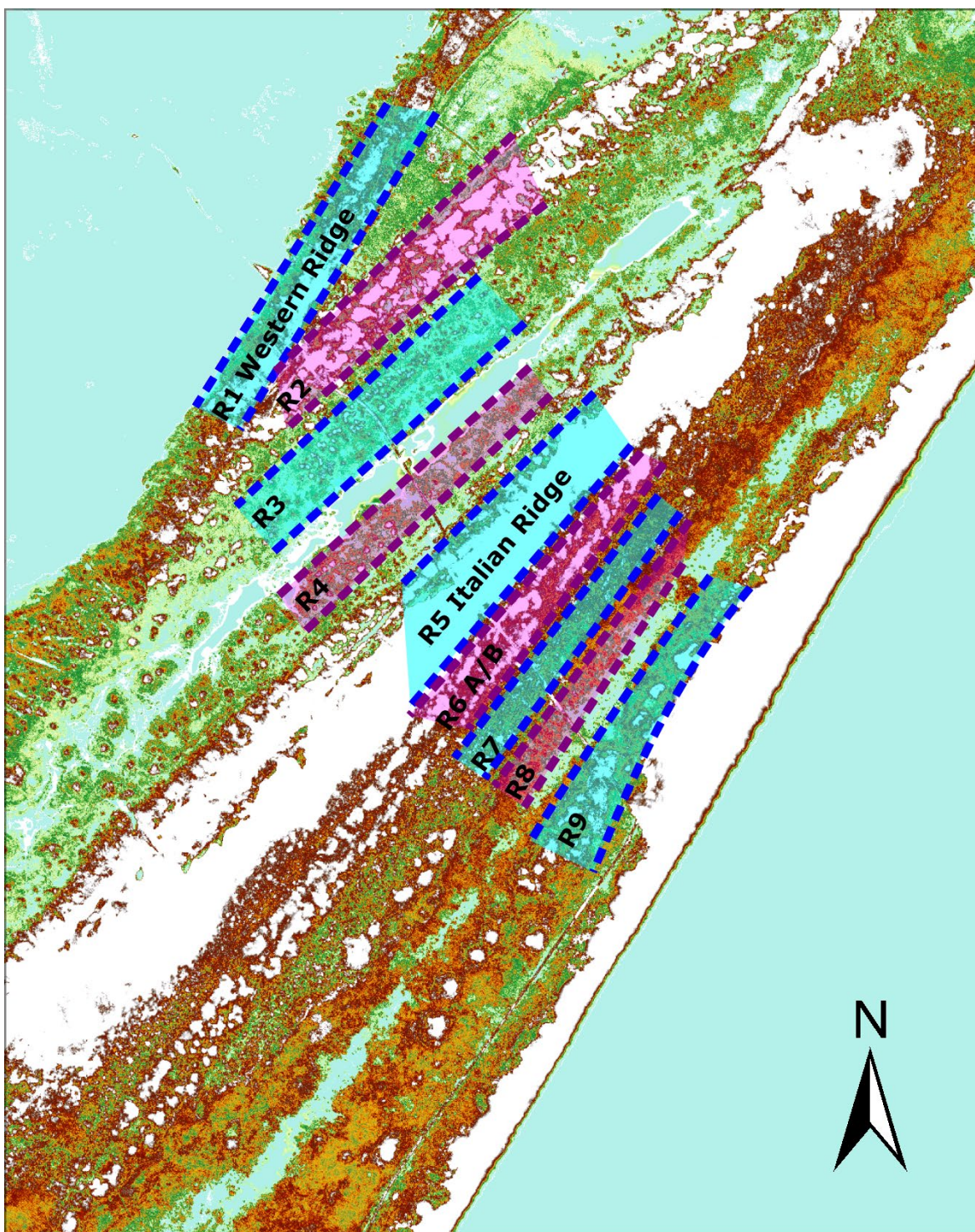


Figure A4.15 – Plan view of study area on north Parramore Island, Virginia, with 2016 CoNED (Coastal National Elevation Database) LiDAR derived elevation. This image is shaded between 0.7 and 1.2 m NAVD88 in order to enhance the detail of the ridges, highlighted here in alternating shades of blue and violet. Elevations in white are out of shader range.

